Philosophiæ Doctor Thesis

University of Wrocław
Faculty of Physics and Astronomy

Transport Properties of Hot QCD Matter in the Quasiparticle Approach

Author:
Valeriya Mykhaylova

Supervisor:
Dr. hab. Chihiro Sasaki, Prof. UWr

Wrocław
2023

„Questions you cannot answer are far better for you than the answers you cannot question"

Yuval Noah Harari

Acknowledgements

First of all, I would like to express my deep sense of gratitude and appreciation to my supervisor, Dr. hab. Chihiro Sasaki, Prof. UWr, who constantly inspires me to grow professionally by her own example. She is a great teacher and mentor, and I am grateful for her sincere support, active guidance, and patience.

I would also like to give the warmest thanks to my collaborator and former supervisor, Prof. Dr. hab. Krzysztof Redlich. I appreciate that he once recognized me as a future physicist and has been accompanying me on this entertaining journey ever since.

Words cannot express the gratitude to my parents, Iryna Mykhaylova and Maksym Mykhaylov, who always did and do their best by loving, undoubtedly trusting, and believing in me.

From the bottom of my heart, I would like to thank my high school physics teacher, Ivan M. Moyseienko, whose extraordinary talent encouraged me to enter the world of science.

I am also thankful to Tomasz Bonus, Kornel Witkowski, dr Michał Marczenko, and dr Marcus Bluhm, for sharing valuable knowledge that improved my computing skills.

Lastly, I would like to acknowledge that my doctoral research has been financially supported by the Stefan Banach Scholarship Programme (2017 – 2021) provided by the Polish National Agency for Academic Exchange and Max Born Scholarship (2021) awarded by the City Council of Wrocław. Further, in the day of the Thesis submission, I am a principal investigator in the project „Transport of Charm Quarks in the Quark-Gluon-Plasma", operating under PRELUDIUM 20 grant No. UMO-2021/41/N/ST2/02615 (2022 – Ongoing) provided by the National Science Center in Poland.

Abstract

One of the main achievements of relativistic heavy ion collisions is providing signatures of the formation of the quark-gluon plasma (QGP). This deconfined phase of strongly interacting matter is explored theoretically by Quantum Chorodynamics (QCD), which is characterized by some peculiar aspects, making it challenging to perform the first-principle computations. Therefore, various effective frameworks have been developed to extend the scope of the theory and approach it in a simplified manner.

In this Thesis, we investigate the transport properties of hot QCD matter in the quasiparticle model. We consider quasiparticle excitations with quark and gluon quantum numbers as effective degrees of freedom in the deconfined phase. The interactions with a hot medium are embodied in dynamical masses of the constituents and temperature-dependent dispersion relations through the effective running coupling extracted from lattice QCD thermodynamics.

We study the temperature and flavor dependence of different transport parameters of the deconfined matter in pure Yang-Mills theory and QCD with light and strange quark flavors. The calculations are performed in kinetic theory under the relaxation time approximation, with relaxation times that depend explicitly on the microscopic two-body scatterings of the quasiparticles.

The shear viscosity to entropy density ratio in pure Yang-Mills theory exhibits a characteristic non-monotonicity, with a minimum at the first-order phase transition. However, the ratio smoothens while showing a minimum near confinement in the presence of dynamical quarks. We illustrate that this agrees with the results of hydrodynamic simulations and perturbative QCD expectations at higher temperatures.

We also investigate the bulk viscosity to entropy density ratio, which in pure gluon plasma exhibits a rapid rise around the phase transition temperature, similar to lattice gauge theory and AdS/CFT observations. However, in the QGP, the non-monotonic structure is totally dissolved due to the substantial contribution of dynamical quarks. We observe an overall significant increase of the specific shear and bulk viscosities in QCD, compared to the Yang-Mills theory, resulting from the presence of dynamical quarks, with a major impact produced by the light quark sector.

Moreover, we compute the bulk to shear viscosity ratio, which near the phase transition temperature, behaves consistently to the scaling with the speed of sound derived in the AdS/CFT. In contrast, it obeys the same parametric dependence as in perturbation theory at high temperatures. This feature is not altered by including dynamical quarks, which, however, retards the system from restoring conformal invariance. This analysis indicates that the employed quasiparticle model nicely captures the theory's weak and strong coupling regimes.

The electrical conductivity of the QGP with quasiquarks is another transport parameter that we have examined in the quasiparticle model. We find that the behavior of the individual flavor contributions agrees qualitatively well with the results of lattice QCD simulations and with a class of phenomenological approaches.

Finally, we employ the acquired shear viscosity in the investigation of charm quark production. By comparing perfect QGP propagating longitudinally with the viscous QGP also expanding in the transverse direction, we observe that the latter setup significantly induces the production of charm-anticharm pairs. However, as QGP approaches the phase transition temperature, the majority of heavy quarks annihilate in the perfect fluid. At the same time, in a viscous medium, the final number of charm-anticharm pairs in certain cases equals the initial one, which agrees with the experimental observations. We find a universal behavior of the charm quark number as a function of temperature and time at the late stage of the QGP evolution. This can be linked to the rate equation used in our calculations, which is characterized by the general property of differential equations to have a universal (attracting) solution.

Streszczenie

Jednym z głównych osiągnięć relatywistycznych zderzeń ciężkich jonów jest dostarczenie dowodów na powstanie w wyniku tych zderzeń plazmy kwarkowo-gluonowej (QGP). Ta faza silnie oddziałującej materii jest opisywana teoretycznie przez Chromodynamikę Kwantową (QCD), której szczególne aspekty utrudniają wykonywanie obliczeń od podstaw. Dlatego opracowano szereg modeli efektywnych, które pozwalają rozszerzyć zakres teorii i w uproszczony sposób podejść do różnego rodzaju zagadnień.

W niniejszej pracy badamy właściwości transportowe gorącej materii QCD w modelu kwazicząstek. Za efektywne stopnie swobody w fazie cząstek uwolnionych przyjmujemy wzbudzenia kwazicząsteczkowe, posiadające liczby kwantowe kwarków i gluonów. Oddziaływania składników materii z otoczeniem są zawarte w dynamicznych masach i zależnych od temperatury energii tychże składników. Zależność została wprowadzona poprzez efektywne sprzężenie, wyprowadzone z termodynamiki QCD obliczonej na sieci.

Badamy zależność różnych parametrów transportu od temperatury i rodzajów kwarków w materii opisanej poprzez czystą teorię Yanga-Millsa oraz przez QCD z uwzględnieniem kwarków lekkich i dziwnych. Do obliczeń używamy kinetycznej teorii z przybliżonym rozwiązaniem metodą czasów relaksacji, które wprost zależą od mikroskopijnych rozproszeń kwazicząstek w ośrodku.

Stosunek lepkości ścinania do gęstości entropii w czystej teorii Yanga-Millsa wykazuje charakterystyczną niemonotoniczność, z minimum obserwowanym przy przejściu fazowym pierwszego rzędu. Jednak zachowanie tego stosunku wygładza się w obecności kwarków dynamicznych. Te obserwacje zgadzają się z wynikami symulacji hydrodynamicznych i oczekiwaniami teorii zaburzeń QCD w wyższych temperaturach.

Badamy również stosunek lepkości objętościowej do gęstości entropii, który w czystej plazmie gluonowej wykazuje szybki wzrost wokół przemiany fazowej, podobnie jak w teorii QCD na sieci i teorii AdS/CFT. Jednak niemonotoniczne zachowanie stosunku lepkości objętościowej do gęstości entropii całkowicie znika w QGP z powodu istotnego udziału kwarków dynamicznych. Obserwujemy ogólny znaczny wzrost ww. stosunku w QCD, w porównaniu do teorii Yanga-Millsa, wynikający z obecności kwazikwarków, przy czym główny wpływ na współczynnik transportu ma sektor kwarków lekkich.

Ponadto obliczamy stosunek lepkości objętościowej do lepkości ścinania, który w pobliżu temperatury przemiany fazowej zachowuje się zgodnie ze skalowaniem z prędkością dźwięku wyprowadzonym w AdS / CFT. W przeciwieństwie do tego, w wysokich temperaturach, stosunek ten podlega zależności parametrycznej, obliczonej w teorii zaburzeń QCD. Ta cecha pozostaje, gdy układ zostaje uzupełniony przez kwarki dynamiczne, lecz ich obecność opóźnia przywracanie niezmienności konforemnej układu. Analiza ta wskazuje, że zastosowany model kwazicząstek dobrze oddaje tryby słabego i silnego sprzężenia w chromodynamiki kwantowej.
Przewodnictwo elektryczne w QGP uwzględniającej kwarki dynamiczne to kolejny parametr transportu, który badamy w modelu kwazicząstek. Obserwujemy, że zachowanie poszczególnych składników przewodnictwa elektrycznego, pochodzących od różnych zapachów kwarków, całkiem dobrze się zgadza z symulacjami QCD na

sieci oraz z obliczeniami przeprowadzonymi w szeregu fenomenologicznych modeli.

Na koniec wykorzystujemy wyznaczoną lepkość ścinania do badania produkcji ciężkich kwarków powabnych. Porównując QGP w postaci płynu doskonałego poruszającego się w kierunku podłużnym do lepkiej QGP rozszerzającej się również w kierunku poprzecznym, obserwujemy, że ta druga konfiguracja znacznie indukuje produkcję ciężkich kwakrów i antykwarków. Jednak gdy QGP zbliża się do temperatury przemiany fazowej, większość ciężkich kwarków anihiluje w płynie doskonałym. Jednocześnie w ośrodku lepkim końcowa liczba ciężkich kwarków w określonych przypadkach jest równa ich liczbie początkowej, co zgadza się z danymi doświadczalnymi. Obserwujemy uniwersalne zachowanie liczby kwarków powabnych jako funkcji temperatury i czasu na późnym etapie ewolucji QGP. Zachowanie to można to powiązać z równaniem produkcji kwakrów, które charakteryzuje ogólna właściwość równań różniczkowych do posiadania uniwersalnego (przyciągającego) rozwiązania.

List of Publications

Peer Reviewed Articles

- Valeriya Mykhaylova, Marcus Bluhm, Chihiro Sasaki, Krzysztof Redlich, Quark-flavor dependence of the shear viscosity in a quasiparticle model, *Phys. Rev. D 100* (2019) 3, 034002, 10.1103/PhysRevD.100.034002.

- Valeriya Mykhaylova, Shear viscosity to electrical conductivity ratio in the quasiparticle model, *Eur. Phys. J. ST* 229 (2020) 22-23, 3487-3496, 10.1140/epjst/e2020-000116-9.

- Valeriya Mykhaylova and Chihiro Sasaki, Impact of quark quasiparticles on transport coefficients in hot QCD, *Phys. Rev. D* 103 (2021) 1, 014007, 10.1103/PhysRevD.103.014007.

Conference Proceedings

- Valeriya Mykhaylova, Flavor-dependent transport parameters of the quark–gluon plasma within the quasiparticle model, *Acta Phys. Polon. Supp.* 13 (2020) 4, 829-834, 10.5506/APhysPolBSupp.13.829.

- Valeriya Mykhaylova, Interviewing the weak with strong coupling regimes via the bulk to shear viscosity ratio in QCD, *Acta Phys. Pol. B Proc. Suppl.* 14 (2021) 2, 271-279, 10.5506/APhysPolBSupp.14.271.

- Valeriya Mykhaylova, The Role of Strange Quasiquarks in Transport Properties of the QGP, *EPJ Web Conf.* 259 (2022) 10007, 10.1051/epjconf/202225910007.

- Valeriya Mykhaylova, Quasiparticle perspective on transport properties of hot QCD matter, *Proceedings of the IFJ PAN Particle Physics Summer Student Alumni Conference 2022*, Institute of Nuclear Physics PAS, Kraków (2022), e-Print: 2210.13539 [hep-ex], 49-52, 10.48733/978-83-63542-30-6.

- Valeriya Mykhaylova, Charm quark fugacity in hot QCD, *EPJ Web Conf.* 274 (2022) 05006, 10.1051/epjconf/202227405006.

Hearby, I would like to declare that I have provided a major contribution to the articles listed above. I have performed on my own such essential steps as the analytical evaluation of the cross sections between massive quasiparticles, computation of the relaxation times, and all numerical calculations of various transport and dynamical parameters. The peer-reviewed publications present an original systematic study of the role of different quark flavors in transport coefficients of the deconfined matter. I have also provided the leading contribution to the writing process and the vast majority of figures.

The most recent article exhibits the first outcomes of my scientific project conducted under the PRELUDIUM 20 grant mentioned previously, which I have fully prepared on my own.

List of Abbreviations

(in alphabetical order)

- AdS/CFT – Anti-de Sitter/Conformal Field Theory
- c.m. – center-of-mass [reference frame]
- CSC – Color SuperConductor
- DQPM – Dynamical QuasiParticle Model
- d.o.f. – degree(s) of freedom
- EoS – Equation of State
- FRG – Functional Renormalization Group
- GRG – Glueball Resonance Gas
- HRG – Hadron Resonance Gas
- HTL – Hard Thermal Loop
- KSS – Kovtun-Son-Starinets [bound]
- LAS – Large Angle Scattering [assumption]
- LHC – Large Hadron Collider
- LHS – Left-Hand Side
- lQCD – lattice Quantum Chromodynamics
- LRF – Local Rest Frame
- NJL – Nambu-Jona-Lasinio [model]
- NLL – Next-to-Leading-Log [order]
- pQCD – perturbative Quantum Chromodynamics
- QCD – Quantum Chromodynamics
- QGP – Quark-Gluon Plasma
- QPM – QuasiParticle Model
- RHIC – Relativistic Heavy Ion Collider
- RTA – Relaxation Time Approximation
- SU(n) – Special Unitary group of degree n

Spis treści

Structure of the Thesis

The research in this Thesis is outlined as follows:

Chapter 1 introduces the essential elements of strong interactions and our motivation to study the transport properties of the QGP. After briefly discussing the main QCD features in Section 1.1, we focus on the phenomena occurring in the deconfined matter and the corresponding transport parameters. Section 1.2 contains an overview of previous studies of the QGP transport properties approached from various perspectives. In Chapter 2, we introduce the general concept of the phenomenological quasiparticle model employed in this research. Chapter 3 discusses how transport coefficients, such as the shear and the bulk viscosity, emerge in the description of viscous fluid dynamics, while Chapter 4 shows how they can be derived in kinetic theory using Boltzmann equation in the relaxation time approximation (Section 4.1).

We present a detailed computation of the relaxation times of quasiparticles in Section 4.2. Various numerical results obtained in this research are comprehensively discussed in Chapter 5, e.g. see Section 5.1 for the specific shear viscosity, Section 5.2 for the specific bulk viscosity, or Section 5.4 for the electrical conductivity. The investigation of the charm quark production in perfect and viscous QGP is contained in Chapter 6. The conclusions of our research are given in Chapter 7.

Additionally, in Appendix A, we provide a step-by-step analytical evaluation of the scattering amplitudes for the elementary cross sections of massive particles, while in Appendix B, the calculation of the weight factor entering the transport cross section is presented.

Rozdział 1

Introduction

In a scientific world full of uncertainties, relativity, and unknowns, exploring strong interactions from experimental and theoretical perspectives has proven to be a powerful source of knowledge about the matter and fields existing in the Universe. Over the last several decades, the fundamental theory of strong interactions – Quantum Chromodynamics (QCD) – has remarkably developed, and together with the information collected from ultrarelativistic heavy ion collision experiments, has led to significant progress in understanding the phenomena occurring in strongly interacting matter [1–3].

1.1 Quantum Chromodynamics

The QCD is characterized by a few unique features which make it challenging to describe the physics of strong interactions. The underlying degrees of freedom (d.o.f.) of the theory are quarks (fermions) of different flavors and gluons (gauge bosons), all carrying the color charge associated with the SU(3) gauge group [4].

There is a unique QCD phenomenon known as confinement, which implies that the color-charged elementary particles cannot be isolated; hence it is impossible to observe a single quark as a separate object [1, 5, 6]. This can be understood as the opposite side of asymptotic freedom – a property related to the QCD coupling strength, which increases with the increasing distance between strongly-interacting elementary particles [7, 8].

Another peculiar feature of QCD is the spontaneous chiral symmetry breaking [9]. Associated with the orientation of the particle's spin relative to its direction of motion, the left- and right-handed chirality of quarks can be interchanged in the QCD interaction if the masses of quarks can be neglected [1,6]. The assumption of massless quarks is known as the chiral limit, in which the chiral symmetry in QCD is exact. However, the quarks actually carry constant masses and when confined in hadrons, do not form any degenerate chiral partners but lead to the bound states of opposite parities and prominently distinct masses. This paradoxical observation has been identified with the spontaneous breakdown of chiral symmetry [1, 6, 10].

The lattice gauge theory simulations provide numerical solutions to the QCD equations, in which spontaneous chiral symmetry breaking and confinement are certainly manifested. We utilize one of the lattice QCD (lQCD) results in our studies to take into account the main features of strong interactions, see Chapter 2.

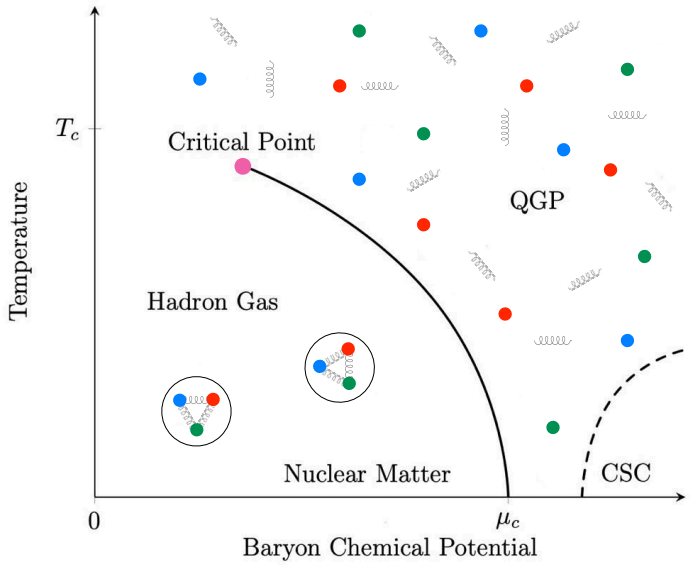

Rysunek 1.1: The hypothetical QCD phase diagram with temperature T shown as a function of baryon chemical potential μ_B. We schematically depict the quarks (circles) and gluons (spirals) in the confined (Nuclear Matter and Hadron Gas) and the deconfined (QGP) phases, with the first-order phase transition between them, indicated by the solid line. The transition becomes a smooth crossover after reaching the Critical Point [11] shown by the pink dot. In addition, at very high μ_B, the matter reaches the color superconducting (CSC) phase [12]. The T_c and μ_c stand for the critical temperature at vanishing μ_B, and critical chemical potential at vanishing T_c, respectively.

One of the important goals of experimental and theoretical approaches to strong interactions is to properly designate the possible phases of the QCD matter. Those are illustrated in Fig. 1.1 by the simplistic QCD phase diagram, which covers various states of strongly interacting matter as functions of temperature T and baryon chemical potential μ_B [1]. At Earth conditions, the quarks, interacting via gluons, are bound in hadrons, such as the proton, neutron, etc. However, for higher T and/or μ_B, i.e. when nuclear matter is strongly heated and/or compressed, the QCD coupling decreases, and quarks and gluons are released from the bound states due to the deconfinement phase transition, creating a particular state of matter known as the Quark-Gluon Plasma (QGP) [1, 6]. Investigation of the transport properties of the QGP with different quark content is the main scope of this Thesis.

Due to the dramatically different conditions at which the deconfined matter is created, one can study its dynamical properties from different theoretical and phenomenological perspectives. Based on the asymptotic freedom, one assumes that in the high-temperature regime, the deconfined matter can be described as a weakly interacting gas, and therefore, perturbative QCD (pQCD) expansion becomes applicable [13]. On the other hand, the significant theoretical evidence for the QGP existence comes from the lQCD simulations, which cover the non-perturbative QCD

regime in the vicinity of the (pseudo)critical temperature T_c at vanishing chemical potential. Currently, the ways of extending the lQCD data to finite μ_B are actively developing [14]. While the lattice and perturbative approaches access the low- and high-temperature QCD regimes, as an alternative, various phenomenological models are used to cover a wide range of temperatures and baryon densities and effectively connect the strongly and weakly coupled sectors of the QCD phase diagram. Motivated to investigate the properties of hot QCD matter in a wide temperature range, starting from the point of the QGP thermalization and finishing when it reaches the hadronic phase, we employ the kinetic quasiparticle model (QPM) and discuss its reliability in the following Chapters.

1.2 Transport Properties of Deconfined Matter

The data collected from the Large Hadron Collider (LHC) and the Relativistic Heavy Ion Collider (RHIC) support the idea that the hot deconfined matter is created at ultrarelativistic heavy ion collisions [2, 15–17]. Moreover, the flow observables, characteristic for strongly coupled media, have been extensively studied in ideal [17–25] and viscous [26–34] hydrodynamics, confirming that the QGP is a strongly coupled fluid.

In particular, it has been shown in [26] that the elliptic flow coefficient v_2 can be parameterized by the ratio of shear viscosity to entropy density, η/s, see Fig. 1.2. The shear viscosity η is a transport parameter measuring the resistance of the fluid against the momentum modifications. In other words, the shear viscosity is related to inner friction, which arises in a longitudinally propagating fluid and causes the irreversible momentum transfer from one part of the fluid to another. The shear viscosity is usually presented as a dimensionless ratio to the total entropy density of the system, η/s, since this specific parameter enters the hydrodynamic simulations of the heavy ion collisions.

Since elliptic flow data shown in Fig. 1.2 can be parameterized to some extent by the ideal hydrodynamics, one recognizes that the QGP constitutes a nearly perfect fluid [17, 23–26]. In fact, one of the values of the specific shear viscosity used in Fig. 1.2, $\eta/s = 1/4\pi \simeq 0.08$, refers to the conjectured lower bound for all fluids in nature and is known as the Kovtun-Son-Starinets (KSS) bound [35], which has been obtained by applying the duality between the strongly coupled gauge and weakly coupled gravity theories. Simulations with an evolution-averaged η/s based on comparisons with combined experimental data from top-RHIC and LHC energies [24, 36, 37] extracted a possible range of $1 < (\eta/s)/(1/4\pi) < 5$, however, those estimates suffered from sizable systematic and statistical errors [38].

In Fig. 1.2, one additionally observes that as p_T increases, the larger values of η/s become more suitable to achieve a better agreement between the hydrodynamic results and the experimental data for the elliptic flow. This implies that the dependence of the shear viscosity on the surrounding conditions is relevant in the description of the QGP properties.

Thus, more realistic studies consider a temperature dependence of the viscosity coefficient [27, 39]. It was found that the combined data favor an increase with T up to a factor of 5 from RHIC to LHC [40]. A possible μ_B-dependence was investigated in [41] finding a moderate increase with increasing μ_B. The wealth of accumulated

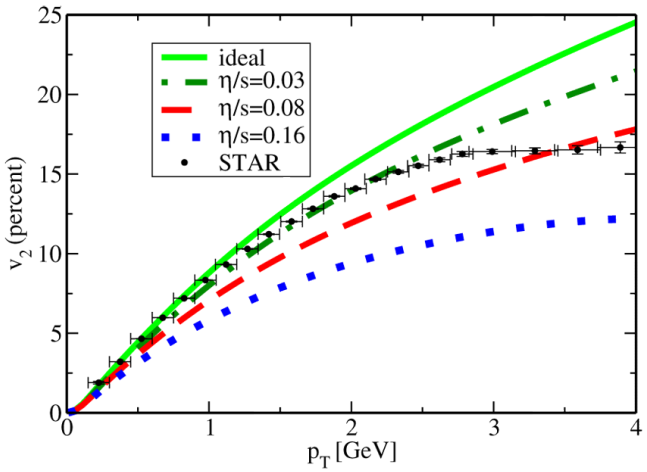

Rysunek 1.2: Figure taken from Ref. [26]. The elliptic flow coefficient v_2 as a function of the transverse momentum p_T. The experimental data from the STAR collaboration are approximated by the hydrodynamic model with different values of the specific shear viscosity η/s, including the ideal fluid case with $\eta/s = 0$.

experimental data also made Bayesian estimate studies for the temperature [42] and chemical potential [43] dependence possible, confirming the previous results.

The transport parameters of different systems are always sensitive to the relevant d.o.f., their properties, and interactions within the fluid. The specific shear viscosity used in Fig. 1.2 is undoubtedly tiny in comparison to the results found for other fluids in nature. In Fig. 1.3, one can see that η/s for the deconfined matter reaches much lower values than the specific shear viscosity of other media, and thanks to this unique property, the QGP is often called „the most perfect fluid known" [15,52]. Note that the collected lattice gauge theory results for η/s consider the pure Yang-Mills theory, i.e. the pure gluon plasma [46–48, 53]. For QCD, including dynamical quarks, no explicit calculations exist. Estimates based on the results for Yang-Mills theory and information from perturbative QCD [54] suggest a slight increase in the presence of dynamical quarks [46, 55].

As an alternative, functional diagrammatic approaches to QCD were recently exploited [56,57] to determine the shear viscosity in Yang-Mills theory from gluon spectral functions via the Kubo relation [58]. Those are in favor of a quasiparticle structure applied in this Thesis. The results presented in [57] are in reasonable agreement with the lattice data and provide an estimate for QCD with $N_f = 2 + 1$ quark flavors also indicating only a slight increase. Both first-principle approaches find a minimal η/s of about 0.2 near the deconfinement transition temperature T_c with a moderate increase with increasing T, which is qualitatively in line with the estimates from fluid dynamical simulations. Similar results can be obtained from perturbation theory with appropriately chosen scales in the running coupling [57, 59].

Since first estimates indicated that η/s of the deconfined matter is close to the KSS-bound, various QCD-like and phenomenological approaches were used to give an explanation for the apparent perfectness of the QGP in terms of relevant d.o.f. The

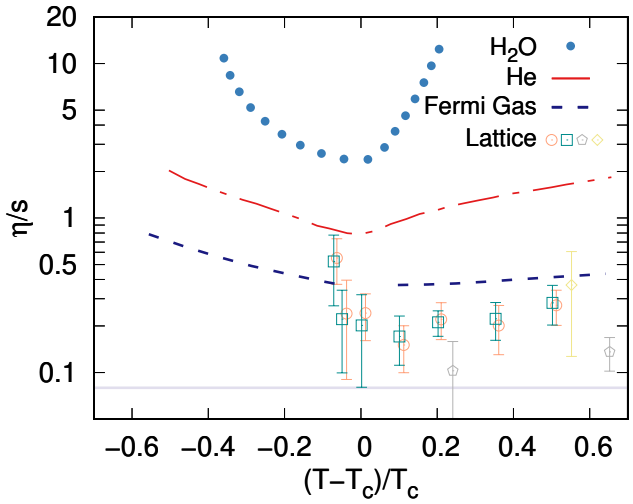

Rysunek 1.3: The shear viscosity to entropy density ratio η/s as a function of the scaled temperature $(T - T_c)/T_c$ for a number of fluids in nature. T_c denotes the critical temperature at the endpoint of the liquid-gas phase transition of water (H_2O, circles) [44] and helium (He, dashed-dotted line) [44] while representing the superfluid transition temperature for ultracold Fermi Gas (dashed line) [45] and the deconfinement temperature for pure SU(3) theory. For the latter, the data collected from lQCD simulations are shown by open symbols: circles and squares [46], pentagons [47], and diamond [48]. The solid horizontal line denotes the KSS lower bound of $\eta/s = 1/(4\pi)$ [35]. Similar figures can be found in [49–51].

specific shear viscosity of quark matter was investigated in Nambu-Jona-Lasinio (NJL) model [60–67], the Polyakov-loop improved linear sigma model [68], or a Polyakov-loop extended Quark-Meson model [69]. Further investigations were also made regarding a Gribov-Zwanziger plasma [70]. Moreover, kinetic theory within partonic transport simulations was exploited [71–74] as well as anisotropic fluid dynamics [75,76], both supporting the idea of a medium composed of quasiparticle excitations.

It was a widespread paradigm that a quasiparticle description could not account for the perfect fluidity observed for deconfined strongly interacting matter. The first quantitative determination of the specific shear viscosity for pure Yang-Mills theory described with massive quasiparticles has been found, refuting this paradigm, an $\eta/s \simeq 0.2$ with a negligible T-dependence by using the Green-Kubo formalism [77]. Based on the early works of [78,79], kinetic theory calculations considered a medium composed of quasiparticles without residual mean field interaction [61,80] and for pure Yang-Mills theory with mean field interaction term [81–84]. This idea was extended to describe interacting hadronic matter at vanishing [85] and finite chemical potential [86]. Further QPM predictions for QCD matter were presented in [87] and in [88,89], by taking into account the possible formation of turbulences in an expanding QGP. Modeling quasiparticle interactions, the QPM was further extended by including a finite collisional width in the quasiparticle spectral functions [90–92].

Alongside the shear viscosity, another significant transport coefficient accompanying the evolution of the deconfined matter is the bulk viscosity ζ. This parameter

indicates the dissipation of the energy occurring in a fluid with a changing volume, i.e., ζ reflects the reaction of a strongly coupled system to its expansion or compression.

Following the specific shear viscosity η/s, one usually studies the dimensionless ratio of the bulk viscosity to the entropy density, ζ/s, since these quantities are employed in the hydrodynamic equations [6, 93–95] and reflect the deviation of the medium from local thermodynamic equilibrium.

The early studies of the bulk viscosity have investigated its origin in the heavy-ion collisions [96], as well as its role in the clusterization of the QGP [97]. It has also been shown that the bulk viscosity vanishes in the conformally invariant theories [35]. Further results of the Green-Kubo approach [98,99] and the quasiparticle Nambu-Johna-Lasinio model [61] predicted a rapid increase of ζ/s near the phase transition temperature. Around T_c, the specific shear viscosity is anticipated to have a minimum close to the conjectured KSS bound [35], while the ratio ζ/s is expected to exhibit a rapid rise around T_c, indicating its relevance for the hydrodynamic evolution of the QGP.

The bulk viscosity of the deconfined matter has been evaluated in various frameworks, such as the effective quasiparticle models [61, 80, 81, 83, 85, 87], applying the parton-hadron string dynamics [90], as well as the Nambu-Johna-Lasinio approach [61, 62, 65, 66, 100], the dynamical quasiparticle model (DQPM) [91, 101], the Polyakov-loop extended Quark-Meson model [102], the Green-Kubo formalism [98,103,104] and the holographic QCD [105–107]. Additionally, the ζ/s ratio is considered in the analysis of Gribov-Zwanziger plasma [108–110], while its criticality has been used to probe the possible endpoint of the chiral phase transition [61, 100, 111]. At present, the lattice gauge theory simulations are able to compute the bulk viscosity in pure SU(3) theory only [47, 48, 112, 113].

In contrast to the shear and bulk viscosities, the electrical conductivity σ, which quantifies the ability of an arbitrary system to conduct the electric charge, has been evaluated in lQCD, also with quarks taken into account [114–119]. Since the QGP consists of electrically charged quarks, it is meaningful to investigate the charge current in the deconfined matter to deepen the exploration of its dynamical properties.

It has been noticed that the electrical conductivity of the QGP influences the diffusion of the magnetic field in medium [120], as well as the soft dilepton emission [121] and the photon production rate [122, 123]. Along with the results from lattice gauge theory, the electrical conductivity of strongly interacting matter has been deduced from the experimental data of the non-central heavy-ion collisions, where strong electric and magnetic fields are produced [124–127]. The magnitude of the electrical conductivity is also relevant for the chiral magnetic effect, which indicates the violation of the CP-symmetry [4] in strong interactions [128].

The electrical conductivity of the deconfined matter has been examined using various methods, among which are phenomenological quasiparticle models [129–131], the Green-Kubo formalism [129, 130, 132], the DQPM [91, 101, 133], the Polyakov Quark-Meson model [102], the Anti-de Sitter/Conformal Field Theory (AdS/CFT) correspondence [134] and the Color String Percolation approach [135].

The characteristic property of the deconfined matter, considered the potentially important probe in diagnosing the QCD dynamics, is its flavor composition [136]. In this Thesis, we investigate the above-discussed transport parameters in hot QCD matter with different numbers of quark flavors: pure gluon plasma with $N_f = 0$, and the QGP consisting of gluons, light quarks (as degenerate up and down flavors), and strange quarks ($N_f = 2 + 1$). We compute the shear and bulk viscosities, as well as the electrical conductivity within kinetic theory under the relaxation time approximation (RTA) [60, 78, 137], combined with well-established quasiparticle model [80, 81, 85, 87, 101, 131, 138]. The results will be presented in Chapter 5.

Moreover, we utilize the specific shear viscosity η/s to investigate charm quark production in QGP with $N_f = 2 + 1$ quark flavors. Due to their large masses, charm quarks are expected to survive through the evolution of the deconfined matter. Hence their interactions with the QGP constituents are expected to deliver more information about the non-trivial QCD dynamics in the deconfined phase. The precise determination of transport parameters as functions of temperature and chemical potential and their incorporation into fluid dynamical simulations is one of the main steps towards understanding the evolution of strongly interacting matter.

Rozdział 2

Quasiparticle Model

In this Chapter, we introduce the concept of the quasiparticle model, whose variations have been successfully applied in previous studies of different QGP properties [83,92,101,130,131,139–141]. While some of the systematic approaches to strong interactions, such as pQCD or lattice gauge theory, are restricted to certain values of the coupling/temperature, the advantage of the phenomenological quasiparticle model is based on the possibility to aces both low- and high-temperature limits, and therefore effectively connect the non-perturbative and perturbative QCD regimes by constraining the model parameters.

The idea of quasiparticles has been widely used in strongly correlated systems [142] and solid state physics, for example, to simplify the description of the electron moving in an arbitrary (semi)conductor. One can „hide" the interactions between the electron and surrounding atoms into the medium-dependent effective mass, which in turn allows postulating that massive quasielectron moves freely in a solid state [143]. For the analysis of the deconfined matter, the notion of quasiparticles requires a reliable prescription of encoding strong interactions into the effective masses of quarks and gluons. This is achieved by making use of the expressions acquired from Hard Thermal Loop (HTL) approach, which has proved to be a crucial tool to study the (near-)equilibrium QGP properties in a systematic and gauge-independent way [144].

The HTL arose as a resummation scheme for the diagrammatic approach to QCD. It has been observed that at high temperatures, the resummation procedure is necessary to consistently account for the contributions at leading order in the coupling constant g [145]. Such contributions emerge from the one-loop diagrams (hard thermal loops), which by definition consider hard internal momentum of the order of T, and soft external momenta proportional to gT [145–147].
At high temperatures, the HTL approach supports and justifies a picture of weakly interacting massive quasiparticles, as determined by the HTL propagators [87, 148]. The earlier lQCD investigations of pure Yang-Mills theory also provided a major hint that the theory contains effectively massive gluons since at high temperature, the presence of low-momentum massive gluon modes has been pointed out [149].

2.1 Dynamical Masses

In general, the effective mass of the quasiparticles can be understood as arising from the energy contained in a strongly coupled system determined by the correlation range of the interactions [87]. As each quark and gluon propagates through the medium, it becomes dressed by the dynamically generated medium-dependent self-energy Π_i, emerging from the interactions with other QGP constituents. Mathematically speaking, the effective masses of gluons g, light l, and strange s quarks, as well as the corresponding anti-quarks, are defined in the QPM by

$$m_i^2 = \left(m_i^0\right)^2 + \Pi_i \,, \tag{2.1}$$

where we include the current particle masses m_i^0 with $m_g^0 = 0$, $m_l^0 = 5$ MeV and $m_s^0 = 95$ MeV. For Π_i we employ the asymptotic forms of the gauge independent HTL self-energies [150–152], which at $\mu_B = 0$ read

$$\Pi_g(T) = \left(3 + \frac{N_f}{2}\right) \frac{G(T)^2}{6} T^2, \tag{2.2}$$

$$\Pi_l(T) = 2\left(m_l^0 \sqrt{\frac{G(T)^2}{6} T^2} + \frac{G(T)^2}{6} T^2\right), \tag{2.3}$$

$$\Pi_s(T) = 2\left(m_s^0 \sqrt{\frac{G(T)^2}{6} T^2} + \frac{G(T)^2}{6} T^2\right), \tag{2.4}$$

where the perturbative coupling has been replaced by an effective running coupling $G(T)$, which in a high-temperature regime resembles the perturbative one for thermal momenta, $p \sim T$. To describe pure Yang-Mills thermodynamics, the above prescription is modified by setting $N_f = d_{l,\bar{l},s,\bar{s}} = 0$. Note that as an average medium effect, the dynamical masses are momentum-independent [149] while exhibiting explicit and implicit dependence on temperature.

2.2 Effective Runing Coupling

Once the interactions are accounted as guided above, a system of quasiparticles can be treated as a dilute gas of weakly interacting massive constituents. In the present QPM, the deconfined matter is described by dynamical quarks and gluons with effective masses and a residual mean field interaction which depends on the temperature [138]. The complexity of the correlations is assumed to be encoded in the quasiparticle dispersion relations, while the longitudinal plasmon and quark-hole excitations are, instead, considered to be exponentially suppressed [153].

Based on the kinetic theory, the entropy density of the deconfined matter with $N_f = 2 + 1$ at $\mu_B = 0$, is given by the sum of different quasiparticle contributions,

$$s = \sum_{i=g,l,\bar{l},s,\bar{s}} d_i \int \frac{d^3p}{(2\pi)^3} \frac{\left(\frac{4}{3}p^2 + m_i^2\right)}{E_i T} f_i^0 \,, \tag{2.5}$$

where d_i is the spin-color degeneracy factor, which explicitly depends on the number of colors $N_c = 3$ as $d_{l,\bar{l}} = 2N_cN_l = 12$ for $N_l = 2$ light (anti)quark flavors,

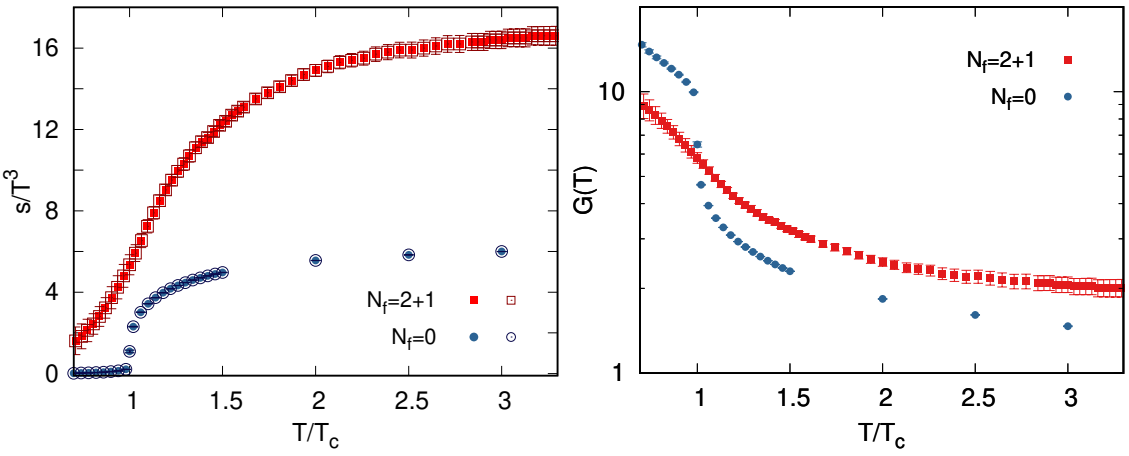

Rysunek 2.1: Left: Scaled entropy density s/T^3 as a function of scaled temperature T/T_c. The quasiparticle model results (full symbols) are shown along with the lattice gauge theory results for pure Yang-Mills theory ($N_f = 0$) [154] (open circles) and for QCD with $N_f = 2 + 1$ [155] (open squares). Following the lQCD approach, we use $T_c = 260$ MeV and $T_c = 155$ MeV for $N_f = 0$ and $N_f = 2 + 1$, respectively. Right: The corresponding effective coupling $G(T)$ as a function of scaled temperature T/T_c employed in the description of the scaled entropy density in the left panel. The errorbars highlight the estimates for the uncertainties obtained on the lattice for s/T^3 [154, 155], which are then transferred to the result for the effective coupling $G(T)$.

$d_{s,\bar{s}} = 2N_c = 6$ for strange (anti)quarks and $d_g = 2(N_c^2 - 1) = 16$ for left- plus right-handed transversal gluons [138]. The distribution function f_i^0 reads

$$f_i^0 = (\exp(E_i/T) \pm 1)^{-1}, \tag{2.6}$$

where $E_i = \sqrt{p^2 + m_i^2}$ denotes the dispersion relation (energy) of the on-shell propagating quasiparticle. The $\pm$ sign represents Fermi-Dirac $(+)$ and Bose-Einstein $(-)$ statistics in thermal equilibrium. Note that we use natural units in all of the expressions provided in this Thesis, i.e. $k_B = \hbar = c = 1$ [6].

Figure 2.1 shows our results for the scaled entropy density s/T^3 compared to state-of-the-art lattice gauge theory outcomes for pure Yang-Mills theory [154] and $N_f = 2+1$ QCD with physical quark masses [155]. The temperature dependence of the effective coupling $G(T)$ is adjusted in the QPM to describe the lattice data and accommodate non-perturbative effects near the deconfinement transition temperature T_c. The results for $G(T)$ are shown in Fig. 2.1 (right). The depicted error bars reflect possible variations in $G(T)$ due to the errors reported for the lattice data shown in the left panel of Fig. 2.1. The corresponding effective quasiparticle masses are exhibited in Fig. 2.2.

While the changes in the entropy density in Yang-Mills theory indicate a first-order phase transition, see Fig. 2.1 (left), s/T^3 is continuous for T around T_c in $N_f = 2+1$ QCD. Through the presence of dynamical quarks, the scaled entropy density is increased by about a factor $2 - 3$ in the deconfined phase. This is reflected in the behavior of the effective coupling $G(T)$, see Fig. 2.1 (right). Except for $T \lesssim T_c$,

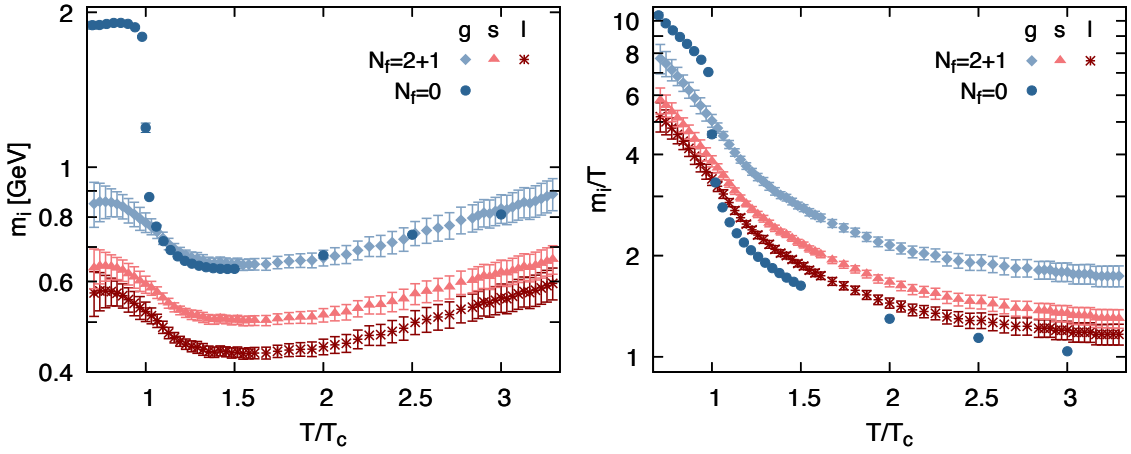

Rysunek 2.2: The effective mass $m_i(T)$ (left) and the effective mass scaled with temperature m_i/T (right) as a function of T/T_c for different quasiparticle species. In both panels, the same symbols stand for gluons (diamonds), strange (triangles), and light (stars) quarks in QCD with $N_f = 2+1$, while circles represent the dynamical masses of gluons in pure Yang-Mill theory.

where the effective coupling and, thus, the gluon quasiparticle mass must become large to describe the sudden drop in the Yang-Mills entropy density, $G(T)$ is larger for QCD than for Yang-Mills theory. Moreover, at larger T, both couplings exhibit comparable slopes. This is in line with the perturbatively expected behavior of the β-function and its N_f-dependence [138].

The QPM is capable of describing the lattice data for s/T^3 with the effective coupling $G(T)$ and the corresponding temperature-dependent masses calculated via Eq. (2.1) and shown in Fig. 2.2. For $N_f = 0$, an abrupt change in the effective gluon mass near T_c is responsible for describing a jump in the entropy density at the first-order phase transition. For $N_f = 2+1$, the temperature profile of $G(T)$ becomes much milder and smoother at any temperature, which then influences the behavior of the effective masses in full QCD. While m_i/T at high T vanishes logarithmically in line with the perturbative coupling for $p \sim T$, (see right panel of Fig. 2.2), $m_i(T)$ itself (left panel) rises approximately linearly with T in this regime, exhibits a minimum somewhat above T_c, and becomes large near T_c. Similar behavior has been observed in former studies for SU(2) [156] and SU(3) [157] theories. In the left panel of Fig. 2.2, when plotted as a function of T/T_c, the gluon effective mass is found to be comparable for Yang-Mills theory and QCD. The apparent N_f-independence in the shown temperature interval is a consequence of the compensation of two effects, the N_f-dependence in the dynamically generated gluon self-energy $\Pi_g(T)$ in Eq. (2.2), including the behavior of $G(T)$, and the N_f-dependence of the (pseudo-)critical temperature.

For the main scope of this Thesis, we adopt the effective coupling $G(T)$ shown in Fig. 2.1, additionally justifying its validity by computing the speed of sound squared, c_s^2, which contains the coupling's derivative. However, to ensure the thermodynamic consistency, broken by the medium-dependent dispersion relations [158], evaluating the thermodynamic quantities at $\mu_B = 0$, one has to introduce the

temperature-dependent bag function, $B(T)$. The latter will provide an additional medium dependence, through which all thermodynamic quantities will reproduce the ideal gas formulas [87, 101, 159].

2.3 Speed of Sound

The speed of sound squared can be obtained from the entropy density expressed as a function of temperature via

$$c_s^2 = \frac{s}{T}\left(\frac{\partial s}{\partial T}\right)^{-1}, \tag{2.7}$$

with the entropy density defined by Eq. (2.5). The results are presented in Fig. 2.3 for pure Yang-Mills theory (left) and for QCD with $N_f = 2+1$ (right).

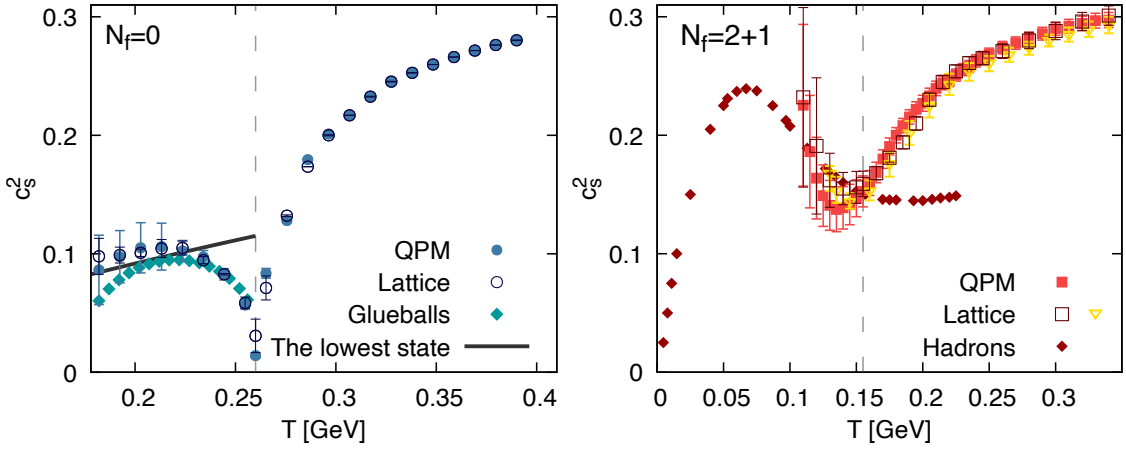

Rysunek 2.3: Speed of sound squared as a function of temperature. Left: The result for pure Yang-Mills theory obtained in the quasiparticle model (full circles) is compared with c_s^2 deduced from the lattice data [154] (open circles), from the glueball resonance gas with the Hagedorn spectrum [154,160] (diamonds), and from the ideal gas of the lowest glueball [161, 162] (solid line). Right: The same quantity but for $N_f = 2+1$ (full squares), in comparison to the corresponding result of the lattice QCD simulations by [155] (open squares) and [163] (triangles) and to the hadron resonance gas with the states below 2.5 GeV [161, 162] (diamonds). The dashed vertical lines indicate both theories' (pseudo)critical temperatures.

In the left panel, one readily finds that the speed of sound squared of the gluon plasma in the QPM is in excellent agreement, both in confined and deconfined phases, with the results deduced from the lattice data for the pressure and energy density in pure Yang-Mills theory [154]. This arises from the effective running coupling $G(T)$ defined with the entropy density in the same lattice setup.

It is also instructive to compare the QPM outcome with the model for a glueball resonance gas (GRG), which can be done with the parametric form for the

entropy density suggested in [154],

$$\frac{s_{\rm conf}(T)}{T^3} = \Big(-0.2\frac{T}{T_c} - 0.134\,F(T)\Big), \tag{2.8}$$

$$F(T) = \log\Big[1.024 - \frac{T}{T_c}\Big]. \tag{2.9}$$

The above parameterization includes the contribution from the GRG beyond the two-particle threshold, i.e., considering the Hagedorn density of states [160]. The resultant c_s^2 is found easily as

$$c_s^2 = \frac{(1.024\,T_c - T)\Big(0.2\frac{T}{T_c} + 0.134\,F(T)\Big)}{(0.412\,T_c - 0.402\,T)F(T) + T\Big(0.686 - 0.8\frac{T}{T_c}\Big)}, \tag{2.10}$$

which well captures the behavior near T_c as seen in Fig. 2.3.

As a useful reference, one takes a simple model for an ideal bosonic gas, including only the lowest glueball. The speed of sound squared is calculated analytically as in the form [161, 162]

$$c_s^2 = \Big(3 + \frac{m_0^2 K_2(m_0/T)}{4T^2 K_2(m_0/T) + m_0 T K_1(m_0/T)}\Big)^{-1}, \tag{2.11}$$

where $K_{1,2}$ are the modified Bessel functions of the second kind. The parameter m_0 denotes the glueball mass, and we take $m_0 = 2$ GeV. The comparison with the GRG and the QPM approaches, as well as with lattice results, clearly illustrates that it is insufficient to describe the thermodynamics near T_c with the lowest state only, and Eq. (2.11) fails even qualitatively although it describes the c_s^2 better at lower temperature.

In Fig. 2.3 (right), we present the c_s^2 of the QGP with $N_f = 2 + 1$ quark flavors, computed in the QPM and hadron resonance gas (HRG) model, as well as in lattice QCD. Within the errors, the overall behavior of the QPM result is fairly consistent with lattice QCD [155, 163]. The HRG model [161] describes the c_s^2 relatively well near the crossover, and an apparent deviation from the lattice data emerges just above T_c, indicating that the hadronic picture of the QCD thermodynamics breaks down.

The c_s^2 exhibits a non-monotonicity around the corresponding T_c in the two theories, whereas this behavior is much more robust in pure Yang-Mills theory. This observation is linked to the rapid change of the entropy density as a function of temperature at the first-order phase transition. At higher temperatures, the c_s^2 approaches the Stefan-Boltzmann limit, $c_s^2 = 1/3$. Related to that, in Section 5.3, we will explore how the system recovers its conformality depending on the number of quark flavors.

We have explicitly demonstrated that the QPM captures the non-perturbative properties of the bulk thermodynamic quantities not only in the deconfined phase but also somewhat below T_c in pure Yang-Mills theory and full QCD with dynamical quarks. However, we emphasize that such an agreement with the hadronic picture in

the confined phase would not be expected for transport coefficients since they carry the details of kinematics with entirely different constituents, i.e., hadrons versus quarks and gluons.

Rozdział 3

Relativistic Hydrodynamics

Before proceeding to the kinetic theory framework used in our research, we would like to illustrate how transport parameters, such as shear and bulk viscosity, emerge in relativistic viscous hydrodynamics. We start with the idealized case of perfect fluid [6] and then introduce the dissipative processes considered in viscous media [10].

3.1 Ideal Hydrodynamics

The essential building block of the hydrodynamic equations is the conservation of the energy-momentum (stress-energy) tensor $T^{\mu\nu}$, given by [6, 10, 93, 94],

$$\partial_\mu T^{\mu\nu} = 0. \tag{3.1}$$

For perfect fluid in global equilibrium, $T^{\mu\nu}$ is defined as

$$T_0^{\mu\nu} = \Big[(\epsilon + P)u^\mu u^\nu - P g^{\mu\nu}\Big] = \epsilon\, u^\mu u^\nu - P\Delta^{\mu\nu}, \tag{3.2}$$

where ϵ and P stand for the energy density and isotropic pressure, respectively, defined in the local rest frame (LRF) of the fluid element [6]. The u^μ denotes the four-velocity (flow vector) of the fluid, which in LRF reads $u^\mu = (1, \vec{0})$, while $g^{\mu\nu} = \mathrm{diag}(1, -1, -1, -1)$ is the metric tensor and $\Delta^{\mu\nu} = g^{\mu\nu} - u^\mu u^\nu$ is the operator, projecting onto the space orthogonal to u^μ.

Further, in local equilibrium, the stress-energy tensor of a perfect fluid is obtained by postulating that ϵ and u^μ depend on the spatial coordinate x [10],

$$T_0^{\mu\nu}(x) = \epsilon(x)\, u^\mu(x) u^\nu(x) - P(\epsilon(x))\Delta^{\mu\nu}(x). \tag{3.3}$$

Here, along with the flow vector $u^\mu(x)$, another primary fluid variable is the local temperature $T(x)$. The relativistic energy-momentum tensor of a perfect fluid is the most general symmetric tensor, which becomes independent of any derivatives, once it is expressed in terms of $u^\mu(x)$ and $T(x)$ [10].

From the stress-energy tensor $T^{\mu\nu}$ given by Eq. (3.2), and the conservation law from Eq. (3.1), one can directly obtain the entropy density conservation equation [6, 10],

$$u^\mu \partial_\mu s = 0. \tag{3.4}$$

However, to solve the equations of motion of a perfect fluid, in addition to the above equations, the equation of state (EoS) of the system should be known, e.g., pressure as a function of the energy density, $P(\epsilon)$.

Perfect fluid dynamics holds in the limit of local thermal equilibrium, meaning that the mean free path, i.e., the distance a particle travels freely between two nearest scatterings, is sufficiently small. When this condition is violated, the system starts to deviate from local thermodynamic equilibrium, resulting in a set of dissipative effects. Those occur due to the irreversible transfer of momentum (and charge) from one part of the system to another, naturally leading to the extension of the framework to viscous hydrodynamics.

3.2 Viscous Hydrodynamics

The dissipative processes reflecting the thermodynamic irreversibility of motion are the characteristic features of any fluid in nature. Due to the presence of inner friction (viscosity) and, eventually, thermal conduction between the fluid elements, a reasonable description of the relativistic fluid requires careful consideration of these phenomena.

For a viscous medium, the energy-momentum tensor is usually expressed as a linear combination of the tensor shown in Eq. (3.2) and an additional, dissipative term, resulting into [164, 165]

$$T^{\mu\nu} = T_0^{\mu\nu} + \Pi^{\mu\nu}, \tag{3.5}$$

where the viscous $\Pi^{\mu\nu}$ component is usually defined, in the absence of any charges, as a sum of the shear stress tensor $\pi^{\mu\nu}$ and the bulk pressure Π [10, 166],

$$\Pi^{\mu\nu} = \pi^{\mu\nu} + \Pi\Delta^{\mu\nu}. \tag{3.6}$$

Further, the shear stress tensor reads

$$\pi^{\mu\nu} = 2\eta\sigma^{\mu\nu}, \tag{3.7}$$

with the shear viscosity coefficient η and the shear flow tensor

$$\sigma^{\mu\nu} = 2\Delta^{\mu\nu}_{\alpha\beta}\partial^{\alpha}u^{\beta}. \tag{3.8}$$

Above, $\Delta^{\mu\nu}_{\alpha\beta}$ is the projection operator of the form [10, 83]

$$\Delta^{\mu\nu}_{\alpha\beta} = \frac{1}{2}(\Delta^{\mu}{}_{\alpha}\Delta^{\mu}{}_{\beta} + \Delta^{\nu}{}_{\alpha}\Delta^{\nu}{}_{\beta}) - \frac{1}{3}\Delta^{\mu\nu}\Delta_{\alpha\beta}. \tag{3.9}$$

The bulk pressure Π, which enters Eq. (3.6) is defined as the first-order divergence of the flow vector [10],

$$\Pi = -\zeta\partial_{\mu}u^{\mu}, \tag{3.10}$$

introducing the bulk viscosity coefficient ζ. Investigation of the temperature and flavor dependence of the shear and bulk viscosities in hot QCD is a primary goal of

this research.

We emphasize that for conformal fluids, whose EoS obeys $\epsilon = 3P$, the trace of the energy-momentum tensor vanishes, leading to $\Pi = 0$. As a straightforward consequence, the bulk viscosity also vanishes in conformally invariant systems, $\zeta = 0$ [167]. In Section 5.3, we will employ our results for the bulk viscosity to study how hot QCD matter approaches the conformal limit, depending on the considered number of quark flavors.

One can show that through the definitions provided by Eqs. (3.7) and (3.10), the second law of thermodynamics is automatically satisfied [168], $\partial_\mu \mathcal{S}^\mu > 0$, with $\mathcal{S}^\mu$ representing the entropy four-current. With this assumption, supplemented by the conservation equations, one obtains the hydrodynamic framework known as the relativistic Navier-Stokes theory.

Using the formulation of Navier-Stockes hydrodynamics, and assuming that the EoS of the medium is known, the transport coefficients can be directly obtained from Green-Kubo relations [58, 169], by computing the correlation functions of the energy-momentum tensor provided in Eq. (3.5). This is considered one of the main approaches to transport properties of the QCD matter [98, 103, 104, 129, 130, 132].

The relativistic hydrodynamics specified in Navier-Stokes theory develops, however, a series of issues connected to linear instabilities around equilibrium and the acausal transmission of signals [170–172]. To fix such conceptual difficulties, Israel and Stewart developed a second-order hydrodynamic formalism [168,173], which appears to be the most popular framework used in the contemporary studies of the relativistic fluid dynamics [38, 174–178].

Rozdział 4

Kinetic Theory

The kinetic theory describes the macroscopic properties of the system in terms of its microscopic structure, as we have already seen in the definition of the entropy density given by Eq. (2.5). Therefore, the equilibrium thermodynamic quantities are defined in the QPM as standard phase-space integrals over the thermal distribution functions of dynamical quarks and gluons, which obey medium-dependent dispersion relations. The thermodynamic integrals are dominated by excitations with thermal momenta $p \sim T$.

In QCD with $N_f = 2 + 1$, for a medium composed of quasiparticles, the energy-momentum tensor in local thermal equilibrium reads [61, 80]

$$T_0^{\mu\nu} = \sum_{i=g,l,\bar{l},s,\bar{s}} d_i \int \frac{d^3p}{(2\pi)^3} \frac{p^\mu p^\nu}{E_i} f_i^0, \tag{4.1}$$

where the sum runs over different quasiparticle species carrying the four-momenta of the general form $p^\mu = (E, \vec{p})$. The distribution function f_i^0 for fermions or bosons is given by Eq. (2.6), with the temperature-dependent quasiparticle energy E_i and degeneracy factors d_i. In pure Yang-Mills theory, the expression for $T_0^{\mu\nu}$ naturally reduces to the gluon term, applying the corresponding effective coupling for $N_f = 0$. A more sophisticated form of the energy-momentum tensor can be found in [81], where it also incorporates the mean field term depending on the quasiparticle self-energy.

The transport parameters are always related to the dissipative phenomena occurring in non-equilibrated systems. Therefore we now postulate that the deconfined matter appears slightly out of equilibrium, which implies that the quasiparticle distribution function also deviates from its equilibrium value f_i^0 by the infinitesimal change δf_i,

$$f_i = f_i^0 + \delta f_i, \tag{4.2}$$

where f_i denotes the non-equilibrium value of the statistics.

It straightforwardly follows from the above assumption that the stress-energy tensor also departs from equilibrium, reading

$$T^{\mu\nu}(f_i) = T_0^{\mu\nu}(f_i^0) + \delta T^{\mu\nu}(\delta f_i), \tag{4.3}$$

where $\delta T^{\mu\nu}(\delta f_i)$ considers the dissipative processes quantified by different dynamical and transport coefficients. The δf_i can be obtained from the Boltzmann equation discussed in the next section.

4.1 Boltzmann Equation

For each quasiparticle species i with medium-dependent dispersion relation, the Boltzmann kinetic transport equation is defined as

$$\left(p_i^\mu \partial_\mu + m_i F_i^\mu \partial_{p_i^\mu}\right) f_i = \mathcal{C}_i[\{f_i\}]\,. \tag{4.4}$$

The second term on the left-hand side (LHS) contains an external force on the quasiparticles, $F_i^\mu = \partial^\mu m_i$ with $p_{i,\mu} F_i^\mu = 0$, induced by the residual mean field interaction as a consequence of the temperature-dependent effective mass [81]. This term can be neglected for simplicity, however it is essential when making contact between the kinetic theory description and fluid dynamics discussed in Chapter 3, by defining a covariantly conserved energy-momentum tensor from which transport coefficients can be determined [179].

Since we consider the system to be out of but near the local thermal equilibrium, it allows us to expand the Boltzmann equation around its equilibrium solution f_i^0, such that the LHS of Eq. (4.4) can be written in terms of gradients of the thermodynamic variables. The collision operator $\mathcal{C}_i[\{f_i\}]$ is taken as linearized in the deviation $\delta f_i = f_i - f_i^0$ from equilibrium. Assuming that the distribution function f_i relaxes to its equilibrium value f_i^0 in the time interval τ, the collision term in the relaxation time approximation (RTA) takes the form [180]

$$\mathcal{C}_i[\{f_i\}] = -\frac{p_i^\mu u_\mu}{\tau_i}\delta f_i\,, \tag{4.5}$$

where τ_i is the relaxation time for species i in the presence of other quasiparticles. We recall that in the LRF of the fluid, $u_\mu = (1, \vec{0})$.

In the simplified RTA, neglecting the external force entering Eq. (4.4), one can find the explicit form of the leading-order deviation of the energy-momentum tensor from local thermal equilibrium [80],

$$\delta T^{\mu\nu} = -\sum_{i=g,l,\bar{l},s,\bar{s}} d_i \int \frac{d^3p}{(2\pi)^3}\frac{p^\mu p^\nu}{E_i^2} p^\alpha \partial_\alpha[\tau_i f_i^0], \tag{4.6}$$

which depends on the relaxation times τ_i of the quasiparticles. A more complex structure of $\delta T^{\mu\nu}$ can be found in [81–84], with the mean field interaction term taken into account.

The transport parameters of the deconfined matter can be derived by collecting Eqs. (4.3) and (4.6), and matching the out-of-equilibrium kinetic expression for $T^{\mu\nu}$ with its corresponding definition in fluid dynamics, see Eqs. (3.5)-(3.10). The step-by-step derivation can be found in [131] for the electrical conductivity σ, and in [78, 80, 81] for the shear η and bulk ζ viscosities. However, final expressions differ from each other, depending on the consideration/neglection of the mean field interaction term. We will provide the formulas employed in the QPM at the beginning of the corresponding sections. See η in Eq. (5.1), ζ in Eq. (5.5), as well as σ in Eq. (5.12).

Essentially, the Boltzmann equation provides a complete description of the microscopic dynamics only for systems in the dilute regime, whereas a precise examination of the high-density fluids requires higher-order corrections. Therefore, the distribution functions exhibit small fluctuations and tend to restore their equilibrium values exponentially.

The RTA is valid in a diluted system, i.e., when the mean free path λ is greater than the average interparticle distance d [60, 181],

$$\lambda \sim \tau \gg d \sim n^{-1/3}, \tag{4.7}$$

where n is the total particle number density of the system. In the QPM, we find that at T_c in pure Yang-Mills theory, $\tau \sim 0.4$ fm and $d \sim 10^{-4}$ fm. When the temperature reaches 3 T_c, the relaxation time remains of the same order, whereas the average distance between the quasiparticles decreases to the order of 10^{-6} fm. Thus, the condition, $\tau \gg d$, is satisfied in the range of temperatures considered in this Thesis. Similar numbers satisfying the requirement are also found in QCD with $N_f = 2+1$.

Once the validity region of the RTA is cross-checked, we proceed with the computation of the relaxation times τ_i, which need to be evaluated to obtain the resulting transport parameters.

4.2 Relaxation Time Computation

In various approaches based on the kinetic theory, the momentum-averaged form of the relaxation time (or the mean free path) is commonly used to conveniently estimate the interactions between the system's constituents [60, 61, 78, 139, 181, 182]. In the original relaxation time approximation utilized in our model [183], the relaxation time τ is also introduced as a mean. However, depending on the microscopic dynamics of the theory, τ can exhibit a strong momentum dependence which results in extremely different values of transport coefficients [85]. Nevertheless, we assume that the momentum-averaged relaxation time gives a correct order of magnitude of the transport parameters investigated in the present quasiparticle approach [184].

In general, the relaxation time is inversely related to the number density of scattering partners and the corresponding scattering cross section, which for a multicomponent system follows in a matrix form as $\hat{\tau}^{-1} = \hat{n}\hat{\bar{\sigma}}$ [180]. For QCD with $2+1$ quark flavors, this explicitly reads

$$\begin{pmatrix} \tau_l^{-1} \\ \tau_{\bar{l}}^{-1} \\ \tau_s^{-1} \\ \tau_{\bar{s}}^{-1} \\ \tau_g^{-1} \end{pmatrix} = \begin{pmatrix} \bar{\sigma}_{ll} & \bar{\sigma}_{l\bar{l}} & \bar{\sigma}_{ls} & \bar{\sigma}_{l\bar{s}} & \bar{\sigma}_{lg} \\ \bar{\sigma}_{\bar{l}l} & \bar{\sigma}_{\bar{l}\bar{l}} & \bar{\sigma}_{\bar{l}s} & \bar{\sigma}_{\bar{l}\bar{s}} & \bar{\sigma}_{\bar{l}g} \\ \bar{\sigma}_{sl} & \bar{\sigma}_{s\bar{l}} & \bar{\sigma}_{ss} & \bar{\sigma}_{s\bar{s}} & \bar{\sigma}_{sg} \\ \bar{\sigma}_{\bar{s}l} & \bar{\sigma}_{\bar{s}\bar{l}} & \bar{\sigma}_{\bar{s}s} & \bar{\sigma}_{\bar{s}\bar{s}} & \bar{\sigma}_{\bar{s}g} \\ \bar{\sigma}_{gl} & \bar{\sigma}_{g\bar{l}} & \bar{\sigma}_{gs} & \bar{\sigma}_{g\bar{s}} & \bar{\sigma}_{gg} \end{pmatrix} \begin{pmatrix} n_l^0 \\ n_{\bar{l}}^0 \\ n_s^0 \\ n_{\bar{s}}^0 \\ n_g^0 \end{pmatrix}, \tag{4.8}$$

where

$$n_i^0 = d_i \int \frac{d^3p}{(2\pi)^3} f_i^0 \tag{4.9}$$

is the T-dependent particle number density of the quasiparticle species i in equilibrium. As mentioned previously, τ_i generally depends on the energy E_i of the

quasiparticle, while we approximate τ_i by its mean value, using the energy-averaged cross sections $\bar{\sigma}_{ij}$ discussed below.

From Eq. (4.8), one finds the explicit form of the relaxation time for light quarks,

$$\tau_l^{-1} = \frac{n_l^0}{2}\Big[\bar{\sigma}_{ud\to ud} + \bar{\sigma}_{uu\to uu}\Big] + n_s^0\bar{\sigma}_{us\to us} + n_{\bar{s}}^0\bar{\sigma}_{u\bar{s}\to u\bar{s}}$$
$$+ \frac{n_{\bar{l}}^0}{2}\Big[\bar{\sigma}_{u\bar{u}\to u\bar{u}} + \bar{\sigma}_{u\bar{u}\to d\bar{d}} + \bar{\sigma}_{u\bar{u}\to s\bar{s}} + \bar{\sigma}_{u\bar{u}\to gg} + \bar{\sigma}_{ud\to ud}\Big] + n_g^0\bar{\sigma}_{ug\to ug}, \tag{4.10}$$

or for gluons

$$\tau_g^{-1} = n_l^0\,\bar{\sigma}_{gu\to gu} + n_{\bar{l}}^0\,\bar{\sigma}_{g\bar{u}\to g\bar{u}} + n_s^0\,\bar{\sigma}_{gs\to gs} + n_{\bar{s}}^0\,\bar{\sigma}_{g\bar{s}\to g\bar{s}}$$
$$+ n_g^0[\bar{\sigma}_{gg\to gg} + \bar{\sigma}_{gg\to u\bar{u}} + \bar{\sigma}_{gg\to d\bar{d}} + \bar{\sigma}_{gg\to s\bar{s}}]. \tag{4.11}$$

Note that in pure Yang-Mills theory, we have only $\tau_g^{-1} = n_g^0\bar{\sigma}_{gg\to gg}$. The above-presented scheme is general and has also been used in [78, 92, 185, 186] to evaluate the relaxation times. However, other models involve cross sections different from that used in our quasiparticle approach. We also note that the relaxation time defined above is independent of momentum since it is introduced as a mean. However, with given scattering amplitudes, one can evaluate the momentum-dependent relaxation times, including inelastic collisions as instructed in [85].

The individual energy-averaged cross sections for the binary scattering processes in the medium are given by [60]

$$\overline{\sigma}_{12\to 34}(T) = \int_{s_{\rm th}}^{\infty} ds \int_{t_{\rm min}}^{t_{\rm max}} dt\, \frac{d\sigma_{12\to 34}}{dt}(s,t;T)$$
$$\times \sin^2\theta(s,t;T)(1\pm f_3^0)(1\pm f_4^0)P(s;T)\,. \tag{4.12}$$

We note that $\bar{\sigma}$ depends on T both explicitly via the equilibrium distribution functions $f_i^0(s;T)$ and implicitly via $G(T)$ and $m_{i=1\ldots4}(T)$. In writing Eq. (4.12) we have assumed that the center-of-mass (c.m.) of the system is at rest in the medium, such that all entering quantities can be expressed in terms of the Mandelstam variables s, t, and u, defined in Appendix A. Taking into account the possible phase-space occupation in the final state, the factors $(1\pm f_i^0)$ represent the in-medium effects on the cross sections, corresponding to Bose enhancement (for gluons) or Pauli blocking (for quarks and antiquarks). The integration limits in the four-momentum transfer, $t_{\rm min}$ and $t_{\rm max}$, are determined from the condition $-1 \leqslant \cos\theta \leqslant 1$, where θ is the scattering angle, while $s_{\rm th} = \max[(m_1+m_2)^2, (m_3+m_4)^2]$.

Further, following [60, 61, 181], we include into Eq. (4.12) the phenomenological weight-factor $\sin^2\theta$ signaling the dominance of large angle scatterings for the momentum transfer. This procedure is known as the large angle scattering (LAS) assumption, and $\overline{\sigma}_{12\to 34}(T)$ is the so-called transport cross section, relevant for the viscosity coefficients [187]. Although the small angle scatterings prevail in the deconfined matter, they are not sufficient to transport the momenta of order $p \sim T$, typical for relativistic fluids [59]. Since the transport cross section is reduced in comparison to the isotropic one [60], it results in an increase in the relaxation time. We

will come back to this issue in Section 5.1 by illustrating how LAS assumption affects the shear viscosity coefficient, see Fig. 5.3. The exact computation of the $\sin^2\theta$ for different scatterings can be found in Appendix B.

Finally, $P(s;T)$ in Eq. (4.12) denotes the probability of finding a pair (3 4) in the final state with c.m. energy squared s,

$$P(s;T) = C\sqrt{(s-m_1^2-m_2^2)^2-4m_1^2m_2^2}\, f_3^0\, f_4^0 v_{\rm rel}(s;T)\,,$$

where the normalization constant C is fixed via

$$\int_{s_{\rm th}}^{\infty} ds\; P(s;T) = 1, \tag{4.13}$$

and $v_{\rm rel}(s;T)$ is the relative velocity between the two initial quasiparticles

$$v_{\rm rel}(s;T) = \frac{2s\sqrt{(s-m_1^2-m_2^2)^2-4m_1^2m_2^2}}{s^2-(m_1^2-m_2^2)^2}\,. \tag{4.14}$$

The differential cross section $d\sigma/dt$ for the process $(1,2)\to(3,4)$ entering Eq. (4.12) is obtained from the corresponding total scattering amplitude squared $|\mathcal{M}|^2$ via

$$\frac{d\sigma_{12\to34}}{dt}(s,t;T) = \frac{1}{16\pi((s-m_1^2-m_2^2)^2-4m_1^2m_2^2)}|\mathcal{M}_{12\to34}|^2(s,t;T). \tag{4.15}$$

In $|\mathcal{M}|^2$, we sum over the spin/polarization and color d.o.f. in the final state and, since the degeneracy factors d_i are included already in Eqs. (5.1) and (4.8), average over the initial state. The individual amplitudes are computed perturbatively at tree level for the elementary two-body scattering processes $qq\to qq$, $qq'\to qq'$, $q\bar{q}\to q\bar{q}$, $q\bar{q}'\to q\bar{q}'$, $\bar{q}\bar{q}\to\bar{q}\bar{q}$, $gg\to gg$, $q\bar{q}\to q'\bar{q}'$, $q\bar{q}\to gg$ and $gg\to q\bar{q}$ among the massive quasiparticles, where $q=u,d,s$ and also exchanged gluons obey Eq. (2.1). It would be interesting to study the temperature dependence of the transport parameters when the cross sections include higher-order corrections or when more inelastic processes, e.g., $g\to gg$, $gg\to ggg$, are considered.

The (anti)quark and gluon propagators, suppressing color indices, are modified in the QPM, respectively, as

$$\frac{i}{\not{p}-m_{l,\bar{l},s,\bar{s}}} \quad\text{and}\quad \frac{-ig^{\mu\nu}}{p^2-m_g^2}. \tag{4.16}$$

The exchanged gluon is dressed by interactions with the medium. Therefore by expressing the gluon propagator in the Feynman gauge, we directly enforce the on-shellness condition for the quasiparticles in the QGP. For the coupling, we employ the effective coupling $G(T)$ shown in Fig. 2.1. As a useful example, in Appendix A, we provide the step-by-step calculation of some scattering amplitudes for scatterings of massive particles. We note that in the limit of $m_{i=1\ldots4}\to 0$, our analytic expressions for all the differential cross sections $d\sigma/dt$ agree with those presented in [4, 185, 188].

With the above-described setup, we compute the relaxation times τ_i in pure Yang-Mills theory and QCD for $N_f = 2+1$. The corresponding results as functions of T/T_c

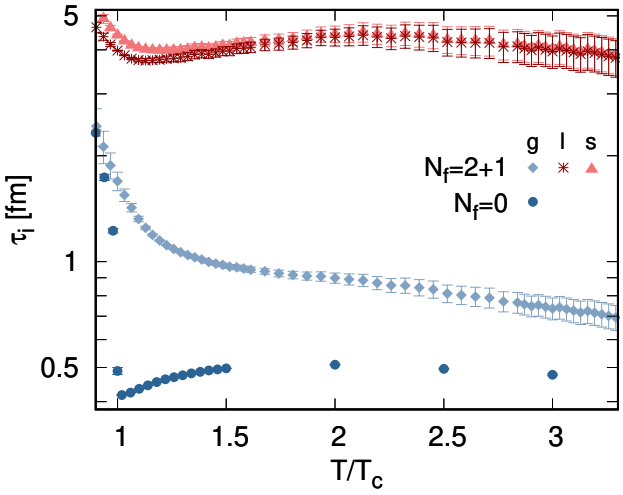

Rysunek 4.1: The relaxation time τ_i as a function of the scaled temperature T/T_c for different quasiparticle species. Pure Yang-Mills theory result for τ_g (circles) is presented along with the results in $N_f = 2+1$ QCD, with diamonds showing gluons, stars representing light quarks, and triangles standing for strange quarks. The QCD results shown for τ_l and τ_g are obtained via Eqs. (4.10) and (4.11), respectively.

are exhibited in Fig. 4.1. In pure Yang-Mills theory, τ_g exhibits a sharp minimum around T_c and a shallow maximum for about $2T_c$ before slowly decreasing with increasing temperature. The pronounced non-monotonicity near T_c is caused by the behavior of the QPM coupling $G(T)$.

A qualitatively similar observation can be made for light and strange quarks in QCD. However, τ_l and τ_s are an order of magnitude larger, and both extrema are smooth (via the smooth coupling behavior in the vicinity of the QCD crossover) and shifted towards slightly higher temperatures. Moreover, one observes that the current quark mass m_i^0 plays a considerable role only for $T < 1.5\,T_c$. In contrast, τ_g in QCD remains a monotonically decreasing function of T/T_c that is roughly a factor $4-5$ smaller than $\tau_{l,s}$. In the next Chapter, we will see that all transport parameters discussed in this Thesis directly depend on the relaxation times of the quasiparticles. Therefore, it is clear that the main contribution to them will stem from the quark and antiquark sectors. Furthermore, the increase of τ_g from pure Yang-Mills theory to QCD highlights the impact of dynamical quarks in the QGP on the effectiveness of gluons at equilibrating the momentum degradations.

Our major assumption in this study is that all the transport parameters for a given particle species carry a common relaxation time. Each parameter is characterized by a particular dissipative phenomenon formed in the viscous fluid, thus, the corresponding relaxation times are, in general, different. The shear viscosity emerges at the longitudinal fluid motion; hence it is sensitive to the changes in the transverse momentum density, which are carried on the microscopic level by the elastic binary scattering processes included in Eq. (4.8). The bulk viscosity, on the other hand, characterizes the diffusion of the particles during a uniform expansion of the medium, therefore its relaxation time essentially depends on the inelastic collisions changing the number density of the excitations [189]. In this context, within a scalar field theory [104], response functions of the energy-momentum tensor have been

carefully examined to derive the shear and bulk relaxation times. Further, electrical conductivity measures the transfer of the electric charge separately from the momentum transfer, therefore resulting in a different relaxation time from those for the shear and bulk viscosities. We will not take those complications into account and will proceed with the computations of a set of transport parameters employing the relaxation times τ_i presented in Fig. 4.1, aiming to clarify the dynamical role of the quasiquarks in the QGP.

Rozdział 5

Transport Parameters in Relaxation Time Approximation

As discussed in Section 1.2, the hot QCD medium has unique transport properties which can help to identify the dynamics of the matter produced at the early stages of the heavy ion collisions. In this chapter, we discuss the role of transport parameters, such as shear and bulk viscosity, as well as electrical conductivity, in the evolution of the deconfined matter with different numbers of quark flavors. The results in pure Yang-Mills theory will be juxtaposed to that in QCD with $N_f = 2 + 1$ to investigate the impact of dynamical quarks and gluons onto the transport coefficients. In addition, we will compare our results with the alternative QCD approaches, such as lattice gauge theory, AdS/CFT, or perturbative QCD calculations.

5.1 Shear Viscosity

We study the temperature and flavor dependence of the specific shear viscosity of strongly interacting matter in a framework with quasiparticle d.o.f. presented in Chapter 2.

In kinetic theory for the QGP with $N_f = 2 + 1$, the shear viscosity is defined as [78–81, 85, 179]

$$\eta = \frac{1}{15T} \sum_{i=g,l,\bar{l},s,\bar{s}} \int \frac{d^3p}{(2\pi)^3} \frac{\vec{p}^4}{E_i^2} \, d_i \, \tau_i \, f_i^0 (1 \pm f_i^0). \tag{5.1}$$

The upper (lower) sign corresponds to Fermi-Dirac (Bose-Einstein) statistics f_i^0 given by Eq. (2.6). We recall that E_i is the temperature-dependent dispersion relation, d_i is the degeneracy factor, both defined as for Eq. (2.5), and τ_i is the relaxation time shown in Fig. 4.1 for each quasiparticle species.

It is clear that at vanishing baryon chemical potential, $\mu_B = 0$, the contributions of quarks and antiquarks become equal, thus in QCD, Eq. (5.1) can be rewritten as

$$\eta = \eta_g + 2(\eta_l + \eta_s), \tag{5.2}$$

while in pure Yang-Mills theory we have $\eta = \eta_g$, applying the appropriate effective coupling.

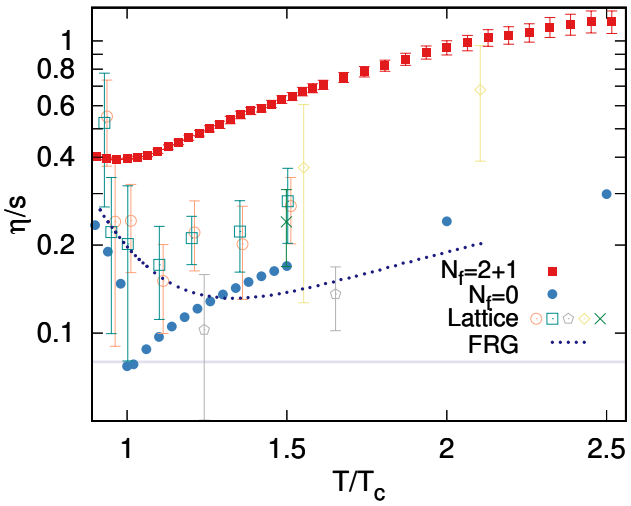

Rysunek 5.1: Shear viscosity to entropy density ratio as a function of T/T_c for pure Yang-Mills theory in the quasiparticle model (full circles) and QCD with $N_f = 2 + 1$ (full squares). For comparison, the corresponding lattice gauge theory results from [46] (open circles and open squares), [47] (pentagons), [48] (diamonds), and [53] (cross) are shown. The dotted line indicates the parametric representation of the results from the functional diagrammatic approach (FRG) [57], while the horizontal solid line represents the KSS-bound of $1/4\pi$ [35].

Following the general trend, we present numerical results in the form of the specific shear viscosity to entropy density ratio, η/s. This allows us to systematically compare the QPM outcomes in both theories, as well as to juxtapose them with the other approaches, such as lattice gauge theory, perturbative QCD calculations, or a variety of effective models. Furthermore, thanks to the additivity of the transport parameters, we carefully analyze the individual contributions coming from each quasiparticle sector. This part of the research lies at the center of our efforts and helps to understand the impact of the dynamical quarks and gluons on the properties of hot QCD matter with different quark content.

In Fig. 5.1, we show the temperature dependence of the shear viscosity to entropy density ratio for pure Yang-Mills theory. The ratio exhibits an abrupt, non-monotonic change in its behavior around the first-order phase transition, with a pronounced minimum at T_c and a mild, monotonic increase for larger T. This behavior can be traced back to the effective coupling $G(T)$ and the entropy density $s(T)$. It is an intriguing observation that the minimum of the specific shear viscosity reaches the KSS lower bound of $1/4\pi$, without any fine-tuning of the relaxation time τ_g, as it was, for example, done in [71]. We further compare our results with available data from lattice gauge theory calculations [46–48, 53] and with the results from employing the gluon spectral function in the functional diagrammatic approach [57]. Overall, our results agree remarkably with the bulk of information collected from the first-principle approaches. The global behavior found in [57] is within the reported errors well captured by our model in a wide range of temperatures, in particular for T above $1.3\,T_c$, see the dotted line in Fig. 5.1 for a parametric representation. However, near the critical temperature, we find a significantly stronger non-monotonicity with a minimal η/s around T_c instead of slightly above T_c as a natural consequence of

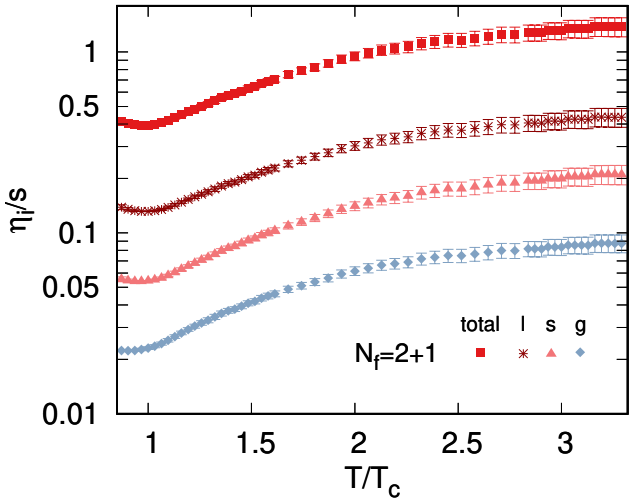

Rysunek 5.2: Shear viscosity to total entropy density ratio as a function of T/T_c in QCD with $N_f = 2{+}1$. The individual contributions η_i/s from light quarks (stars, as a sum of up and down flavors) and strange quarks (triangles), with equal contributions from their anti-quarks, as well as from gluons (diamonds) are shown along with the total specific shear viscosity of the QGP (squares), corresponding to Eq. (5.2).

the first-order phase transition.

In Fig. 5.1, a direct comparison of the quasiparticle model results in full QCD and pure Yang-Mills theory reveals a significant impact of the quark sector contributions in the entire temperature range studied in this work. The sizeable increase of η/s in the presence of dynamical quarks is in line with the observations made for the relaxation times, see Fig. 4.1. Although the entropy density is about a factor 2 - 3 larger in QCD, this is not sufficient to balance the overall dominance of the quark and anti-quark contributions. Moreover, the pronounced non-monotonicity at T_c in Yang-Mills theory is significantly smoothened in QCD, reflecting the difference in the order of the underlying phase transition.

Our results for η/s in $N_f = 2 + 1$ QCD are in quantitative contrast to the functional estimate for QCD reported in [57], which indicated only a moderate increase of the ratio for given T/T_c due to the presence of dynamical quarks. While one might argue that our findings are within errors still compatible with the old lattice gauge theory results for pure Yang-Mills theory [48], the bulk of available recent first-principle information is well overestimated by our QCD result. Moreover, we find a minimal η/s that is, at best, at the very upper edge of possible values extracted for the QGP in early fluid dynamical applications [59]. We note, however, that a very similar minimal value of the specific shear viscosity was found in other strongly coupled quantum fluids, namely ultra-cold atomic Fermi gases at or near the unitary limit. The shear viscosity of these physical systems can be studied experimentally, similar to flow experiments in heavy-ion collisions, through the fluid dynamical expansion of a trapped gas after removing the trapping potential [191–193]. Analyzing these experiments with a proper fluid dynamical framework [194] allows one to extract η in the normal fluid phase as a function of temperature and density. In a different study [195], a minimal specific shear viscosity of $\eta/s = 0.5 \pm 0.1$ was found just above the transition temperature to superfluidity. Moreover, an increase

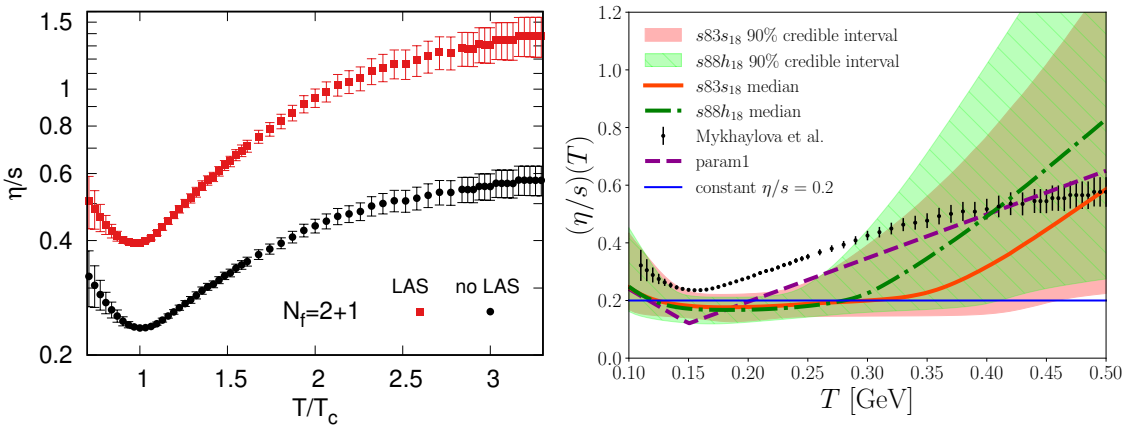

Rysunek 5.3: Left: Shear viscosity to total entropy density ratio as a function of T/T_c in full QCD computed using the relaxation times based on transport cross sections defined in Eq. (4.12) (LAS, squares) and using the isotropic cross sections without the large angle scattering (LAS) assumption (circles). Right: The η/s ratio as a function of temperature for the QGP with $N_f = 2 + 1$ obtained in the QPM (circles) and computed from the Bayesian analysis by comparing a hydrodynamic model to the experimental data with various assumptions. Figure taken from [190]. The black curves in the left and right panels are identical.

of η/s with T could be extracted in line with kinetic theory predictions [196], supporting the idea of an underlying quasiparticle picture for the strongly coupled fluid.

The total ratio η/s in QCD with $N_f = 2 + 1$ quark flavors is additionally shown in Fig. 5.2, alongside the individual contributions from light and strange quark sectors, as well as from gluon one. We find a rather shallow minimum of about 0.4 around the pseudo-critical temperature T_c and a moderate, monotonic increase with T at larger temperatures for the total ratio. Similar behavior can be seen for the individual contributions η_i/s entering Eq. (5.1). This is a consequence of the dynamics encoded in the quasiparticle masses via the effective coupling $G(T)$. Although all the quasiparticles affect each other's relaxation times through the effective masses in the cross sections and number densities entering Eq. (4.8), one clearly observes a hierarchy among the individual contributions that follows the inversed order in the effective quasiparticle masses. As expected, the heaviest quasiparticles are the most effective ones in equilibrating momentum degradations within the QGP. We note that a similar but quantitatively different pattern was reported in [88, 186]. We find $\eta_s/\eta_l < 0.5$ approaching only slowly 0.5 with increasing T while $\eta_g/\eta_l \leqslant 0.2$ in the shown temperature range.

We recall that the results of our studies are based on the transport cross sections with large angle scattering (LAS) approximation. However, to illustrate how this assumption affects the behavior of transport coefficients, we also compute the specific shear viscosity based on the total cross sections, i.e., excluding the weight-factor $\sin^2(\theta)$ from Eq. (4.12). As shown in Fig. 5.3 (left), the η/s in QCD with $N_f = 2 + 1$, the total specific shear viscosity based on transport cross sections is shifted towards higher values, while when the LAS approximation is relaxed, the η/s ratio decreases by a factor of $\sim 2/3$ [60, 138], and appears close to the results of hydrodynamic

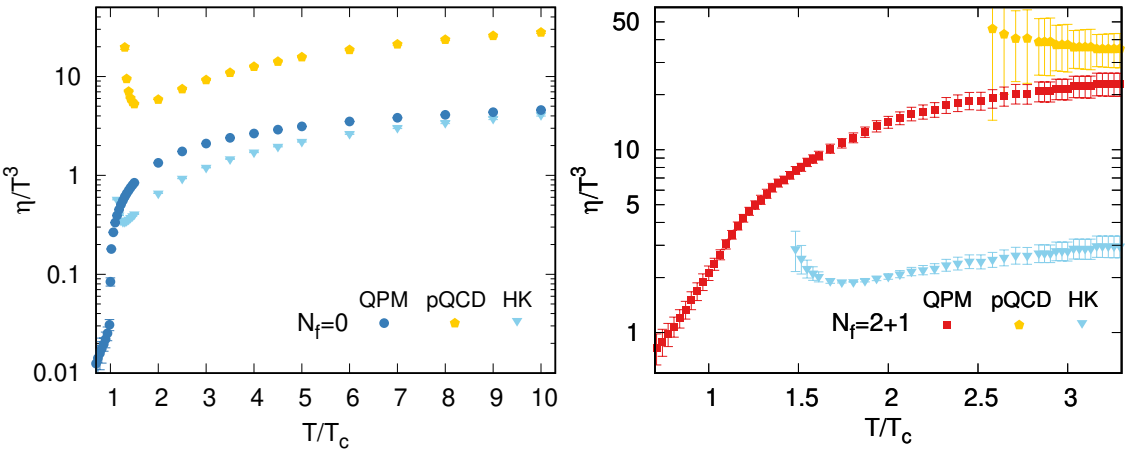

Rysunek 5.4: Scaled shear viscosity η/T^3 as a function of scaled temperature T/T_c for pure Yang-Mills theory (left) and QCD with light and strange quarks (right). The results obtained in the QPM (circles for $N_f = 0$ and squares for $N_f = 2+1$) are shown alongside a couple of perturbative approximations: using the next-to-leading-log coupling-expansion result from Arnold, Moore, and Yaffe [54] (pQCD, hexagons), and applying the parameterized relaxation time at leading-log order given by Hosoya and Kajantie [78] (HK, triangles).

simulations [190] shown in the right panel of Fig. 5.3. For a comprehensive discussion of Fig. 5.3 (right), we refer the reader to [190]. Here, we simply would like to emphasize that the QPM result for η/s with no LAS assumption agrees with the hydrodynamic outcomes much better than the result based on the transport cross sections. Therefore, in Chapter 6, for the investigation of charm quark production in viscous QGP, we adopt the time evolution found by [190] using our η/s result shown in Fig. 5.3 (right).

Alongside the specific η/s ratio, one can effectively examine the shear viscosity coefficient by constructing a dimensionless ratio of η/T^3, which naturally comes out of the dimension of the entropy density, and the shear viscosity as well. Therefore, in Fig. 5.4, we compare the shear viscosity of the deconfined matter obtained in the quasiparticle model with perturbative QCD expectations. The next-to-leading-log (NLL) expansion in the running coupling g as derived by Arnold, Moore and Yaffe [54] gives the following result for the shear viscosity

$$\eta_{\mathrm{NLL}} = \frac{T^3}{g^4}\left[\frac{\eta_1}{\ln(\mu_*/m_D)}\right] \tag{5.3}$$

with coefficients $\eta_1 = 27.126$ and $\mu_*/T = 2.765$ for $N_f = 0$, while $\eta_1 = 106.66$ and $\mu_*/T = 2.957$ for $N_f = 3$. The Debye screening mass reads $m_D^2 = (1 + N_f/6)g^2T^2$ for $SU(3)$ symmetry group [54]. Another perturbative parametrization of the shear viscosity was proposed by Hosoya and Kajantie [78], reading

$$\eta = \frac{64\pi^4}{675}\frac{T^3}{g^4\ln(4\pi/g^2)}\left[\frac{21\,N_f}{6.8\,(1+0.12(2\,N_f+1))} + \frac{16}{15\,(1+0.06\,N_f)}\right]. \tag{5.4}$$

The two terms in the square bracket mark the contributions from massless quarks and gluons, respectively, which are both proportional to the relaxation times parametrized at leading-log order in g.

In the perturbative expressions given by Eqs. (5.3) and (5.4), we replace the running coupling with our effective coupling $G(T)$ corresponding to the applied number of quark flavors. For pure Yang-Mills theory presented in the left panel of Fig. 5.4, we find that the scaled shear viscosity obtained in the QPM can be quantitatively approximated by Eq. (5.4) proposed by Hosoya and Kajantie [78], although it considers a system of massless gluons. The NLL perturbative result for η/T^3 [54] overestimates the QPM result, even at the temperature of the order of $10\,T/T_c$.

We observe the opposite tendency in the full QCD case (see the right panel of Fig. 5.4), where at high temperatures, η/T^3 in the quasiparticle model approaches within errors the pQCD expectation from Eq. (5.3). However, there is a significant difference between the QPM result and the approximation proposed in [78]. Since the latter describes a system of massless quarks and gluons, we can directly see the influence of the quasiparticle masses on the shear viscosity in the QGP. The result particularly depends on the number of quark flavors, since for the pure gluon plasma, the results of our Eq. (5.1) and Eq. (5.4) with $N_f = 0$ appear much closer to each other.

The shear viscosity obtained in this section is essential for the bulk to shear viscosity ratio ζ/η, which is used to illustrate the restoration of conformal invariance in pure Yang-Mills theory and QCD with quarks [184]. Parameterized by the speed of sound squared, the ζ/η ratio additionally points out the non-perturbative and perturbative QCD regimes, both well-captured in the present QPM. These and other issues will be discussed in Section 5.3. Further, in Section 5.5, we will utilize the specific shear viscosity to study its ratio to the electrical conductivity [197], while in Section 6.1, the η/s will be taken into account in the analysis of charm quark production in viscous QGP [198].

5.2 Bulk Viscosity

In this Section, we present a detailed analysis of the specific bulk viscosity ζ/s, which quantifies the energy dissipation in a system with changing volume, whether it is expanding or being compressed.

In analogy to the shear viscosity coefficient, we determine the bulk viscosity ζ from kinetic theory, assuming that the system deviates slightly from thermal equilibrium and using the Boltzmann kinetic equation in the RTA. The bulk viscosity of the hot QCD matter composed of quark and gluon quasiparticles reads [81, 85]

$$\zeta = \frac{1}{T}\sum_{i=g,l,\bar{l},s,\bar{s}} \int \frac{d^3p}{(2\pi)^3} d_i f_i^0 (1 \pm f_i^0) \frac{\tau_i}{E_i^2} \left\{ \left(E_i^2 - T^2 \frac{\partial \Pi_i}{\partial T^2} \right) c_s^2 - \frac{p^2}{3} \right\}^2 , \tag{5.5}$$

with the same quantities as for the shear viscosity η in Eq. (5.1). We additionally recall that c_s^2 is the speed of sound squared given by Eq. (2.7), while $\Pi_i(T)$ is the quasiparticle self-energy given by Eqs. (2.2) – (2.4). One can deduce the bulk viscosity of the gluon plasma by setting $N_f = 0$ and $i = g$, and applying the effective coupling appropriate for pure Yang-Mills theory. Note that in QCD at vanishing chemical potential, the particle and antiparticle contributions to the bulk viscosity

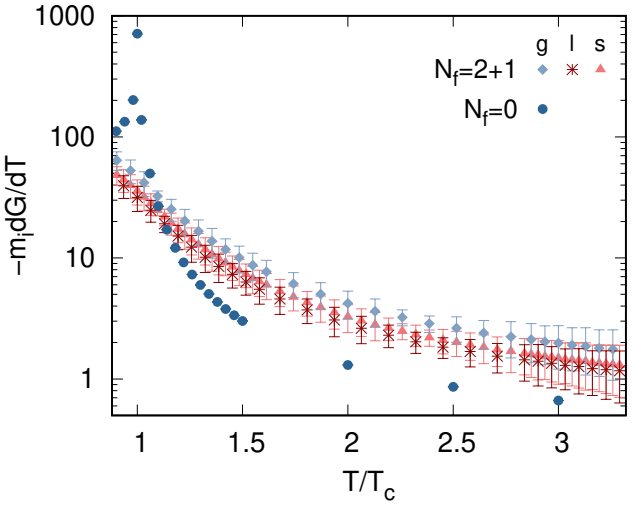

Rysunek 5.5: Temperature derivative of the effective coupling multiplied by the negative quasiparticle masses as a function of T/T_c. The result in pure Yang-Mills theory (circles) is compared to those for each quasiparticle species in QCD with $2+1$ quark flavors: gluons (diamonds), light quarks (stars), and strange quarks (triangles).

become equal, and ζ can be simplified in the same manner as the shear viscosity in Eq. (5.2).

It is clear that the definition of the bulk viscosity is more complex than that for the shear parameter, see Eq. (5.1), since ζ incorporates the speed of sound squared c_s^2, as well as the term $-\partial\Pi_i(T)/\partial T^2$. The derivative of the self-energy readily generates a temperature derivative of the effective coupling in the form of $-m_i\, dG/dT$. Since this term plays an essential role in the behavior of the bulk viscosity, we compute it separately for each quasiparticle species, both in pure Yang-Mills theory and QCD with quarks. The numerical results are presented in Fig. 5.5. In pure Yang-Mills theory, the derivative $-m_g\, dG/dT$ exhibits a prominent maximum at the critical temperature T_c. In contrast, in QCD with $N_f = 2+1$, for any constituents, it varies smoothly, and the strong non-monotonicity seen in the $N_f = 0$ case disappears.

One finds that the characteristic features of the quasiparticle masses and their thermal profiles are encoded into the resultant bulk viscosity to entropy density ratio ζ/s shown in Fig. 5.6. In pure Yang-Mills theory above T_c, the QPM result is fairly consistent with the collected data sets from lattice gauge theory [112, 113, 199], as well as to that from an approach based on the gauge-gravity correspondence [105]. In the confined phase, the lattice results show that the ratio continuously decreases as temperature increases toward T_c, but this behavior is not captured either by the holography or the QPM frameworks. As emphasized in Section 2, the present quasiparticle model is unsuitable for describing the kinematics of glueballs, which is essential to evaluate the total cross sections below T_c. Therefore, the bulk viscosity in this region should be interpreted with caution. The observed minimum right below T_c and the result at lower temperatures might be the artifacts of the quasiparticle approximation, so they require further justifications in a more refined approach that resembles confinement.

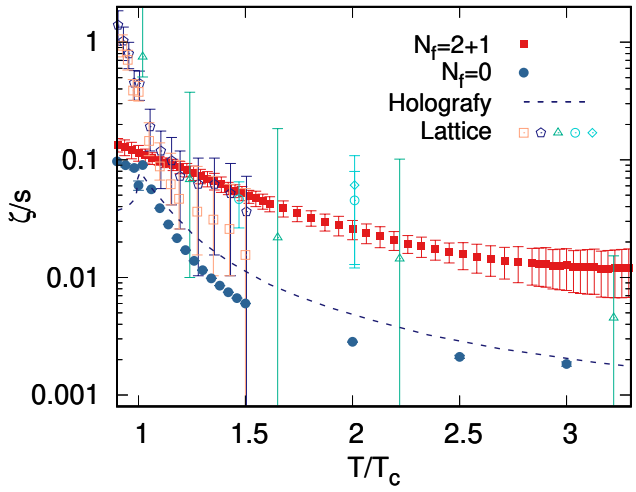

Rysunek 5.6: Total bulk viscosity to entropy density ratio ζ/s in pure Yang-Mills theory (full circles) and QCD with 2+1 quark flavors (full squares) as a function of T/T_c. For comparison, the corresponding lattice gauge theory results from [113] (open squares and hexagons), [199] (open triangles), and [112] (open circles and diamond), as well as the holographic result from [105] (dashed line) are presented.

Fig. 5.6 also exhibits our specific bulk viscosity for the full QCD with quarks. The ζ/s ratio obtained in the quasiparticle model appears above T_c in agreement with the available set of lQCD data [112,113,199], even though the first-principle calculations are performed in the pure SU(3) theory. Furthermore, it is an intriguing observation that in the vicinity of the (pseudo)critical temperature, the bulk viscosity is less flavor-dependent than the shear parameter shown in Fig. 5.1. In the QPM, there is a pronounced, almost constant hierarchy between η/s for $N_f = 0$ and $N_f = 2+1$, on the examined temperature range. Yet our results for ζ/s appear quite close to each other around T_c, while achieving an approximately constant, a factor of 5 difference at higher temperatures, starting from $T \gtrsim 1.5\,T_c$. Hence, the presence of light and strange quasiquarks substantially contribute to the bulk viscosity coefficient, causing a delay of the QGP approaching a non-interacting gas with $\zeta \to 0$ at high T.

Fig. 5.7 shows the total specific bulk viscosity of the QGP for $N_f = 2+1$, along with the contributions coming from different quasiparticle species. The $\zeta_{l,\,s,\,g}/s$ ratios are evaluated individually by using $i = l, s, g$ terms of the sum given by Eq. (5.5) and dividing them by the total entropy density from Eq. (2.5). The light quarks bring the main impact to the total bulk viscosity of the QGP, while the contributions of strange quarks and gluons are relatively suppressed by their larger effective masses, as illustrated in Fig. 2.2 and Fig. 5.5. We find that the strange quarks and gluons contribute almost equally to the bulk viscosity coefficient via different quantum statistics encoded in the characteristic derivatives of the self-energies. The quantitative resemblance between ζ_s/s and ζ_g/s is strongly affected by their individual properties coming from the convolution of the degeneracy factors, the relaxation times, and the effective masses entering the corresponding quasiparticle energies in Eq. (5.5). This is a clear distinction to the specific shear viscosity shown in Fig. 5.2, where the

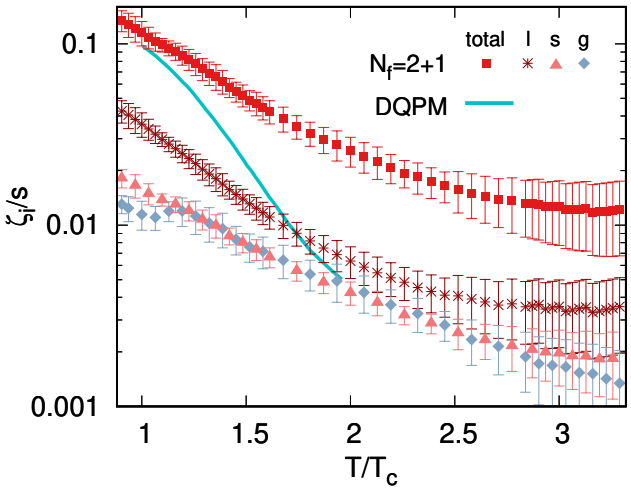

Rysunek 5.7: The bulk viscosity to entropy density ratio as a function of T/T_c in full QCD with quarks. The total QPM result (squares) is compared to the individual contributions coming from light quark (stars), strange quark (triangles), and gluon (diamonds) sectors. The antiparticle contributions are not included in the shown ratios $\zeta_{l(s)}/s$, but equal the particle ones. The total ζ/s computed in the dynamical quasiparticle model (DQPM, solid line) for $N_f = 2+1$ [101] is also depicted.

strange-quark component is larger than the gluon one at any temperature [138].

Further, in Fig. 5.7, the total QPM result in full QCD is confronted with that evaluated in the dynamical quasiparticle model [101]. The overall behavior as functions of T/T_c in the two approaches is similar, whereas the ζ/s in the DQPM decreases much faster with the increasing temperature. The observed difference can be traced back to the fact that in the DQPM, the quasiparticles carry finite lifetimes, which reproduce the same lattice equation of state [155] but modify the expressions for the relaxation times. This may explain the gap between the two results at high temperatures. In addition, as discussed in the previous section, following the standard prescription, we evaluated the transport cross sections applying the LAS approximation [60, 61, 181], while this is not considered in [101].

The rapid growth of the bulk viscosity close to the deconfinement phase transition is an outstanding feature of the SU(3) dynamics. While changing two orders of magnitude close to T_c, the specific bulk viscosity vanishes at very high temperatures, $\zeta/s \to 0$ as $T \to$ inf, implying that the hot QCD medium reaches the conformal limit, $m_i \to 0$. Therefore, the bulk viscosity is considered as a measure for the violation/restoration of conformal invariance [99]. In the next section, we adopt the outcomes presented in Fig. 5.6 to investigate the dynamical properties of the deconfined matter depending on the considered number of quark flavors. As will be shown later on, combined with the shear viscosity, the bulk coefficient is capable of pointing out the weak and strong coupling limits of QCD, which are both well-captured in the present quasiparticle model.

5.3 Bulk to Shear Viscosity Ratio

In the previous sections, we have illustrated how differently the deconfined matter's specific shear and bulk viscosities behave close to the (pseudo)critical temperature. The η/s ratio then exhibits its minimum, reaching the $1/4\pi$ KSS bound in the pure Yang-Mills case, and consistently increases with an increasing temperature. On the other hand, the specific bulk viscosity ζ/s has a maximum at T_c and then decreases, even by two orders of magnitude, on the examined temperature interval.

Since the dynamics of η and ζ drastically change with temperature, it is undoubtedly connected to the behavior of the running coupling, in our case, to the effective coupling $G(T)$. By taking the high-temperature limit in Eqs. (2.7) and (5.5), we find that the bulk viscosity ζ vanishes as the speed of sound squared approaches the value of 1/3, i.e., the Stefan-Boltzmann limit. Therefore, one can parameterize the ζ/η ratio by the c_s^2 to investigate the weak- and strong-coupling QCD domains.

For the viscosities evaluated perturbatively at high temperature, the ratio ζ/η is given unambiguously by [54, 200]

$$\frac{\zeta}{\eta} = 15\left(\frac{1}{3} - c_s^2\right)^2. \tag{5.6}$$

Quantitatively the same trend has been observed for an interacting photon gas [201], and in scalar field theory [189].

In contrast, for strongly-coupled theories along with gauge/gravity duality [202], the ratio behaves as [203]

$$\frac{\zeta}{\eta} \propto \left(\frac{1}{3} - c_s^2\right), \tag{5.7}$$

which differs from Eq. (5.6) by the power of the c_s^2.

Yet another non-perturbative approach, which describes the Yang-Mills plasma based on the Gribov-Zwanziger quantization [204, 205], leads to the ratio ζ/η linearly proportional to the quantity $\Delta c_s^2 = 1/3 - c_s^2$ [70], thus to an intriguing agreement with the result from gauge-gravity duality. In a similar QPM framework for pure Yang-Mills theory, it has been shown that the ratio ζ/η linearly depends on Δc_s^2 near the first-order phase transition, whereas it scales quadratically with Δc_s^2 at high temperature [81].

The bulk to shear viscosity ratio can be computed straightforwardly from Eqs. (5.5) and (5.1) by employing the corresponding effective coupling and masses for pure Yang-Mills theory and QCD with $N_f = 2 + 1$. Based on the previous observations in [81, 206, 207], the full QPM results in two theories will be compared with the linear and quadratic dependence on Δc_s^2:

$$\text{Linear:} \quad \frac{\zeta}{\eta} = \alpha\left(\frac{1}{3} - c_s^2\right) + \beta, \tag{5.8}$$

$$\text{Quadratic:} \quad \frac{\zeta}{\eta} = \gamma\left(\frac{1}{3} - c_s^2\right)^2 + \delta, \tag{5.9}$$

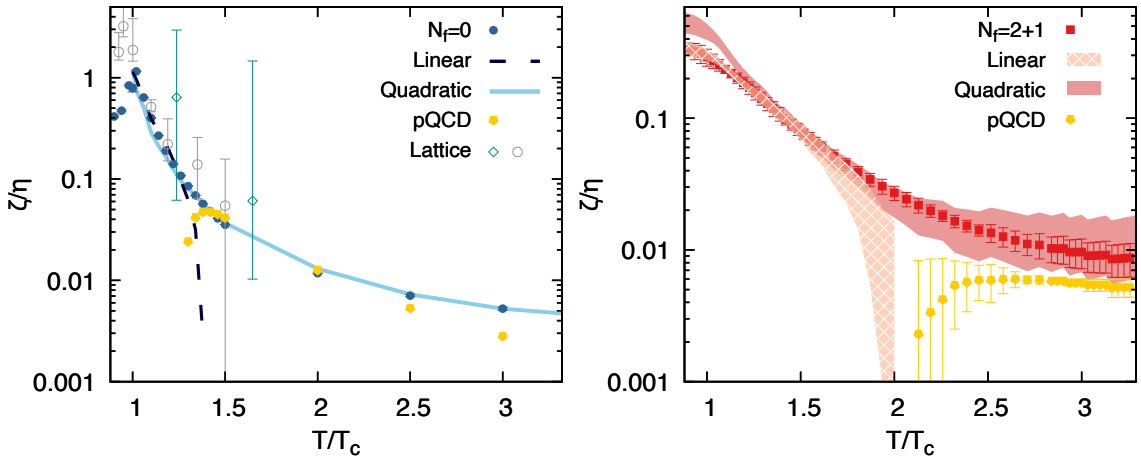

Rysunek 5.8: The bulk to shear viscosity ratio as a function of T/T_c. Left, pure Yang-Mill theory: The exact QPM result (full circles), parameterized by linear (dashed line) and quadratic (solid line) ansatzes, using Eqs. (5.8) and (5.9), with the fit parameters $\alpha = 4.5, \beta = -0.3$, $\gamma = 12$, $\delta = 0.002$. The lQCD data are deduced from [47, 199] (open diamonds), and [46, 113] (open circles). Right, full QCD: The ζ/η in the QPM (full squares), shown along with linear (checkered band) and quadratic (plain-colored band) parametrizations in the c_s^2, here $\alpha = 2.15, \beta = -0.085$, $\gamma = 14$, $\delta = 0$. In both panels, the pQCD result (pentagons) is computed from Eq. (5.3) and (5.10) [54, 200] with the corresponding $G(T)$.

with fit parameters α, β, γ and δ, assuming equal relaxation times for the shear and bulk viscosities.

Figure 5.8 presents the bulk to shear viscosity ratio in pure Yang-Mills theory (left) and in QCD with $N_f = 2 + 1$ (right). Consistently to the earlier study in thermodynamics with $N_f = 0$ [81, 139], the QPM result is well captured by the linear ansatz (5.8) near T_c, and by the quadratic one (5.9) at the higher temperature. A clear changeover from the linear to quadratic scaling emerges at $T \simeq 1.3\,T_c$. Near T_c the ζ/η in the QPM agrees reasonably well with the same quantity deduced from the available lattice data [47, 199] and [46, 113]. Above $T \simeq 1.4\,T_c$, it is in line with the pQCD prediction [54, 200], obtained from the next-to-leading-log (NLL) expansion in the weak coupling. We recall that in this approximation, the shear viscosity is given by Eq. (5.3),

$$\eta_{\rm NLL} = \frac{T^3}{g^4}\left[\frac{\eta_1}{\ln(\mu_*/m_D)}\right],$$

while the bulk viscosity is expressed in the NLL as

$$\zeta_{\rm NLL} = \frac{g^4\,T^3}{16\pi^2}\left[\frac{A}{\ln(\mu_2^*/m_D)}\right]. \tag{5.10}$$

For $N_f = 0$, the set of parameters reads $\eta_1 = 27.126$, $\mu_1^*/T = 2.765$, $A = 0.443$ and $\mu_2^*/T = 7.14$, while for $N_f = 3$, $\eta_1 = 106.66$, $\mu_1^*/T = 2.957$, $A = 0.657$ and $\mu_2^*/T = 7.77$ [54, 200].

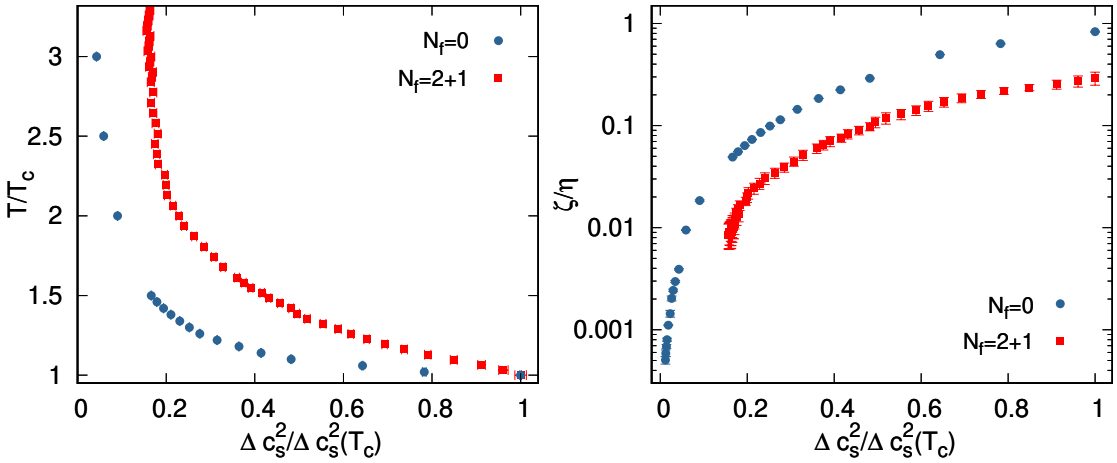

Rysunek 5.9: The scaled temperature (left) and the bulk to shear viscosity ratio (right) as functions of the conformality measure, $\Delta c_s^2 = 1/3 - c_s^2$, normalized by its value at T_c in pure Yang-Mills theory (full circles) and QCD with $N_f = 2+1$ (full squares).

Shown in the right panel of Fig. 5.8, the QPM result for $N_f = 2+1$ retains the same features observed in the Yang-Mills case. However, the changeover between the two scaling behaviors appears at a higher temperature, $T \simeq 2\,T_c$. One observes a somewhat more significant distinction from the pQCD result, arising from the presence of the dynamical quarks in the system.

Since the non-vanishing ζ quantifies how far the system appears from the conformal limit, to look closer into the connection between the bulk viscosity and conformality, in Fig. 5.9, we show a flavor dependence of the ζ/η ratio as a function of the measure Δc_s^2 (right panel), as well as the explicit temperature profiles of c_s^2 at and above T_c (left panel). Fig. 5.9 can be easily read by starting from the right-hand side of each panel, when $T = T_c$ in both theories, and then going to the left, in the direction of the temperature increase. One finds that the speed of sound squared in QCD approaches its conformal value ($\Delta c_s^2 = 0$, or equivalently, $c_s^2 = 1/3$) at high temperatures considerably slower than in Yang-Mills theory, due to the presence of dynamical quarks. Consequently, the appearance of dynamical quarks delays the restoration of conformal invariance. Furthermore, the changeover of the two scalings of ζ/η ratio given by Eqs. (5.8) and (5.9) is preserved, and one recognizes the regions with linear and quadratic behavior in the c_s^2.

This subject finalizes our investigation of the shear and bulk viscosities in hot QCD with different numbers of quark flavors. The more advanced studies of the viscosity coefficients incorporate the additional factors present at heavy ion collisions, such as the momentum anisotropy [72], the finite chemical potential and chiral phase transition [186], the impact of the magnetic field [208, 209], and many others.

5.4 Electrical Conductivity

The electrical conductivity σ is another valuable transport parameter in the investigation of the dynamical and transport properties of QCD. In the medium

with non-zero electrical conductivity, σ characterizes the linear response of the system to the external electric field, which generates the electrically charged current. Mathematically speaking, it can be expressed by the vector form of Ohm's Law [131],

$$\vec{J} = \sigma \vec{E}, \tag{5.11}$$

where $\vec{J}$ denotes the electric current, while $\vec{E}$ stands for the applied electric field. In ultrarelativistic heavy ion collisions, the electrical conductivity quantifies the reaction of the deconfined matter to the produced electric field.

In kinetic theory under the RTA, the electrical conductivity of hot QCD medium with $N_f = 2 + 1$ reads [131]

$$\sigma = \frac{1}{3T} \sum_{i=u,\bar{u},d,\bar{d},s,\bar{s}} \int \frac{d^3p}{(2\pi)^3} \frac{p^2}{E_i^2} q_i^2 d_i \tau_i f_i^0 (1 - f_i^0), \tag{5.12}$$

where the quark electric charge q_i is given explicitly by $q_u = -q_{\bar{u}} = 2\,e/3$ for up, and $q_{d,s} = -q_{\bar{d},\bar{s}} = -e/3$ for down and strange (anti)quarks. The electron charge reads $e = \sqrt{4\pi\alpha}$ with the fine structure constant $\alpha \simeq 1/137$. In contrast to our previous notation, due to the different electric charges of up and down quarks, their contributions are evaluated separately in the electrical conductivity. We first compute σ_u and σ_d with new degeneracy factors $d_{u,\,d,\,s} = 6$, and then denote the contribution from light quark sector as $\sigma_l = \sigma_u + \sigma_d$.

Due to the charge neutrality of gluons, they do not directly contribute to the above equation. Therefore, in the pure Yang-Mills theory, the deconfined matter is characterized by vanishing electrical conductivity, $\sigma_g = 0$. However, one should keep in mind that the interactions with dynamical gluons are encoded in the relaxation times of light and strange quasiquarks entering Eq. (5.12).

In the left panel of Fig. 5.10, we present the electrical conductivity scaled by the temperature, σ/T, including the results of various approaches. The QPM result is quite consistent with the earlier study [129], where σ has been evaluated in the Green-Kubo formalism and in the RTA. A slight difference from the approach employed in [129] arises from such key features as the parameterization of the effective coupling reproducing the same EoS as used in our QPM [155], as well as the alternative definition of the effective mass of quarks,

$$m_q^2 = g^2 T^2/3, \tag{5.13}$$

with no dependence on the bare mass m_i^0. The above expression implies that all dynamical quarks are degenerate, unlike in our QPM, with strange quarks distinguished from the light flavors. We have already seen that the larger mass suppresses the individual contribution to shear and bulk viscosity from the strange quark sector, see Figs. 5.2 and 5.7.

Moreover, in the alternative quasiparticle framework by Puglisi et al. [129], the relaxation times are computed from the cross sections of the form [130]

$$\sigma_{tr}^{ij}(s) = \beta^{ij} \frac{G^4}{16\pi m_D^2} \frac{s}{s + m_D^2} h(a), \tag{5.14}$$

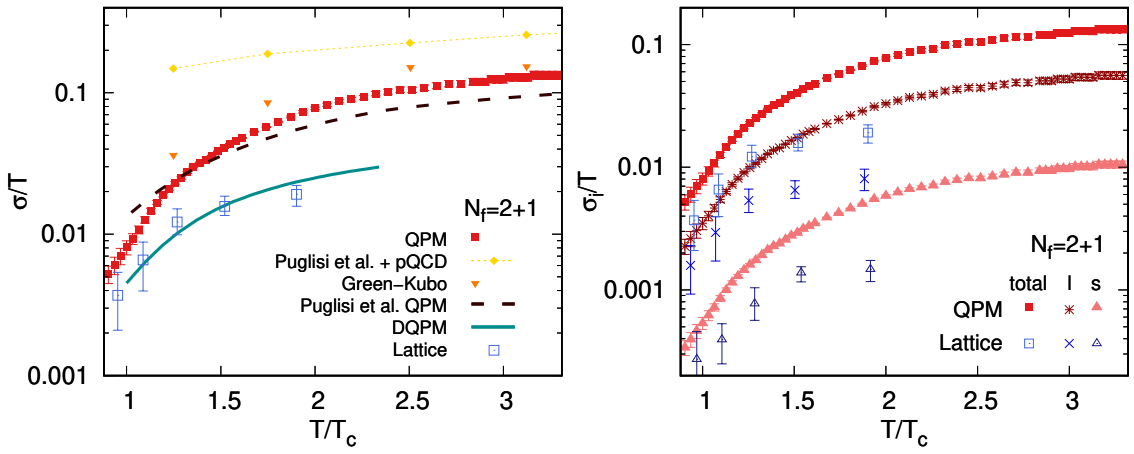

Rysunek 5.10: Left: The total electrical conductivity scaled with temperature as a function of T/T_c. Besides our QPM result (full squares), we show the results in other approaches collected in [129]: the pQCD-based calculation (diamonds), the Green-Kubo formalism (triangles), and the QPM with a different setup (dashed line). The solid line corresponds to the DQPM result [101], while the result of the lattice simulations is shown by open squares [118, 119]. Right: The total σ/T ratio of the QGP (full squares) along with the light (stars) and strange (triangles) quark components. The corresponding lattice data is deduced from [118, 119] for the total electrical conductivity (open squares) and for light and strange quark contributions (crosses and open triangles, respectively). Here, our $\sigma_{l,s}/T$ ratios do not include the antiparticle contributions for a direct comparison to the lattice QCD data which considers just the particles.

where β^{ij} is the coefficient referring to the different scatterings of quarks and gluons, $\beta^{qq} = 16/9$, $\beta^{qq'} = 8/9$, $\beta^{qg} = 2$, $\beta^{gg} = 9$. The Debye mass $m_D^2 = G^2(T)T^2$ is originated from the HTL approach, s denotes the Mandelstam variable, while $h(a) = 4a(1+a)[(2a+1)\ln(1+1/a) - 2]$ with $a = m_D^2/s$ represents anisotropy of the scatterings [130].

The result corresponding to pQCD estimation in Fig. 5.10 (left) is obtained from the alternative QPM utilizing the perturbative coupling [129]

$$g_{\mathrm{pQCD}} = \frac{8\pi}{9} \ln^{-1}\left[\frac{2\pi T}{\Lambda_{\mathrm{QCD}}}\right], \tag{5.15}$$

where Λ_{QCD} is the QCD scale parameter [4]. Since the present quasiparticle framework captures the non-perturbative QCD features through the effective coupling $G(T)$, our result tends to approach the pQCD estimation only at high temperatures. Similar behavior has also been observed for the specific shear viscosity in pure Yang-Mills theory and QCD with quarks, see Fig. 5.4.

Further, near T_c, we find that the QPM fairly captures the behavior of σ/T found in the lattice QCD simulations [118, 119], see open symbols in the left panel of Fig. 5.10. We also recognize an overall qualitative agreement of our σ/T with the DQPM result [101], although, in this approach, σ/T yields a somewhat smaller value at any temperature. A similar trend was already observed in the case of the specific bulk viscosity ζ/s, see Fig. 5.7. The quantitative difference between the two effective approaches arises due to the finite widths of the quasiparticles employed

in [101] and the LAS assumption in the QPM [138], the application of which leads to a systematic upward-shift of any transport parameter.

To look into the role of different quark flavors in the total electrical conductivity, we present the individual contributions from light and strange quark sectors.

The right panel of Fig. 5.10 exhibits that the light-quark contribution is larger than that of the strange quarks, as anticipated with their mass differences shown in Fig. 2.2. The corresponding lattice data [119] near T_c is relatively compatible with the QPM result, whereas the discrepancy between them emerges at $T \simeq 1.5\,T_c$ and increases gently with temperature. This can be attributed to the fact that the lattice setup includes the pion mass $m_\pi = 384(4)$ MeV [119], heavier than the physical one used in our model-building. In fact, by increasing the bare mass of light quarks, we obtain a decrease in electrical conductivity, which is smaller than the result with physical quark masses at any temperature.

5.5 Shear Viscosity to Electrical Conductivity Ratio

We now make use of the results for the electrical conductivity discussed above and the specific shear viscosity presented in Section 5.1 to compute their relative ratio, $(\eta/s)/(\sigma/T)$. In the pioneering work discussing this coefficient [130], it was shown that $(\eta/s)/(\sigma/T)$ complements the ratio of gluon to quark scattering rates and appears to be independent of the effective coupling. Therefore, the relation between these quantities may help us to understand the comparative role of gluons to quarks in the evolution of the QGP.

From Eqs. (5.1) and (5.12), it follows that the electrical conductivity depends on the relaxation times of quarks. At the same time, the shear viscosity contains an additional term created by the presence of gluons. Therefore, the quantity $(\eta/s)/(\sigma/T)$ depends on the ratio of gluon to light and strange quarks relaxation times.

The shear viscosity also differs from the electrical conductivity by its temperature dependence, which among other terms, is encoded in the ratio p^4/E_i^2 in Eq. (5.1), and p^2/E_i^2 in Eq. (5.12). Since η and σ equivalently depend on the effective coupling and masses, we expect that the influence of these details cancels to a large extent in the $(\eta/s)/(\sigma/T)$ ratio. As a result, the shear viscosity to electrical conductivity remains sensitive only to the ratio $\tau_g/(\tau_l + \tau_s)$. This observation agrees with the conclusion in [130], although the same relaxation times for all types of quarks were assumed, unlike in our approach, where strange quarks are distinguished from the light ones.

Fig. 5.11 exhibits the temperature dependence of the ratio $(\eta/s)/(\sigma/T)$ in various quasiparticle approaches for QCD with $N_f = 2 + 1$. Our result is acquired from the total η/s and σ/T shown in Fig. 5.2 and 5.10, respectively. The impact of the LAS assumption applied in Eq. (4.12) vanishes, leading to identical outcomes for $(\eta/s)/(\sigma/T)$ ratio based either on the transport or isotropic cross sections.

Despite a few discrepancies in the models' setup, we find an excellent agreement

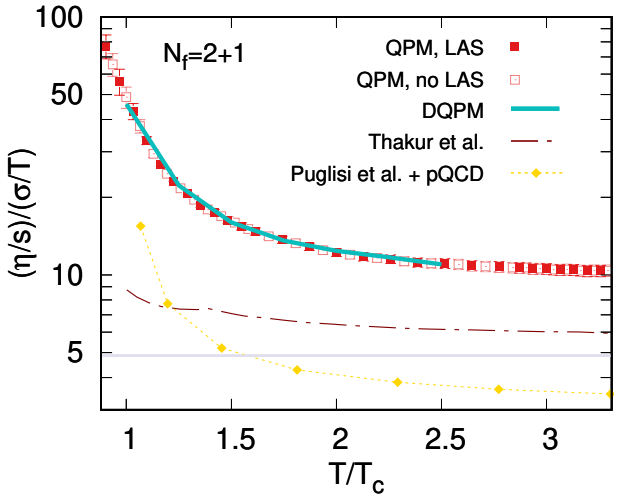

Rysunek 5.11: The ratio of the shear viscosity to the electrical conductivity as a function of T/T_c obtained in different QPM approaches. The results from our quasiparticle model based on transport (LAS, full squares) and isotropic (no LAS, open squares) cross sections are presented along with the dynamical quasiparticle model [101] (DQPM, solid line), and the quasiparticle approaches by Thakur et al. [131] (dash-dotted line) and Puglisi et al. with pQCD components [130] (diamonds). The horizontal line indicates the value $(\eta/s)/(\sigma/T) = 4/(e^2 N_c^2) \approx 4.85$ obtained from AdS/CFT correspondence [35, 134].

between the DQPM [101] and our QPM approach. While η and σ in both frames are evaluated using Eqs. (5.1) and (5.12), with the effective couplings determined from the lQCD entropy density [155], the DQPM additionally incorporates finite widths of the quasiparticles [101]. Moreover, their relaxation times are defined from the isotropic cross sections, i.e., by excluding the phenomenological weight factor $\sin^2\theta(s,t,m_{i,j,i',j'}(T))$ from Eq. (4.12). Our detailed study justifies that the influence of the effective coupling and masses is compensated. We also find a similar cancellation mechanism for finite widths of the quasiparticles in the $(\eta/s)/(\sigma/T)$ ratio. The observed agreement can be traced back to the relaxation times, which are modeled similarly and depend on the same types of the two-body scattering processes [92, 138]. Thus, both approaches equivalently maintain the microscopic interactions between the constituents of the deconfined matter.

Fig. 5.11 also shows the result of Thakur et al. [131] obtained in the alternative quasiparticle framework. There, the dynamical quarks and gluons are dressed with the self-energies proposed in Eqs. (2.2) – (2.4), however, significant simplifications are done by taking the relaxation times as for massless particles [78], see Eq. (5.4), and applying the coupling based on the former lQCD data for pure SU(3) theory [211]. These assumptions lead to a systematic underestimation of the shear viscosity to electrical conductivity ratio obtained by Thakur et al. [131]. The ratio, in this case, also appears to be the least sensitive to temperature changes. Compared to the other approaches, it remains approximately constant in the explored temperature range, exhibiting a slight increase near T_c.

We further juxtapose our $(\eta/s)/(\sigma/T)$ to the result acquired in the quasiparticle pic-

ture by Puglisi et al. [130] which uses the pQCD-type cross sections and coupling from Eqs. (5.14) and (5.15), as well as the identical relaxation times for all quark flavors. The behavior of $(\eta/s)/(\sigma/T)$ is qualitatively compatible with the QPM and DQPM results. However, it is more than 2 times suppressed in the whole temperature interval due to the much higher values of the scaled electrical conductivity σ/T [197], see Fig. 5.10.

In general, the $(\eta/s)/(\sigma/T)$ ratio in the quasiparticle models shows a pronounced increase toward the pseudocritical temperature and is expected to reach an approximately constant value at higher temperatures. In contrast, from the AdS/CFT predictions for η/s [35] and σ/T [134], one obtains $(\eta/s)/(\sigma/T) = 4/(e^2 N_c^2) \approx 4.85$, i.e., a constant value at any temperature.

More advanced studies of the shear viscosity to electrical conductivity ratio in QCD consider the momentum anisotropy [131], the influence of magnetic field [212], or very high density of the system [135].

Rozdział 6

Charm Quark Production

The information collected from the experimental and theoretical investigations of charm quarks and their bound state, charmonium ($c\,\bar{c}$), proved, as has been predicted in [213], that they can be used as direct probes of the dynamics of the quark-gluon plasma [2, 214–218].

Therefore it is highly important to analyze not only the production of charmonium in heavy ion collisions but also the production mechanism of charm quarks in the quark-gluon plasma. If one describes the QGP in terms of massless quarks and gluons, the charm quark production will be insignificant due to the large amount of energy required to produce the massive charm-anticharm pair [219]. However, if the system is expressed in terms of massive (quasi)particles, especially with dynamically generated effective masses, the scatterings among them may significantly increase the production of charm quarks in the deconfined medium. Therefore inspired by [136, 182, 219–221], we investigate the process of the charm quark production in hot QCD and study how their number changes with changing properties of the deconfined matter.

As previously, we consider the QGP with $N_f = 2{+}1$ to be in thermal equilibrium and describe it using the quasiparticle d.o.f. with effective masses and coupling discussed in Chapter 2. While dynamical quarks and gluons contribute to the EoS, charm quarks are added to the system as „obstacles" with constant masses, $m_c = 1.3$ GeV, which do not impact the thermodynamics of the QGP [222]. Initially, charm quarks are out of chemical equilibrium, which is quantified by the fugacity parameter λ_c, indicating the deviation of the statistical phase space density from f_c^0 [182]. Therefore, in contrast to the equilibrium statistics for light (strange) quarks and gluons given in Eq. (2.6), the charm quarks are described by Jüttner distribution for fermions [220, 223],

$$f_c(\lambda_c) = \lambda_c \Big(e^{E_c/T} - \lambda_c \Big)^{-1}, \tag{6.1}$$

where $E_c = \sqrt{p^2 + m_c^2}$ denotes the charm quark energy. The above expression coincides with Fermi-Dirac distribution from Eq. (2.6) for $\lambda_c = 1$, i.e., once the charm quarks equilibrate.

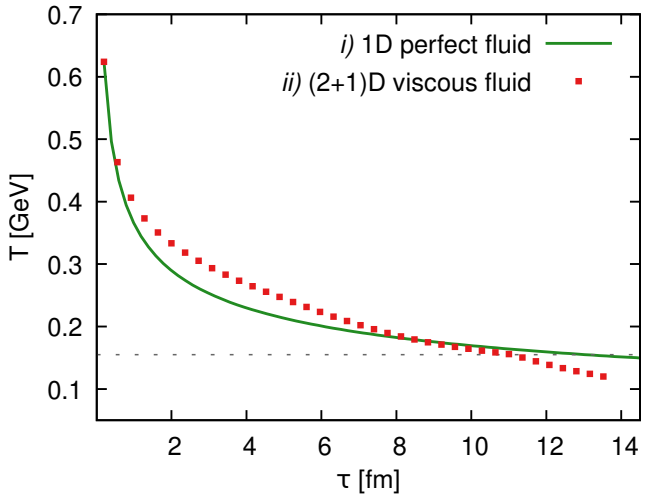

Rysunek 6.1: The temperature T as a function of time τ for longitudinal propagation of perfect QGP (1D, solid line) and 2+1-dimensional expansion of viscous QGP (squares) Both evolution schemes consider the deconfined matter with $N_f = 2 + 1$ and carry the same initial conditions, $\tau_0 = 0.2$ fm, $T_0 = 0.624$ GeV [190]. The dashed line represents the QCD pseudocritical temperature, $T_c = 0.155$ GeV [155].

6.1 Time Evolution of the QGP

We study the evolution of charm quarks in hot QCD, assuming two different scenarios of the medium expansion:

i) Longitudinal (1D) propagation of perfect fluid, known as Bjorken flow, with time evolution specified by the scaling solution [224]

$$T(\tau) = T_0(\tau_0) \left(\frac{\tau_0}{\tau}\right)^{1/3}, \tag{6.2}$$

where τ denotes the time, and $T_0(\tau_0)$ denotes the initial conditions. The prescription is known as Bjorken flow [224].

ii) Longitudinal and transverse, i.e., (2+1)D, expansion of the viscous fluid, whose time evolution is acquired from the second order viscous hydrodynamic simulations [190] incorporating the temperature-dependent specific shear viscosity η/s computed in the QPM from the isotropic cross sections [138], see Fig. 5.3 (right). This QPM result appears to be in line with η/s obtained from hydrodynamic simulations [190].

Both systems are considered as boost-invariant [6], and share common initial conditions, $T_0 = 0.624$ GeV, $\tau_0 = 0.2$ fm [190]. This allows us to illustrate how the shear viscosity, as well as the number of dimensions, affects the QGP lifetime.

Fig. 6.1 shows the time evolution of the QGP in *i*) and *ii*) cases. We observe that the curves coincide numerically, even though they describe different fluids (perfect and viscous) expanding in various numbers of dimensions (1D and (2+1)D, respectively). Applying the same initial conditions illustrates that viscous QGP evolving in (2+1)D

reaches the crossover temperature T_c faster than the perfect deconfined medium propagating longitudinally, with a time difference of around 2 fm. This observation agrees with a general expectation that the energy dissipation is larger in a more viscous fluid expanding in more dimensions, leading to a shortened lifetime of such a system. We recall that at the pseudocritical temperature shown in Fig. 6.1, one expects a crossover phase transition from the deconfined to the hadronic phase.

6.2 Rate Equations

To find how the fugacity of charm quarks λ_c, and therefore the number of $c\bar{c}$ pairs, changes with temperature and time, following [220, 221] we utilize the rate equation defined as

$$\partial_\mu n_c^\mu(\lambda_c) = \partial_\mu[n_c(\lambda_c)\, u^\mu] = R_c \left[1 - \left(\frac{n_c(\lambda_c)}{n_c^0}\right)^2\right], \tag{6.3}$$

with the out-of-equilibrium number density of charm quarks

$$n_c(\lambda_c) = d_c \int \frac{d^3p}{(2\pi)^3}\, f_c(\lambda_c), \tag{6.4}$$

containing the spin-color degeneracy factor $d_c = 6$. The charm quark number density becomes $n_c(\lambda_c = 1) = n_c^0$ in equilibrium. We recall that u^μ is the four-velocity of the fluid discussed in Chapter 3. The production rate of charms quarks R_c is defined as

$$R_c = \frac{1}{2}\, \bar{\sigma}_{gg\to c\bar{c}}\, (n_g^0)^2 + \bar{\sigma}_{l\bar{l}\to c\bar{c}}\, (n_l^0)^2 + \bar{\sigma}_{s\bar{s}\to c\bar{c}}\, (n_s^0)^2, \tag{6.5}$$

and depends on the thermal-averaged cross sections computed at the leading order for massive (quasi)particles [222], as well as on the number density of dynamical quarks and gluons in equilibrium, see Eq. (4.9). Additionally, the factor of 1/2 in the above equation is introduced to avoid the double counting of gluons [182].

In contrast to our previous studies [138, 184, 197], where we employ the transport cross sections [60, 61, 181], this research incorporates the total (isotropic) cross sections computed from Eq. (4.12) by excluding the large angle scattering assumption. The rate equation satisfies the assumption that as charm quarks reach the chemical equilibrium, the production and annihilation rates become equal [221], which implies that the square bracket in Eq. (6.3) vanishes, leading to $\partial_\mu n_c^{0\,\mu} = 0$.

For a purely longitudinal propagation described by the i) scenario, one can simplify the LHS of Eq. (6.3), assuming the flow velocity of the system is in the LRF, $u^\mu = (1, 0, 0, 0)$ [182, 220],

$$\partial_\mu[n_c(\lambda_c)\, u^\mu] = u^\mu \partial_\mu n_c(\lambda_c) + n_c(\lambda_c)\partial_\mu u^\mu = \frac{\partial n_c(\lambda_c)}{\partial \tau} + \frac{n_c(\lambda_c)}{\tau}. \tag{6.6}$$

On the other hand, for (2+1)D evolution in ii), the flow velocity changes because of an additional propagation in the transverse plane. For the purpose of this calculations, we express the flow velocity in cylindrical coordinates [6] and rewrite the LHS

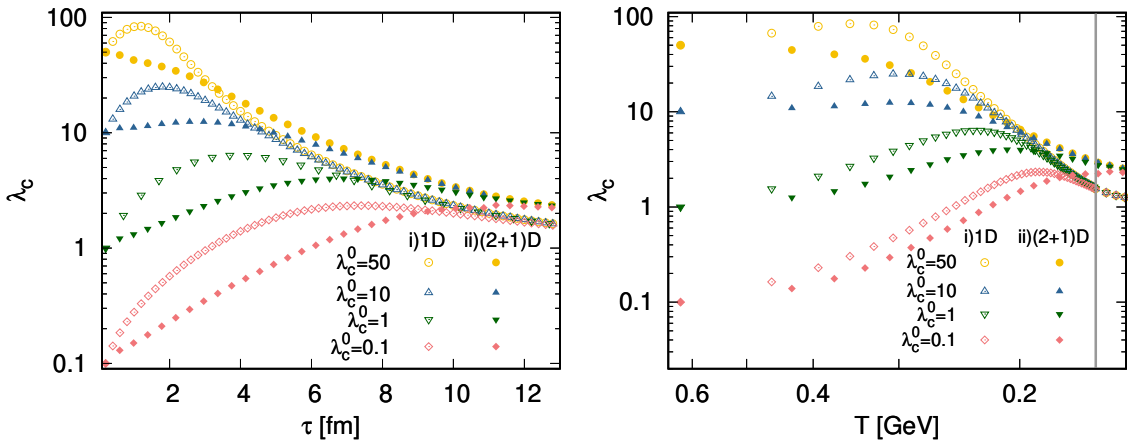

Rysunek 6.2: The charm quark fugacity λ_c as a function of time (left) and correspondingly temperature (right) for different initial values of λ_c^0. The open bullets show λ_c in the i) case of perfect QGP propagating only longitudinally, while full symbols represent the ii) evolution of hot QCD medium expanding in (2+1)D, with temperature-dependent shear viscosity taken into account. The vertical line in the right panel indicates the QCD pseudocritical temperature.

of Eq. (6.3) as [221, 225],

$$\partial_\mu[n_c(\lambda_c)\,u^\mu] = \frac{1}{\tau\,R^2(\tau)}\frac{\partial}{\partial\tau}\left(\tau\,R^2(\tau)\,n_c(\lambda_c)\,\langle u^\tau\rangle\right), \tag{6.7}$$

where $R(\tau)$ is the transverse radius of the system given by

$$R(\tau) = R_0 + a(\tau-\tau_0)^2. \tag{6.8}$$

We apply $R_0(\tau_0) = 7$ fm [219, 225, 226] for the initial radius, and $a = 0.043$ fm^{-1} for the transverse acceleration. This value satisfies the condition of the QGP evolution in (2+1)D, where it hadronizes at $\tau \simeq 11$ fm [198], see Fig. 6.1.

Further, $\langle u^\tau\rangle$ in Eq. (6.7) is the averaged time component of the four-velocity, which is expressed in terms of the transverse radius as [221, 225, 227]

$$\langle u^\tau\rangle = \frac{2}{R^2(\tau)}\int_0^{R(\tau)} dr\left[\left(\frac{dR(\tau)}{d\tau}\right)^2\frac{r}{R(\tau)}\right]^{-1/2}, \tag{6.9}$$

assuming the uniform density distribution in the transverse plane.

Once Eq. (6.3) is rewritten as guided in Eq. (6.6) or Eq. (6.7), depending on the expansion scenario, we solve it numerically for the arbitrary initial values λ_c^0 of the charm quark fugacity [222].

The time evolution of the charm quark fugacity is presented in the left panel of Fig. 6.2. In perfect QGP undergoing the Bjorken flow (the i) case), the charm quark fugacity first increases with time and then decreases, independently of its initial value. The turning point becomes less sharp and shifts towards higher τ for lower λ_c^0. In contrast to that, in the ii) scenario for (2+1)D expansion of viscous QGP, all the $\lambda_c(\tau)$ are flattened. As τ grows, the solutions either slowly increase (for $\lambda_c^0 \ll 1$) or smoothly decrease (for $\lambda_c^0 \gtrapprox 10$) on the whole examined time and

temperature ranges. For the intermediate values of λ_c^0, one can observe a behavior similar to $\lambda_c(\tau)$ in the i) scenario but with a less pronounced turning point.

We additionally observe that for i) and ii) evolutions individually, all the $\lambda_c(\tau)$ tend to overlap each other at high τ. Such a tendency may be related to the universal behavior of the solutions of the differential equations when there exists a particular attractor to which all the other solutions converge [228].

Fig. 6.2 (right) exhibits numerical results for the charm quark fugacity as a function of temperature. The T axis is reversed to correspond to the horizontal (time) axis in the left panel of Fig. 6.2. As a function of temperature, we see that all the fugacities first increase with the decreasing T and then start to drop until they reach the common universal solution for i) and ii) evolutions separately. At the pseudocritical temperature, $\lambda_c \neq 1$, therefore, in the QPM, the charm quarks will not reach the chemical equilibrium. In addition, at $T \simeq 0.2$ GeV and below, the hierarchy between the $\lambda_c(T)$ curves in i) and ii) case changes, and the fugacity in (2+1)D viscous QGP becomes larger than in 1D perfect medium, independently of the initial λ_0. This leads us to the conclusion that at the final stage of the QGP evolution, the resulting number of charm quarks will be higher when the QGP expands in all spatial dimensions with the shear viscosity considered.

6.3 Charm Quark Number

With the behavior of the charm quark fugacity at hand, we can investigate the evolution of the charm number density $n_c(\lambda_c)$ given by Eq. (6.4), and the resulting number of $c\bar{c}$,

$$N_{c\bar{c}}(\lambda_c, \tau) = n_c(\lambda_c)\, V(\tau), \tag{6.10}$$

where the number of charm quark pairs $N_{c\bar{c}}$ equals the product of their number density and the volume $V(\tau)$ of the deconfined matter. In the ii) case of (2+1)D-expanding viscous QGP, we determine the volume from [221, 225]

$$V(\tau) = \pi R^2(\tau)\, \tau, \tag{6.11}$$

with the transverse radius defined in Eq. (6.8). On the other hand, in i) expansion scheme of the perfect fluid propagating longitudinally, the volume does not change in the transverse plane, and the QGP is assumed to be a cylinder with a constant radius. Therefore in the above equation, for 1D evolution, we set $R(\tau) \to R = 7$ fm, which matches the initial radius of the viscous QGP in the ii) scenario.

Fig. 6.3 shows the number of charm quark pairs $N_{c\bar{c}}(\lambda_c, \tau)$ as a function of time (left) and decreasing temperature (right) in hot QCD medium evolving in space and time as described in i) and ii) scenarios. We study the behavior of charm quark number for the following initial values of $c\bar{c}$ pairs: $N_{c\bar{c}}^0 = 13.8$, 20 and 30 [219, 221], which correspond to the initial fugacity: $\lambda_c^0 \simeq 0.05$, 0.071 and 0.12, respectively [198].

While in the QGP obeying 1D perfect fluid scenario, the number of $c\bar{c}$ pairs first mildly grows with time and starts to decrease above $\tau \simeq 3 - 4$, we observe more intensive changes of $N_{c\bar{c}}$ in viscous QGP expanding in 2+1 dimensions, see left panel

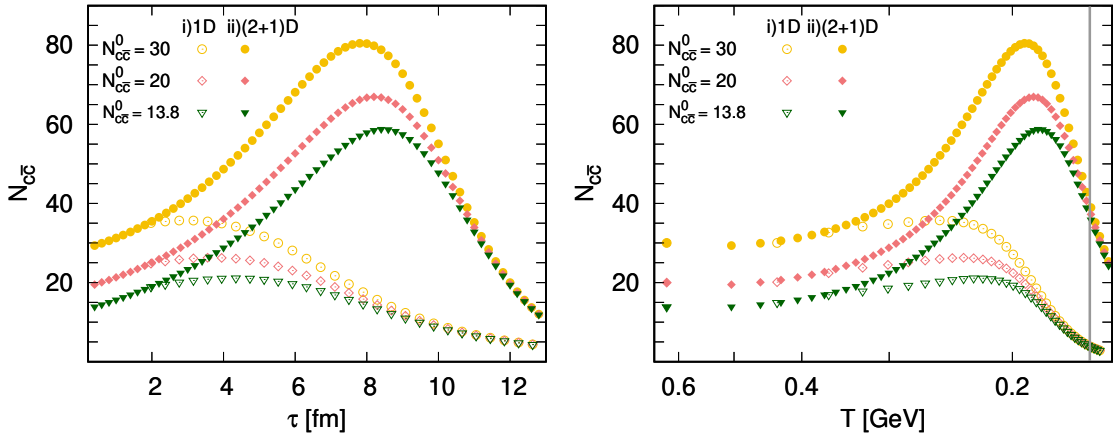

Rysunek 6.3: The number of charm quark pairs $N_{c\bar{c}}$ as a function of time τ (left) and temperature T (right) in the QGP with $N_f = 2 + 1$. The results obtained in the i) 1D case of perfect QGP are shown by open symbols, while full symbols represent the number of charm quarks in viscous QGP expanding additionally in the transverse plane, the ii) (2+1)D scenario. In both panels, the curves start from the initial conditions, $\tau_0 = 0.2$ fm (left) and $T_0 = 0.624$ GeV (right). The right panel additionally exhibits the QCD pseudocritical temperature (vertical line).

of Fig. 6.3. The number of quarks first rapidly increases, exhibiting a pronounced maximum at $\tau \simeq 8$ fm, and decreases afterward even faster, independently of the initial number of charm quark fugacity.

In both dynamical scenarios, we initially see that more charm quarks are produced in the QGP due to the creation and annihilation processes considered in Eq. (6.5). At some point, depending on the QGP dynamics and the initial number of charm quarks, the $c\bar{c}$ pairs start to annihilate, leading to the observation that the resulting curves overlap each other at high τ, i.e., in the vicinity of the pseudocritical temperature. This resembles the behavior of the fugacity λ_c shown in Fig. 6.2.

Further, in the right panel of Fig. 6.3, we readily notice that the maxima of the $N_{c\bar{c}}$ curves are shifted towards lower temperatures for higher initial values of the charm quark number. We also recognize that in perfect QGP described by i) scenario, the final number of the $c\bar{c}$ pairs is $N_{c\bar{c}} \simeq 5$, which is at least 2 times smaller than the numbers incorporated initially. Thus, in the i) framework, most of the charm quarks annihilate before the deconfined matter reaches the hadronic phase.

On the other hand, in the ii) viscous expansion, independent of the initial number of charm quarks, their final number reaches a value of $N_{c\bar{c}} \simeq 35$ at the corresponding time $\tau \simeq 11$ fm (see Fig. 6.1). This implies that in the QPM, all the initially considered heavy quarks survive the evolution of viscous QGP. For certain initial values, even more charm-anticharm pairs are produced, which differs from the experimental observations, where the charm quark number is closely preserved during the QGP evolution [2, 229].

The present QPM outcomes can also be juxtaposed to the alternative quasiparticle frameworks [219, 221], where due to the much shorter lifetime of the QGP, the final number of charm quarks is much higher than observed in Fig. 6.3. However, if we

consider that the QGP hadronizes at $\tau = 6 - 8$ fm, just as in [219, 221], we observe that $N_{c\bar{c}}$ is much higher and clearly depends on the initial value, compared to our actual results.

One should keep in mind that the results shown in Fig. 6.3 are obtained within the simplifying assumption that the light and strange quarks, as well as gluons, remain in chemical equilibrium, while the charm quarks do not contribute to the EoS. The first steps towards improving the current status require the extension of the QPM to QCD with $N_f = 2 + 1 + 1$ [230], and complementing the system of the differential equations, which should consider the out-of-equilibrium scenarios for all quasiparticles presented in the QGP. These are the tasks of our ongoing project, whose results will be reported elsewhere.

Rozdział 7

Conclusions

The main scope of this work was to investigate the transport and dynamical properties of the deconfined matter with different numbers of quark flavors and analyze the role of dynamical quarks and gluons in hot QCD at vanishing chemical potential. For this purpose, we have employed a well-established quasiparticle model (QPM) approach combined with kinetic theory in the relaxation time approximation.

The deconfined matter is described by the dynamical gluons (and quarks) carrying effective masses that depend on the self-energies originating from the hard thermal loop approach. The temperature- and coupling-dependent masses enter the quasiparticles' dispersion relations and are adjusted through the effective coupling to describe the equilibrium entropy density provided by first-principle lQCD simulations. Interestingly, the gluon thermal mass for pure Yang-Mills theory and QCD appeared to be compatible when plotted as a function of scaled temperature T/T_c. This is a consequence of the compensation of the N_f-dependence in the deconfinement transition temperature T_c and the gluon self-energy.

To verify the validity of the QPM to bulk thermodynamic quantities near the phase transition, we have computed the speed of sound squared, c_s^2, in the QPM and the hadron resonance gas model and confronted it with the corresponding lattice results. We found that the QPM captures exceptionally well not only the behavior at high temperature, but also that in the vicinity of the phase transition, and even slightly below T_c. The c_s^2 below but near T_c requires a tower of hadronic resonances, and this non-trivial physics is properly encoded in the effective coupling.

The transport parameters, such as the shear and bulk viscosity, the electrical conductivity, and their various relative ratios, were computed from the kinetic theory expressions, assuming that all transport coefficients are characterized by the common relaxation times τ_i. For the individual quasiparticle species, the τ_i were evaluated from the microscopic scattering amplitudes of the elementary two-body scatterings among the massive quarks and gluons.

We observed that the shear viscosity to entropy density ratio, η/s, exhibits a sharp minimum at T_c in pure Yang-Mills theory which coincides with the KSS bound, $1/4\pi$, conjectured via gauge-gravity duality. The result near T_c is consistent with all the available lattice data within the errors. Moreover, the behavior at tempera-

tures higher than $1.3\,T_c$ agrees fairly well with the functional diagrammatic approach [57]. Introducing quark-quasiparticles strongly modifies the temperature dependence of η/s in QCD with $N_f = 2+1$. The pronounced non-monotonic structure of the ratio at T_c in pure Yang-Mills theory is replaced by a smooth behavior with a shallow minimum around the pseudo-critical temperature in QCD. This modification is also reflected in the behavior of the quasiparticle relaxation times.

In contrast to the functional estimate of η/s for QCD reported in [57], our microscopic calculations reveal a major impact of the dynamics carried by quasiquarks as relevant effective d.o.f. on top of the gluons. The non-trivial dynamics of those quasiparticles enter the scattering cross sections, which significantly contribute to the specific shear viscosity. Another intriguing observation is that the quasiparticle approach in the QCD with quarks yields a scaled shear viscosity, η/T^3, comparable in magnitude to the perturbative QCD result at high temperatures.

We have also illustrated the impact of the large-angle scattering (LAS) approximation, which was applied to evaluate the energy-averaged transport cross sections. The LAS prescription leads to systematically larger contributions to η/s than employing fully isotropic cross sections.

In contrast to the specific shear viscosity, the bulk viscosity to entropy density ratio ζ/s has a more complex structure, thus requires a detailed analysis of its components, e.g., due to its dependence on the temperature derivative of the self-energies and the speed of sound squared. In pure Yang-Mills theory, we observed that the temperature derivative of the gluon effective mass yields a striking peak at the critical temperature and this, though much weakened, results in a mild non-monotonicity in the ratio ζ/s.

We have noticed that the specific bulk viscosity decreases as temperature increases, consistently to the general anticipation, and conformal invariance becomes restored at high temperature. The inclusion of the light and strange quasiquarks considerably modifies the ζ, as well as the entropy density s. For the QGP with $N_f = 2+1$, the ratio ζ/s does not exhibit any apparent non-monotonicity around the crossover. It decreases with increasing temperature much slower than in the $N_f = 0$ case, indicating a larger breaking of scale symmetry.

Given the bulk and shear viscosities, we constructed the ratio ζ/η to confront the linear and quadratic dependence on the measure $\Delta c_s^2 = 1/3 - c_s^2$ representing a deviation from conformal invariance. We found that the ratio scales linearly near T_c, as predicted in the AdS/CFT approach [203], then switches to the quadratic behavior consistently to the perturbative QCD result [54, 200]. The emerging changeover depends on the quark flavors: in pure Yang-Mills theory, it appears at $T \simeq 1.3\,T_c$, whereas in QCD with $N_f = 2+1$ at $T \simeq 2\,T_c$. Thus, the segment in temperature where one finds the system non-perturbative is interestingly extended in the presence of dynamical quarks. The QPM well captures the smooth but N_f-depending changeover to describe the non-perturbative and perturbative domains. Thus, we recognized a systematic connection between the two opposite QCD regimes. We also found that the presence of quasiquarks results in a significant delay in restoring conformal invariance at high temperature, compared with pure Yang-Mills thermo-

dynamics.

We additionally studied the electrical conductivity of the QGP with $N_f = 2 + 1$. The ratio σ/T is observed to be qualitatively consistent with earlier results in a class of the quasiparticle frameworks [101, 129], as well as with the recent lattice QCD results [119]. In particular, the individual contributions to the electrical conductivity were calculated separately for the light and strange quarks and confronted with the corresponding lattice data. Our outcomes are quantitatively close, though systematically lower than the lattice data, which is connected to the fact that the lQCD simulations were carried out for a heavy pion mass.

Further, we have investigated the behavior of the shear viscosity to electrical conductivity ratio, $(\eta/s)/(\sigma/T)$ and observed that it compensates the details of the effective coupling and masses but preserves the overall dependence on the relation between the relaxation times of gluons and quarks. Therefore, the ratio is a valuable quantity to compare the role of quarks and gluons in various effective models. We found a remarkable agreement with the $(\eta/s)/(\sigma/T)$ ratio deduced from the results of the alternative, dynamical quasiparticle model. The observed consistency justifies that both approaches identically accommodate the microscopic interactions between the QGP constituents, despite somewhat different quasiparticle treatments.

Finally, to illustrate the application of the specific shear viscosity, we have explored the evolution of the charm quark fugacity λ_c and the charm quark pairs $N_{c\bar{c}}$ in hot QCD medium with $N_f = 2 + 1$ quark flavors. For the evolution of the QGP, we have adopted the result of the hydrodynamic simulations of viscous QGP expanding in all spatial dimensions, i.e., (2+1)D [190]. We juxtapose this result to Bjorken flow, i.e., the longitudinal (1D) propagation of perfect fluid.

Solving the rate equation for the charm quark fugacity λ_c, we have observed that its behavior depends significantly on the QGP evolution scenario at its early stages. At the same time, as the system approaches the crossover, the dynamics of λ_c becomes universal. This observation is further transferred to the evolution of the number of $c\bar{c}$ pairs, where we have recognized that independently of the initial fugacity λ_c^0, in the QPM, all the solutions are attracted to the same value, individual for 1D and (2+1)D expansions. We have noticed in perfect QGP that the final number of charm quarks is much lower than the initial one. On the other hand, in viscous deconfined medium, for specific values of λ_c^0, the initial and final numbers of $c\bar{c}$ pairs are approximately equal, which coincides with the experimental outcomes.

We have quantified the impact of dynamical quarks on the significant transport parameters in hot QCD. The QPM was shown to provide a systematic link between the non-perturbative and perturbative physics relevant to the transport properties of the deconfined matter. Therefore, the framework developed in this Thesis can be straightforwardly applied to study other transport coefficients and their phenomenological impact on the QCD observables.

Besides, a more realistic estimate requires further extensions going beyond the major assumptions made in this Thesis, i.e., the vanishing baryon chemical potential, the approximation of the solution to Boltzmann equation with the momentum-

independent relaxation time, the application of the common relaxation times for all transport parameters, or the restriction to the binary scatterings only. Those can be implemented into our kinetic approach in the future, offering more reliable medium profiles of the transport coefficients.

Dodatek A

Scattering Amplitudes of Binary Processes

This Appendix contains a detailed computation of the squared scattering amplitudes, $|\mathcal{M}|^2$, of some binary elastic scatterings between massive particles. We work in the center-of-mass (c.m.) reference frame shown in Fig A.1.

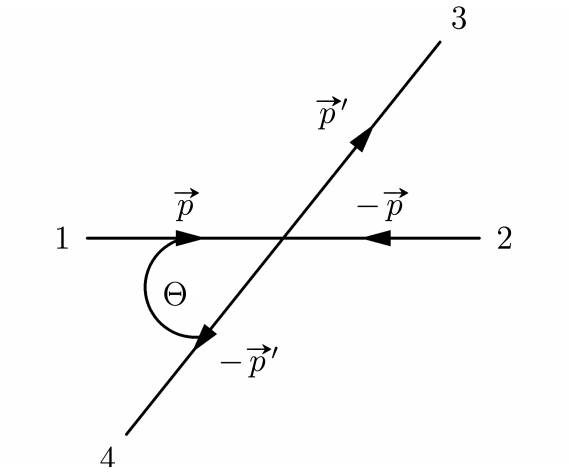

Rysunek A.1: Schematic illustration of the scattering in the center-of-mass frame, where (1,2) denotes the incoming and (3,4) the outgoing scattering partners, and θ is the scattering angle.

The scattering partners carry the momenta, defined as

$$p_i = (E_i, \vec{p}_i), \tag{A.1}$$

while their scalar (dot) product, considering metric tensor $g^{\mu\nu} = (1, -1, -1, -1)$, reads

$$p_i \cdot p_j = E_i E_j - \vec{p}_i \vec{p}_j, \tag{A.2}$$

with the energy $E_i = \sqrt{p_i^2 + m_i^2}$.

We introduce convenient Mandelstam variables, s, t, and u, defined as functions of

the four-momenta of the interacting particles in the c.m.,

$$s = (p_1 + p_2)^2 = m_1^2 + 2p_1 \cdot p_2 + m_2^2 = m_3^2 + 2p_3 \cdot p_4 + m_4^2, \tag{A.3}$$
$$t = (p_1 - p_3)^2 = m_1^2 - 2p_1 \cdot p_3 + m_3^2 = m_4^2 + m_2^2 - 2p_2 \cdot p_4, \tag{A.4}$$
$$u = (p_1 - p_4)^2 = m_1^2 - 2p_1 \cdot p_4 + m_4^2 = m_2^2 + m_3^2 - 2p_2 \cdot p_3. \tag{A.5}$$

It can be shown that in the massless limit, $s + u + t = 0$, while from the above expressions, we obtain

$$s + t + u = m_1^2 + m_2^2 + m_3^2 + m_4^2. \tag{A.6}$$

Further, using the properties of the c.m. frame, it can be shown that

$$E_1 + E_2 = E_3 + E_4 = \sqrt{s}, \tag{A.7}$$

which will be utilized in the following evaluation.

Once the scattering amplitude is known, the differential cross section for two-body scattering can be conveniently computed when expressed as a function of Mandelstam variables,

$$\frac{d\sigma}{dt} = \frac{|\mathcal{M}|^2}{16\pi[(s - m_1^2 - m_2^2)^2 - 4m_1^2 m_2^2]}. \tag{A.8}$$

A.1 $qq' \to qq'$

In this Section, we compute the scattering amplitude for the cross section of two different quark flavors, i.e., $u\,d \to u\,d$, $u\,s \to u\,s$, etc. Note that in our model $m_u = m_d \neq m_s$, therefore in the following derivation, we keep the general masses, $m_i = 1...4$ to prevent simplification of some terms when $m_1 = m_2$, which in case of $u\,s \to u\,s$ is not true.
The Feynman diagram describing the $qq' \to qq'$ process is of the $t-$channel type [4] and is shown in Fig. **??** Along with the $(1,2) \to (3,4)$ notation for incoming and outgoing particles, we additionally use $ij \to i'j'$ below to denote initial- and final-state color factors related to the SU(3) gauge group. The scattering amplitude related to Fig. A.1 reads

$$-i\mathcal{M} = \bar{u}(p_3, s_3)(-ig\gamma^\mu(t)^a_{i'i})u(p_1, s_1)\,\frac{-i\delta_{ab}g_{\mu\nu}}{p_g^2 - m_g^2}\,\bar{u}(p_4, s_4)(-ig\gamma^\nu(t)^b_{j'j})u(p_2, s_2) \tag{A.9}$$

Above, we follow the standard Feynmann rules [4], where $u(p_{i,j}, s_{i,j})$ is a spinor which denotes the incoming fermion with momentum $p_{i,j}$, spin $s_{i,j}$, and additionally with mass $m_{i,j} = m_{i',j'}$ which will explicitly enter the expressions later, and now is skipped to shorten the notation. The outgoing fermion spinor is $\bar{u}(p_{i',j'}, s_{i',j'})$, while $(-ig\gamma^\mu(t)^{a,b}_{i'i})$ denotes vertex and the gluon propagator in Feynmann gauge, mentioned in Section 4.2, reads

$$\frac{-i\delta_{ab}g_{\mu\nu}}{p_g^2 - m_g^2}. \tag{A.10}$$

Rearranging terms in Eq. (A.9) leads to

$$-i\mathcal{M} = ig^2\Big[\bar{u}(p_3,s_3)\gamma^\mu(t)^a_{i'i}u(p_1,s_1)\Big]\frac{\delta_{ab}g_{\mu\nu}}{p_g^2-m_g^2}\Big[\bar{u}(p_4,s_4)\gamma^\nu(t)^b_{j'j}u(p_2,s_2)\Big] = \quad (A.11)$$

$$ig^2(t^a)_{i'i}(t^a)_{j'j}\Big[\bar{u}(p_3,s_3)\gamma^\mu u(p_1,s_1)\Big]\frac{g_{\mu\nu}}{p_g^2-m_g^2}\Big[\bar{u}(p_4,s_4)\gamma^\nu u(p_2,s_2)\Big]. \quad (A.12)$$

$$-i\mathcal{M} = \frac{ig^2}{p_g^2-m_g^2}(t^a)_{i'i}(t^a)_{j'j}\Big[\bar{u}(p_3,s_3)\gamma^\mu u(p_1,s_1)\Big]g_{\mu\nu}\Big[\bar{u}(p_4,s_4)\gamma^\nu u(p_2,s_2)\Big] = \quad (A.13)$$

$$\frac{ig^2}{p_g^2-m_g^2}(t^a)_{i'i}(t^a)_{j'j}\Big[\bar{u}(p_3,s_3)\gamma^\mu u(p_1,s_1)\bar{u}(p_4,s_4)\gamma_\mu u(p_2,s_2)\Big]. \quad (A.14)$$

The squared amplitude is computed as

$$|\mathcal{M}|^2 = (-i\mathcal{M})(-i\mathcal{M})^*, \quad (A.15)$$

which explicitly reads

$$|\mathcal{M}|^2 = \left(\frac{g^2(t^a)_{i'i}(t^a)_{j'j}}{p_g^2-m_g^2}\right)^2\Big[\bar{u}(p_3,s_3)\gamma^\mu u(p_1,s_1)\bar{u}(p_4,s_4)\gamma_\mu u(p_2,s_2)\Big]$$
$$\times\Big[\bar{u}(p_3,s_3)\gamma^\nu u(p_1,s_1)\bar{u}(p_4,s_4)\gamma_\nu u(p_2,s_2)\Big]^*. \quad (A.16)$$

The parameters $(t^a)_{i'i}(t^a)_{j'j}$ are the SU(3) group theory factors, which for the calculation of the scattering cross section must be summed over final and averaged over initial quark colors. The detailed calculation can be found in [4]. Here, we utilize the resulting number, $((t^a)_{i'i}(t^a)_{j'j})^2 = 2/9$. We further apply to Eq. $(A.16)$ the conjugation property, $(\bar{u}_1\gamma_\mu u_2)^* = \bar{u}_2\gamma_\mu u_1$, reading

$$|\mathcal{M}|^2 = \frac{2}{9}\frac{g^4}{(p_g^2-m_g^2)^2}\Big[\bar{u}(p_3,s_3)\gamma^\mu u(p_1,s_1)\bar{u}(p_4,s_4)\gamma_\mu u(p_2,s_2)\Big]$$
$$\times\Big[\bar{u}(p_2,s_2)\gamma_\nu u(p_4,s_4)\bar{u}(p_1,s_1)\gamma^\nu u(p_3,s_3)\Big]. \quad (A.17)$$

Introducing indices in the two brackets above allows to change the order of terms, and naturally leads to the trace :

$$|\mathcal{M}|^2 = \frac{2}{9}\frac{g^4}{(p_g^2-m_g^2)^2}\Big[\bar{u}_a(p_3,s_3)\gamma^\mu_{ab}u_b(p_1,s_1)\bar{u}_c(p_4,s_4)\gamma_{\mu_{cd}}u_d(p_2,s_2)\Big]$$
$$\times\Big[\bar{u}_e(p_2,s_2)\gamma_{\nu_{ef}}u_f(p_4,s_4)\bar{u}_g(p_1,s_1)\gamma^\nu_{gh}u_h(p_3,s_3)\Big] = \quad (A.18)$$

$$= \frac{2}{9}\frac{g^4}{(p_g^2-m_g^2)^2}\Big[u_b(p_1,s_1)\bar{u}_g(p_1,s_1)\gamma^\nu_{gh}u_h(p_3,s_3)\bar{u}_a(p_3,s_3)\gamma^\mu_{ab}\Big]$$
$$\times\Big[u_d(p_2,s_2)\bar{u}_e(p_2,s_2)\gamma_{\nu_{ef}}u_f(p_4,s_4)\bar{u}_c(p_4,s_4)\gamma_{\mu_{cd}}\Big] = \quad (A.19)$$

$$\frac{2}{9}\frac{g^4}{(p_g^2-m_g^2)^2}\mathrm{Tr}\Big[u(p_1,s_1)\bar{u}(p_1,s_1)\gamma^\nu u(p_3,s_3)\bar{u}(p_3,s_3)\gamma^\mu\Big]$$
$$\times\,\mathrm{Tr}\Big[u(p_2,s_2)\bar{u}(p_2,s_2)\gamma_\nu u(p_4,s_4)\bar{u}(p_4,s_4)\gamma_\mu\Big]. \quad (A.20)$$

Under the traces presented in Eq. (A.20), we can use a spin summation, rule [4] for fermions,

$$\sum_{s_1} u(s_1,p_1)\bar{u}(s_1,p_1) = \not{p}_1 + M_1, \tag{A.21}$$

where $\not{p}_1 = \gamma^\mu p_\mu$, with Dirac matrix γ^μ. This leads to

$$|\mathcal{M}|^2 = \frac{2}{9}\frac{g^4}{(p_g^2 - m_g^2)^2}\mathrm{Tr}\Big[(\not{p}_1 + m_1)\gamma^\nu(\not{p}_3 + m_3)\gamma^\mu\Big]\mathrm{Tr}\Big[(\not{p}_2 + m_2)\gamma_\nu(\not{p}_4 + m_4)\gamma_\mu\Big]. \tag{A.22}$$

We now proceed with performing the traces,

$$\mathrm{Tr}[(\not{p}_1 + m_1)\gamma^\mu(\not{p}_3 + m_3)\gamma^\nu] = \tag{A.23}$$

$$\mathrm{Tr}[\not{p}_1\gamma^\mu\not{p}_3\gamma^\nu + \not{p}_1\gamma^\mu m_3\gamma^\nu + m_1\gamma^\mu\not{p}_3\gamma^\nu + m_1\gamma^\mu m_3\gamma^\nu] = \tag{A.24}$$

$$\mathrm{Tr}[p_{1\alpha}\gamma^\alpha\gamma^\mu p_{3\beta}\gamma^\beta\gamma^\nu + p_{1\alpha}\gamma^\alpha\gamma^\mu m_3\gamma^\nu + m_1\gamma^\mu p_{3\beta}\gamma^\beta\gamma^n u + m_1\gamma^\mu m_3\gamma^\nu] = \tag{A.25}$$

$$\mathrm{Tr}[p_{1\alpha}p_{3\beta}\gamma^\alpha\gamma^\mu\gamma^\beta\gamma^\nu + m_1m_3\gamma^\mu\gamma^\nu] = p_{1\alpha}p_{3\beta}\mathrm{Tr}[\gamma^\alpha\gamma^\mu\gamma^\beta\gamma^\nu] + m_1m_3\mathrm{Tr}[\gamma^\mu\gamma^\nu]. \tag{A.26}$$

The Dirac matrices obey various trace identities, among which we use [4]

$$\mathrm{Tr}[\gamma^\alpha\gamma^\mu\gamma^\beta\gamma^\nu] = 4(g^{\alpha\mu}g^{\beta\nu} - g^{\alpha\beta}g^{\mu\nu} + g^{\alpha\nu}g^{\mu\beta}), \tag{A.27}$$

$$\mathrm{Tr}[\gamma^\mu\gamma^\nu] = 4g^{\mu\nu}, \tag{A.28}$$

to rewrite Eq. (A.26) as

$$p_{1\alpha}p_{3\beta}\mathrm{Tr}[\gamma^\alpha\gamma^\mu\gamma^\beta\gamma^\nu] + m_1m_3\mathrm{Tr}[\gamma^\mu\gamma^\nu] = \tag{A.29}$$

$$p_{1\alpha}p_{3\beta}4(g^{\alpha\mu}g^{\beta\nu} - g^{\alpha\beta}g^{\mu\nu} + g^{\alpha\nu}g^{\mu\beta}) + 4m_1m_3g^{\mu\nu} = \tag{A.30}$$

$$4(p_{1\alpha}g^{\alpha\mu}p_{3\beta}g^{\beta\nu} - p_{1\alpha}g^{\alpha\beta}p_{3\beta}g^{\mu\nu} + p_{1\alpha}g^{\alpha\nu}p_{3\beta}g^{\mu\beta}) + 4m_1m_3g^{\mu\nu} = \tag{A.31}$$

$$4(p_1^\mu p_3^\nu - p_1\cdot p_3\ g^{\mu\nu} + p_1^\nu p_3^\mu) + 4m_1m_3g^{\mu\nu} = \tag{A.32}$$

$$4(p_1^\mu p_3^\nu + p_1^\nu p_3^\mu) + 4(m_1m_3 - p_1\cdot p_3)g^{\mu\nu}. \tag{A.33}$$

Similarly, for second trace in Eq. (A.22) we have

$$\mathrm{Tr}[(\not{p}_2 + m_2)\gamma_\mu(\not{p}_4 + m_4)\gamma_\nu] = 4(p_{2\mu}p_{4\nu} + p_{2\nu}p_{3\mu}) + 4(m_2m_4 - p_2\cdot p_4)g_{\mu\nu}. \tag{A.34}$$

Inserting Eqs. (A.33) and (A.34) into Eq. (A.22), we arrive at

$$|\mathcal{M}|^2 = \frac{2}{9}\frac{g^4}{(p_g^2 - m_g^2)^2}\Big[4(p_1^\mu p_3^\nu + p_1^\nu p_3^\mu) + 4(m_1m_3 - p_1\cdot p_3)g^{\mu\nu}\Big]$$

$$\times\Big[4(p_{2\mu}p_{4\nu} + p_{2\nu}p_{3\mu}) + 4(m_2m_4 - p_2\cdot p_4)g_{\mu\nu}\Big] = \tag{A.35}$$

$$\frac{16}{9}\frac{g^4}{(p_g^2 - m_g^2)^2}\Big[p_1^\mu p_3^\nu p_{2\mu}p_{4\nu} + p_1^\mu p_3^\nu p_{2\nu}p_{3\mu} + p_1^\mu p_3^\nu m_2m_4g_{\mu\nu} + \cdots\Big], \tag{A.36}$$

where for all terms in the bracket, we perform the four-vector dot product, e.g.,

$$p_1^\mu p_3^\nu p_{2\mu} p_{4\nu} = (p_1^\mu p_{2\mu})(p_3^\nu p_{4\nu}) = (p_1 \cdot p_2)(p_3 \cdot p_4), \tag{A.37}$$

which leads us to

$$\begin{aligned}|\mathcal{M}|^2 = \frac{16}{9}\frac{g^4}{(p_g^2 - m_g^2)^2}\Big[&(p_1 \cdot p_2)(p_3 \cdot p_4) + (p_1 \cdot p_4)(p_3 \cdot p_2) + (p_1 \cdot p_3)m_2 m_4 \\ &-(p_1 \cdot p_3)(p_2 \cdot p_4) + (p_1 \cdot p_4)(p_3 \cdot p_2) + (p_1 \cdot p_2)(p_3 \cdot p_4) + (p_1 \cdot p_3)m_2 m_4 \\ &-(p_1 \cdot p_3)(p_2 \cdot p_4) + 2(p_2 \cdot p_4)m_1 m_3 + m_1 m_2 m_3 m_4 g_{\mu\nu} g^{\mu\nu} \\ &-m_1 m_3 (p_2 \cdot p_4) g_{\mu\nu} g^{\mu\nu} - (p_1 \cdot p_3)(p_2 \cdot p_4) - (p_1 \cdot p_3)(p_2 \cdot p_4) \\ &-(p_1 \cdot p_3)m_2 m_4 g_{\mu\nu} g^{\mu\nu} + (p_1 \cdot p_3)(p_2 \cdot p_4) g_{\mu\nu} g^{\mu\nu}\Big].\end{aligned} \tag{A.38}$$

Collecting the same terms, and using $g_{\mu\nu} g^{\mu\nu} = 4$, the squared amplitude significantly simplifies to

$$\begin{aligned}|\mathcal{M}|^2 = \frac{16}{9}\frac{g^4}{(p_g^2 - m_g^2)^2}\Big[&(p_1 \cdot p_2)(p_3 \cdot p_4) + (p_1 \cdot p_4)(p_3 \cdot p_2) \\ &-(p_1 \cdot p_3)m_2 m_4 - (p_2 \cdot p_4)m_1 m_3 + 2m_1 m_2 m_3 m_4\Big].\end{aligned} \tag{A.39}$$

One can recognize the four-momentum scalar products entering the above expression with the definitions of the Mandelstam variables, therefore it is convenient to rewrite $|\mathcal{M}|^2$ in terms of s, t, u given by Eqs. (A.3) – (A.5),

$$\begin{aligned}|\mathcal{M}|^2 = \frac{16}{9}\frac{g^4}{(p_g^2 - m_g^2)^2}\Big[&\frac{s - m_1^2 - m_2^2}{2}\,\frac{s - m_3^2 - m_4^2}{2} + \frac{-u + m_1^2 + m_4^2}{2}\,\frac{-u + m_2^2 + m_3^2}{2} \\ &-m_2 m_4 \frac{-t + m_1^2 + m_3^2}{2} - m_1 m_3 \frac{-t + m_4^2 + m_2^2}{2} + 2m_1 m_2 m_3 m_4\Big]\end{aligned} \tag{A.40}$$

We recall that the calculation is performed for $qq' \to qq'$ scattering, therefore $m_1 = m_3$ and $m_2 = m_4$, while the momentum transfer, i.e., the gluon momentum, reads $p_g^2 = t$, since the diagram of this scattering is of the t-channel type [4]. With these modifications, the squared amplitude becomes

$$\begin{aligned}|\mathcal{M}|^2 = \frac{16}{9}\frac{g^4}{(t - m_g^2)^2}\Big[&\frac{(s - m_1^2 - m_2^2)^2}{4} + \frac{(-u + m_1^2 + m_2^2)^2}{4} \\ &+m_2^2 \frac{t - 2m_1^2}{2} + m_1^2 \frac{t - 2m_2^2}{2} + 2m_1^2 m_2^2\Big] =\end{aligned} \tag{A.41}$$

$$\begin{aligned}\frac{16}{9}\frac{g^4}{(t - m_g^2)^2}\Big[&\frac{(s - m_1^2 - m_2^2)^2}{4} + \frac{(-u + m_1^2 + m_2^2)^2}{4} \\ &+m_2^2\Big(\frac{t - 2m_1^2}{2} + m_1^2\Big) + m_1^2\Big(\frac{t - 2m_2^2}{2} + m_2^2\Big)\Big] =\end{aligned} \tag{A.42}$$

$$\frac{16}{9}\frac{g^4}{(t - m_g^2)^2}\Big[\frac{(s - m_1^2 - m_2^2)^2}{4} + \frac{(-u + m_1^2 + m_2^2)^2}{4} + \frac{t(m_1^2 + m_2^2)}{2}\Big]. \tag{A.43}$$

Now we eliminate the variable u, using Eq. (A.6), obtaining the final expression for the scattering amplitude squared mentioned in Section 4.2,

$$|\mathcal{M}|^2 = \frac{16}{9}\frac{g^4}{(t-m_g^2)^2}\Big[\frac{(s-m_1^2-m_2^2)^2}{4} + \frac{(s+t-m_1^2-m_2^2)^2}{4} + \frac{t(m_1^2+m_2^2)}{2}\Big]. \quad \text{(A.44)}$$

Combining the two above equations and setting $m_i = 0$, we obtain the exact expression provided in [4] for $ud \to ud$ cross section.

Applying the crossing symmetry [4] to Eq. (A.44), i.e., by crossing t and s channels, one can straightforwardly obtain the amplitudes for the $q\bar{q} \to q'\bar{q}'$ scatterings.

A.2 $q\bar{q} \to q\bar{q}$ cross section

In this Section we provide the detailed computation of the scattering amplitude for the $q\bar{q} \to q\bar{q}$ process, i.e., for quarks and antiquarks all of the same flavor, $u\bar{u} \to u\bar{u}$, etc. These cross sections are described by the two Feynman diagrams, in s and t channels, therefore the total squared amplitude will be obtained from.

$$|\mathcal{M}|^2 = |\mathcal{M}_s|^2 + |\mathcal{M}_t|^2 + 2\mathcal{M}_s\mathcal{M}_t^* \quad \text{(A.45)}$$

s channel

We now simplify our notation as $u(p_i, s_i) = u_i$, and introduce v_i ($\bar{v}_i$) denoting the incoming (outgoing) antiparticle spinor, with different spin-summation rule,

$$\sum_{s_1} v(s_1,p_1)\bar{v}(s_1,p_1) = \not{p}_1 - M_1. \quad \text{(A.46)}$$

For the diagram in s channel, the scattering amplitude reads

$$-i\mathcal{M}_s = \bar{v}_2(-ig\gamma^\mu t^a_{ij})u_1 - \frac{-i\delta_{ab}g_{\mu\nu}}{p^2-m_g^2}\bar{u}_3(-ig\gamma^\nu t^b_{i'j'})v_4 = \quad \text{(A.47)}$$

$$\frac{g^2}{p_g^2-m_g^2}t^a_{ij}t^a_{i'j'}(\bar{v}_2\gamma^\mu u_1)(\bar{u}_3\gamma_\mu v_4). \quad \text{(A.48)}$$

When squared, the amplitude can be evaluated step-by-step using the techniques presented in the previous section:

$$|\mathcal{M}_s|^2 = \frac{2}{9}\frac{g^4}{(p_g^2-m_g^2)^2}(\bar{v}_2\gamma^\mu u_1)(\bar{u}_3\gamma_\mu v_4)(\bar{v}_4\gamma_\nu u_3)(\bar{u}_1\gamma^\nu v_2) = \cdots = \quad \text{(A.49)}$$

$$\frac{2}{9}\frac{g^4}{(p_g^2-m_g^2)^2}\mathrm{Tr}\left[(\not{p}_2 - m_2)\gamma^\mu(\not{p}_1 + m_1)\gamma^\nu\right]\ \mathrm{Tr}\left[(\not{p}_4 - m_4)\gamma_\mu(\not{p}_3 + m_3)\gamma_\nu\right] = \quad \text{(A.50)}$$

$$\frac{2}{9}\frac{g^4}{(p_g^2-m_g^2)^2}\mathrm{Tr}\left[p_{2\alpha}\gamma^\alpha\gamma^\mu p_{1\beta}\gamma^\beta\gamma^\nu + p_{2\alpha}\gamma^\alpha\gamma^\mu m_1\gamma^\nu - m_2\gamma^\mu p_{1\beta}\gamma^\beta\gamma^\nu - m_2\gamma^\mu m_1\gamma^\nu\right]$$

$$\times\,\mathrm{Tr}\left[p_{4\alpha}\gamma^\alpha\gamma_\mu p_{3\beta}\gamma^\beta\gamma_\nu - m_4\gamma_\mu m_3\gamma_\nu\right] = \quad \text{(A.51)}$$

$$\frac{2}{9}\frac{g^4}{(p_g^2-m_g^2)^2}\Big(p_{2\alpha}p_{1\beta}\mathrm{Tr}[\gamma^\alpha\gamma^\mu\gamma^\beta\gamma^\nu] - m_2m_1\mathrm{Tr}[\gamma^\mu\gamma^\nu]\Big)$$

$$\times\Big(p_{4\alpha}p_{3\beta}\mathrm{Tr}[\gamma^\alpha\gamma_\mu\gamma^\beta\gamma_\nu] - m_4m_3\mathrm{Tr}[\gamma_\mu\gamma_\nu]\Big) \quad \text{(A.52)}$$

Above, $\mathrm{Tr}[p_{2\alpha}\gamma^\alpha\gamma^\mu m_1\gamma^\nu] = \mathrm{Tr}[m_2\gamma^\mu p_{1\beta}\gamma^\beta\gamma^\nu] = 0$ due to the product of the odd number of Dirac matrices. Similar terms are therefore neglected under the second trace in Eq. (A.51).

Using the trace identities

$$\mathrm{Tr}[\gamma^\mu\gamma^\nu\gamma^\rho\gamma^\sigma] = 4(g^{\mu\nu}g^{\rho\sigma} - g^{\mu\rho}g^{\nu\sigma} + g^{\mu\sigma}g^{\nu\rho}), \tag{A.53}$$

$$\mathrm{Tr}[\gamma^\mu\gamma^\nu] = 4g^{\mu\nu}, \tag{A.54}$$

we get:

$$|\mathcal{M}_s|^2 = \frac{2}{9}\frac{g^4}{(p_g^2 - m_g^2)^2}\Big(p_{2\alpha}p_{1\beta}\,4(g^{\alpha\mu}g^{\beta\nu} - g^{\alpha\beta}g^{\mu\nu} + g^{\alpha\nu}g^{\mu\beta}) - m_2m_1 4g^{\mu\nu}\Big)$$
$$\times\Big(p_{4\alpha}p_{3\beta}\,4(g^\alpha_\mu g^\beta_\nu - g^{\alpha\beta}g_{\mu\nu} + g^\alpha_\nu g^\beta_\mu) - m_3m_4 4g_{\mu\nu}\Big) = \tag{A.55}$$

$$\frac{8}{9}\frac{g^4}{(p_g^2 - m_g^2)^2}[p_2^\mu p_1^\nu - (p_2\cdot p_1)g^{\mu\nu} + p_2^\nu p_1^\mu - m_2m_1g^{\mu\nu}]$$
$$\times[p_{4\mu}p_{3\nu} - (p_4\cdot p_3)g_{\mu\nu} + p_{4\nu}p_{3\mu} - m_3m_4g_{\mu\nu}] = \tag{A.56}$$

$$\frac{8g^4}{9(p_g^2 - m_g^2)^2}\Big[p_2^\mu p_{4\mu}p_1^\nu p_{3\nu} - (p_4\cdot p_3)p_2^\mu g_{\mu\nu}p_1^\nu + p_2^\mu p_{3\mu}p_1^\nu p_{4\nu} - m_3m_4p_2^\mu g_{\mu\nu}p_1^\nu$$
$$-(p_2\cdot p_1)p_{4\mu}g^{\mu\nu}p_{3\nu} + (p_2\cdot p_1)(p_4\cdot p_3)g_{\mu\nu}g^{\mu\nu} - (p_2\cdot p_1)p_{4\nu}g^{\mu\nu}p_{3\mu}$$
$$+(p_2\cdot p_1)m_3m_4g^{\mu\nu}g_{\mu\nu} + p_2^\nu p_{3\nu}p_1^\mu p_{4\mu} - (p_4\cdot p_3)p_2^\nu g_{\mu\nu}p_1^\mu + p_2^\nu p_{4\nu}p_1^\mu p_{3\mu}$$
$$-m_3m_4p_2^\nu g_{\mu\nu}p_1^\mu - m_2m_1p_{4\mu}g^{\mu\nu}p_{3\nu}$$
$$+m_2m_1(p_4\cdot p_3)g^{\mu\nu}g_{\mu\nu} - m_2m_1p_{4\nu}g^{\mu\nu}p_{3\mu} + m_1m_2m_3m_4g^{\mu\nu}g_{\mu\nu}\Big]. \tag{A.57}$$

We then rewrite the four-vector products and collect similar terms in the bracket,

$$\Big[\underline{(p_2\cdot p_4)(p_1\cdot p_3)} - \underline{\underline{(p_4\cdot p_3)(p_2\cdot p_1)}} + \underbrace{(p_2\cdot p_3)(p_1\cdot p_4)} - m_3m_4(p_2\cdot p_1)$$
$$-\underline{\underline{(p_2\cdot p_1)(p_4\cdot p_3)}} + \underline{\underline{4(p_2\cdot p_1)(p_4\cdot p_3)}} - \underline{\underline{(p_2\cdot p_1)(p_4\cdot p_3)}} + 4m_3m_4(p_2\cdot p_1)$$
$$+\underbrace{(p_2\cdot p_3)(p_1\cdot p_4)} - \underline{\underline{(p_4\cdot p_3)(p_2\cdot p_1)}} + \underline{(p_2\cdot p_4)(p_1\cdot p_3)} - m_3m_4(p_2\cdot p_1)$$
$$-m_2m_1(p_4\cdot p_3) + 4m_2m_1(p_4\cdot p_3) - m_2m_1(p_4\cdot p_3) + 4m_1m_2m_3m_4\Big], \tag{A.58}$$

and insert it to the Eq. (A.57), obtaining

$$|\mathcal{M}_s|^2 = \frac{8g^4}{9(p_g^2 - m_g^2)^2}\Big[2(p_2\cdot p_4)(p_1\cdot p_3) + 2(p_2\cdot p_3)(p_1\cdot p_4) +$$
$$2m_3m_4(p_2\cdot p_1) + 2m_2m_1(p_4\cdot p_3) + 4m_1m_2m_3m_4\Big] \tag{A.59}$$

Using Mandelstam variables from Eqs. (A.3) – (A.5), and the fact that in the s channel, the momentum transfer is $p_g^2 = s$, we finally get:

$$|\mathcal{M}_s|^2 = \frac{8g^4}{9(p_g^2 - m_g^2)^2}\Big[\frac{(t-2m_2^2)(t-2m_1^2)}{2} + \frac{(u-m_1^2-m_2^2)^2}{2} + 2m_1m_2(s-m_1^2-m_2^2) + 4m_1^2m_2^2\Big] \tag{A.60}$$

t channel

The second diagram for this process is in the t channel,

$$i\mathcal{M}_t = \bar{u}_3(-ig\gamma^\mu t^a_{ii'})u_1\Big(\frac{-i\delta^{ab}g_{\mu\nu}}{p_g^2 - m_g^2}\Big)\bar{v}_2(-i\gamma^\nu g t^b_{jj'})v_4. \tag{A.61}$$

When squared, the scattering amplitude reads

$$|\mathcal{M}_t|^2 = \frac{2}{9}\frac{g^4}{(p_g^2 - m_g^2)^2}(\bar{u}_3\gamma^\mu u_1)(\bar{v}_2\gamma_\mu v_4)(\bar{v}_4\gamma_\mu v_2)(\bar{u}_1\gamma^\mu u_3) = \tag{A.62}$$

$$\frac{2}{9}\frac{g^4}{(p_g^2 - m_g^2)^2}\mathrm{Tr}[(\not{p}_3 + m_3)\gamma^\mu(\not{p}_1 + m_1)\gamma^\nu]\ \mathrm{Tr}[(\not{p}_4 - m_4)\gamma_\mu(\not{p}_2 - m_2)\gamma_\nu] = \tag{A.63}$$

$$\frac{8g^4}{9(p_g^2 - m_g^2)^2}[p_3^\mu p_1^\nu - (p_3\cdot p_1)g^{\mu\nu} + p_3^\nu p_1^\mu + m_1m_3g^{\mu\nu}]$$

$$\times[p_{4\mu}p_{2\nu} - (p_4\cdot p_2)g_{\mu\nu} + p_{4\nu}p_{2\mu} + m_4m_2g_{\mu\nu}] = \cdots = \tag{A.64}$$

$$\frac{8g^4}{9(t-m_g^2)^2}\Big[\frac{(s-m_1^2-m_2^2)^2}{2} + \frac{(u-m_1^2-m_2^2)^2}{2} + t(m_1^2+m_2^2)\Big] \tag{A.65}$$

$s-t$ cross term

In Eq. (A.45), the final term is still missing, which is the cross term between the two channels, $\mathcal{M}_s\mathcal{M}_t^*$. The step-by-step evaluation can be performed by the reader based on the previously given scheme. We provide the final expression, reading

$$\mathcal{M}_s\mathcal{M}_t^* = -\frac{16g^4}{27(s-m_g^2)(t-m_g^2)}$$
$$\times\Big[\frac{(u-m_1^2-m_2^2)^2}{2} - \frac{t(m_1^2+m_2^2)}{2} + m_1m_2(u-s)\Big]. \tag{A.66}$$

Collecting all the terms, we obtain the total squared amplitude of the following form

$$|\mathcal{M}|^2 = |\mathcal{M}_s|^2 + |\mathcal{M}_t|^2 + 2\mathcal{M}_s\mathcal{M}_t^* =$$
$$\frac{8g^4}{9}\Bigg[\frac{1}{(s-m_g^2)^2}\Big\{\frac{(t-2m_2^2)(t-2m_1^2)}{2} + \frac{(u-m_1^2-m_2^2)^2}{2} + 4m_1^2m_2^2$$
$$+2m_1m_2(s-m_1^2-m_2^2)\Big\}$$
$$+\frac{1}{(t-m_g^2)^2}\Big\{\frac{(s-m_1^2-m_2^2)^2}{2} + \frac{(u-m_1^2-m_2^2)^2}{2} + t(m_1^2+m_2^2)\Big\}$$
$$-\frac{2}{3}\frac{1}{(s-m_g^2)(t-m_g^2)}\Big\{\frac{(u-m_1^2-m_2^2)^2}{2} - \frac{t(m_1^2+m_2^2)}{2} + m_1m_2(u-s)\Big\}\Bigg]. \quad \text{(A.67)}$$

Our final expression can be further simplified by eliminating the u variable. We note that for $m_i = 0$, Eq. (A.67) corresponds to the results presented in [4] for $u\bar{u} \to u\bar{u}$ scattering of massless quarks. Moreover, from the above equation, one can obtain other two-body scattering amplitudes from the associated symmetries. Crossing s and u channels delivers the amplitude for the $qq \to qq$ and $\bar{q}\bar{q} \to \bar{q}\bar{q}$ scatterings [4,60].

Dodatek B

Large Angle Scattering Approximation

As stated in Section 4.2, the scatterings with large angle dominate the momentum transfer and therefore considered relevant in the evaluation of the transport parameters. Therefore, in order to compute the transport cross sections under the large angle scattering (LAS) assumption considered in Eq. (4.12), one needs to evaluate a phenomenological weight-factor $\sin^2\theta$, which depends on masses of the (quasi)particles participating in the scattering.

Following Fig. A.1, the scattering angle in the c.m. frame can be expressed in terms of Mandelstam variables as

$$\vec{p}\cdot\vec{p}' = |\vec{p}|\cdot|\vec{p}'|\cos\theta. \tag{B.1}$$

We can further specify the four-vector product between the initial and final states,

$$p_1\cdot p_3 = E_1E_3 - |\vec{p}_1||\vec{p}_3|\cos\theta. \tag{B.2}$$

Combining that with the definition of Mandelstam variable t and Eq. (A.6), we obtain the scattering angle expressed in terms of Mandelstam variables and the (quasi)particle masses,

$$\cos\theta = \frac{s(t-u)+(m_1^2-m_2^2)(m_3^2-m_4^2)}{\sqrt{\lambda(s,m_1^2,m_2^2)}\sqrt{\lambda(s,m_3^2,m_4{}^2)}}, \tag{B.3}$$

with $\lambda(a,b,c)$ given by

$$\begin{gathered}\lambda(a,b,c) = a^2+b^2+c^2-2ab-2ac-2bs = \\ [a-(\sqrt{b}+\sqrt{c})^2][a-(\sqrt{b}-\sqrt{c})^2] = a^2-2a(b+c)+(b-c)^2.\end{gathered} \tag{B.4}$$

The $\sin^2\theta$ factor is then computed from the trigonometric identity

$$\begin{gathered}\sin^2\theta = 1-\cos^2\theta = \\ 1-\frac{[s(t-u)+(m_1^2-m_2^2)(m_3^2-m_4^2)]^2}{[s^2-2s(m_1^2+m_2^2)+(m_1^2-m_2^2)^2]\,[s^2-2s(m_3^2+m_4^2)+(m_3^2-m_4^2)^2]}\,.\end{gathered} \tag{B.5}$$

Now we can simplify the above equation to the case when $m_1=m_2=m_3=m_4$, which corresponds to the scatterings $qq\to qq$, $q\bar{q}\to q\bar{q}$, and $gg\to gg$, considered

in this Thesis. Using the relations between Mandelstam variables for particles with identical masses, $s+t+u=4m^2$, i.e., $u=4m^2-s-t$, we get

$$sin^2\theta = 1 - \frac{[s(t-u)]^2}{[s^2-4sm^2]\,[s^2-4sm^2]} = 1 - \frac{s^2(t-4m^2+s+t)^2}{[s^2-4sm^2]^2} = \tag{B.6}$$

$$\frac{[s-4m^2]^2-(2t+s-4m^2)^2}{[s-4m^2]^2} = \frac{-4t(t+s-4m^2)}{[s-4m^2]^2}, \tag{B.7}$$

which corresponds to the result given in [61] for $u\bar{u} \to u\bar{u}$ scattering studied in the NJL model.

There are other explicit forms of $\sin^2\theta$, depending on the masses of initial and final paticles. For example, for scatterings of the type $q\bar{q} \to q'\bar{q}', q\bar{q} \leftrightarrow gg$, where identical masses of initial states differ from the masses of final ones, i.e, $m_1 = m_2$ and, separately, $m_3 = m_4$.

In Eq. (B.5), we, therefore, change the notation to identify equal masses. Using $m_2 \to m_1$ and $m_4 \to m_3$, we get

$$\sin^2\theta = 1 - \frac{[s(t-u)]^2}{[s^2-2s(m_1^2+m_1^2)]\,[s^2-2s(m_3^2+m_3^2)]} = \tag{B.8}$$

$$1 - \frac{s^2(t-(2m_1^2+2m_3^2-t-s))^2}{s(s-4m_1^2)\,s(s-4m_3^2)} = 1 - \frac{(2t+s-2m_1^2-2m_3^2)^2}{(s-4m_1^2)\,(s-4m_3^2)} = \tag{B.9}$$

$$-\frac{4[m_1^4+m_3^4-2m_3^2t-2m_1^2(m_3^2+t)+t(s+t)]}{(s-4m_1^2)(s-4m_3^2)}. \tag{B.10}$$

Finally, $\sin^2\theta$ for the processes with $m_1 = m_3$ and outgoing $m_2 = m_4$, such as $qq' \to qq'$, $q\bar{q}' \to q\bar{q}'$, or $qg \to qg$. Simplifying Eq. (B.5) by using $m_3 \to m_1,\ m_4 \to m_2$, the scattering angle reads

$$\sin^2\theta = 1 - \frac{[s(t-u)+(m_1^2-m_2^2)^2]^2}{[s^2-2s(m_1^2+m_2^2)+(m_1^2-m_2^2)^2]^2} = \tag{B.11}$$

$$1 - \frac{[s(2t+s-2m_1^2-2m_2^2)+(m_1^2-m_2^2)^2]^2}{[s^2-2s(m_1^2+m_2^2)+(m_1^2-m_2^2)^2]^2} = \tag{B.12}$$

$$-\frac{4st[m_1^4+m_2^4-2m_2^2s-2m_1^2(m_2^2+s)+s(s+t)]}{[s^2-2s(m_1^2+m_2^2)+(m_1^2-m_2^2)^2]^2}. \tag{B.13}$$

We note that the formulas obtained above are valid not only for quasiparticles with medium-dependent masses but for any scatterings of particles, i.e., with constant masses, as well as with vanishing masses. For the latter, one obtains the relevant expressions by setting $m_i = 0$.

Bibliografia

[1] B. Friman, C. Hohne, J. Knoll, S. Leupold, J. Randrup, R. Rapp, and P. Senger, eds., The CBM physics book: Compressed baryonic matter in laboratory experiments, *Lect. Notes in Phys.* 814, 2011.

[2] A. Andronic, P. Braun-Munzinger, K. Redlich, and J. Stachel, Decoding the phase structure of QCD via particle production at high energy, *Nature* 561, 7723, 321–330, 2018.

[3] P. A. Zyla *et al.*, Review of Particle Physics, *PTEP* 8, 083C01, 2020.

[4] M. E. Peskin and D. V. Schroeder, An Introduction to quantum field theory. *Reading, USA: Addison-Wesley,* 1995.

[5] K. G. Wilson, Confinement of quarks, *Phys. Rev. D* 10, 2445–2459, 1974.

[6] W. Florkowski, Phenomenology of Ultra-Relativistic Heavy-Ion Collisions. *World Scientific*, 2010.

[7] D. J. Gross and F. Wilczek, Ultraviolet behavior of non-abelian gauge theories, *Phys. Rev. Lett.* 30, 1343–1346, 1973.

[8] H. D. Politzer, Reliable perturbative results for strong interactions?, *Phys. Rev. Lett.* 30, 1346–1349, 1973.

[9] Y. Nambu and G. Jona-Lasinio, Dynamical Model of Elementary Particles Based on an Analogy with Superconductivity. I., *Phys. Rev.* 122, 345–358, 1961.

[10] D. Blaschke, K. Redlich, C. Sasaki, and L. Turko, eds., Understanding the Origin of Matter: Perspectives in Quantum Chromodynamics, *Lect. Notes in Phys.* 999, 2022.

[11] L. Turko, Looking for the Phase Transition—Recent NA61/SHINE Results, *Universe* 4, 3, 52, 2018.

[12] M. G. Alford, A. Schmitt, K. Rajagopal, and T. Schäfer, Color superconductivity in dense quark matter, *Rev. Mod. Phys.* 80, 1455–1515, 2008.

[13] J. P. Blaizot, E. Iancu and A. Rebhan, Thermodynamics of the high temperature quark gluon plasma, [arXiv:hep-ph/0303185 [hep-ph]], 2003.

[14] S. Borsanyi, J. N. Guenther, R. Kara, Z. Fodor, P. Parotto, A. Pasztor, C. Ratti, and K. K. Szabo, Resummed lattice QCD equation of state at finite baryon density: Strangeness neutrality and beyond, *Phys. Rev. D* 105, 11, 114504, 2022.

[15] E. Shuryak, Physics of Strongly coupled Quark-Gluon Plasma, *Prog. Part. Nucl. Phys.* 62, 48–101, 2009.

[16] B. V. Jacak and B. Muller, The exploration of hot nuclear matter, *Science* 337, 310–314, 2012.

[17] M. Luzum and P. Romatschke, Conformal Relativistic Viscous Hydrodynamics: Applications to RHIC results at $\sqrt{s_{NN}} = 200$ GeV, *Phys. Rev. C* 78, 034915, 2008. [Erratum: Phys.Rev.C 79, 039903 (2009)].

[18] D. Teaney, J. Lauret, and E. V. Shuryak, Flow at the SPS and RHIC as a quark gluon plasma signature, *Phys. Rev. Lett.* 86, 4783–4786, 2001.

[19] P. Huovinen, P. F. Kolb, U. W. Heinz, P. V. Ruuskanen, and S. A. Voloshin, Radial and elliptic flow at RHIC: Further predictions, *Phys. Lett. B* 503, 58–64, 2001.

[20] T. Hirano and K. Tsuda, Collective flow and two pion correlations from a relativistic hydrodynamic model with early chemical freezeout, *Phys. Rev. C* 66, 054905, 2002.

[21] W. Broniowski, M. Chojnacki, W. Florkowski, and A. Kisiel, Uniform Description of Soft Observables in Heavy-Ion Collisions at $\sqrt{s_{NN}} = 200$ GeV, *Phys. Rev. Lett.* 101, 022301, 2008.

[22] B. Schenke, S. Jeon, and C. Gale, (3+1)D hydrodynamic simulation of relativistic heavy-ion collisions, *Phys. Rev. C* 82, 014903, 2010.

[23] U. W. Heinz, The Strongly coupled quark-gluon plasma created at RHIC, *J. Phys. A* 42, 214003, 2009.

[24] H. Song and U. W. Heinz, Extracting the QGP viscosity from RHIC data - A Status report from viscous hydrodynamics, *J. Phys. G* 36, 064033, 2009.

[25] B. Schenke, S. Jeon, and C. Gale, Anisotropic flow in $\sqrt{s} = 2.76$ TeV Pb+Pb collisions at the LHC, *Phys. Lett. B* 702, 59–63, 2011.

[26] P. Romatschke and U. Romatschke, Viscosity Information from Relativistic Nuclear Collisions: How Perfect is the Fluid Observed at RHIC?, *Phys. Rev. Lett.* 99, 172301, 2007.

[27] H. Song, S. A. Bass, and U. Heinz, Elliptic flow in 200 A GeV Au+Au collisions and 2.76 A TeV Pb+Pb collisions: insights from viscous hydrodynamics + hadron cascade hybrid model, *Phys. Rev. C* 83, 054912, 2011. [Erratum: Phys.Rev.C 87, 019902 (2013)].

[28] K. Dusling and D. Teaney, Simulating elliptic flow with viscous hydrodynamics, *Phys. Rev. C* 77, 034905, 2008.

[29] P. Bozek, Bulk and shear viscosities of matter created in relativistic heavy-ion collisions, *Phys. Rev. C* 81, 034909, 2010.

[30] B. Schenke, S. Jeon, and C. Gale, Elliptic and triangular flow in event-by-event (3+1)D viscous hydrodynamics, *Phys. Rev. Lett.* 106, 042301, 2011.

[31] P. Bozek and I. Wyskiel-Piekarska, Particle spectra in Pb-Pb collisions at $\sqrt{S_{NN}} = 2.76$ TeV, *Phys. Rev. C* 85, 064915, 2012.

[32] S. Ryu, J. F. Paquet, C. Shen, G. S. Denicol, B. Schenke, S. Jeon, and C. Gale, Importance of the Bulk Viscosity of QCD in Ultrarelativistic Heavy-Ion Collisions, *Phys. Rev. Lett.* 115, 13, 132301, 2015.

[33] S. Ryu, J.-F. Paquet, C. Shen, G. Denicol, B. Schenke, S. Jeon, and C. Gale, Effects of bulk viscosity and hadronic rescattering in heavy ion collisions at energies available at the BNL Relativistic Heavy Ion Collider and at the CERN Large Hadron Collider, *Phys. Rev. C* 97, 3, 034910, 2018.

[34] L. Du and U. Heinz, (3+1)-dimensional dissipative relativistic fluid dynamics at non-zero net baryon density, *Comput. Phys. Commun.* 251, 107090, 2020.

[35] P. Kovtun, D. T. Son, and A. O. Starinets, Viscosity in strongly interacting quantum field theories from black hole physics, *Phys. Rev. Lett.*, 94, 111601, 2005.

[36] H. Song, S. A. Bass, U. Heinz, T. Hirano, and C. Shen, Hadron spectra and elliptic flow for 200 A GeV Au+Au collisions from viscous hydrodynamics coupled to a Boltzmann cascade, *Phys. Rev. C* 83, 054910, 2011. [Erratum: Phys.Rev.C 86, 059903 (2012)].

[37] U. Heinz and R. Snellings, Collective flow and viscosity in relativistic heavy-ion collisions, *Ann. Rev. Nucl. Part. Sci.* 63, 123–151, 2013.

[38] A. Jaiswal and V. Roy, Relativistic hydrodynamics in heavy-ion collisions: general aspects and recent developments, *Adv. High Energy Phys.* 2016, 9623034, 2016.

[39] H. Niemi, G. S. Denicol, P. Huovinen, E. Molnar, and D. H. Rischke, Influence of the shear viscosity of the quark-gluon plasma on elliptic flow in ultrarelativistic heavy-ion collisions, *Phys. Rev. Lett.* 106, 212302, 2011.

[40] H. Niemi, K. J. Eskola, and R. Paatelainen, Event-by-event fluctuations in a perturbative QCD + saturation + hydrodynamics model: Determining QCD matter shear viscosity in ultrarelativistic heavy-ion collisions, *Phys. Rev. C* 93, 2, 024907, 2016.

[41] I. A. Karpenko, P. Huovinen, H. Petersen, and M. Bleicher, Estimation of the shear viscosity at finite net-baryon density from $A + A$ collision data at $\sqrt{s_{\rm NN}} = 7.7 - 200$ GeV, *Phys. Rev. C* 91, 6, 064901, 2015.

[42] J. E. Bernhard, J. S. Moreland, S. A. Bass, J. Liu, and U. Heinz, Applying Bayesian parameter estimation to relativistic heavy-ion collisions: simultaneous characterization of the initial state and quark-gluon plasma medium, *Phys. Rev. C* 94, 2, 024907, 2016.

[43] J. Auvinen, J. E. Bernhard, S. A. Bass, and I. Karpenko, Investigating the collision energy dependence of η/s in the beam energy scan at the BNL Relativistic Heavy Ion Collider using Bayesian statistics, *Phys. Rev. C* 97, 4, 044905, 2018.

[44] N. I. of Standards and T. (U.S.), NIST Chemistry Webbook: NIST Standard Reference Database Number 69. *NIST*, 2000.

[45] C. Cao, E. Elliott, H. Wu, and J. E. Thomas, Searching for perfect fluids: quantum viscosity in a universal fermi gas, *New Jour. of Phys.* 13, 075007, 2011.

[46] N. Astrakhantsev, V. Braguta, and A. Kotov, Temperature dependence of shear viscosity of $SU(3)$–gluodynamics within lattice simulation, *JHEP* 04, 101, 2017.

[47] H. B. Meyer, A Calculation of the shear viscosity in SU(3) gluodynamics, *Phys. Rev. D* 76, 101701, 2007.

[48] A. Nakamura and S. Sakai, Transport coefficients of gluon plasma, *Phys. Rev. Lett.* 94, 072305, 2005.

[49] S. Cremonini, U. Gursoy, and P. Szepietowski, On the Temperature Dependence of the Shear Viscosity and Holography, *JHEP* 08, 167, 2012.

[50] A. Adams, L. D. Carr, T. Schäfer, P. Steinberg, and J. E. Thomas, Strongly Correlated Quantum Fluids: Ultracold Quantum Gases, Quantum Chromodynamic Plasmas, and Holographic Duality, *New J. Phys.* 14, 115009, 2012.

[51] R. A. Lacey, N. N. Ajitanand, J. M. Alexander, P. Chung, W. G. Holzmann, M. Issah, A. Taranenko, P. Danielewicz, and H. Stoecker, Has the QCD Critical Point been Signaled by Observations at RHIC?, *Phys. Rev. Lett.* 98, 092301, 2007.

[52] K. Eskola, Nearly perfect quark–gluon fluid, *Nature Physics* 15, 08, 2019.

[53] S. W. Mages, S. Borsányi, Z. Fodor, A. Schäfer, and K. Szabó, Shear Viscosity from Lattice QCD, *PoS* LATTICE2014 232, 2015.

[54] P. B. Arnold, G. D. Moore, and L. G. Yaffe, Transport coefficients in high temperature gauge theories. 2. Beyond leading log, *JHEP* 05, 051, 2003.

[55] H. B. Meyer, Transport properties of the quark-gluon plasma from lattice QCD, *Nucl. Phys. A* 830, 641–648, 2009.

[56] M. Haas, L. Fister, and J. M. Pawlowski, Gluon spectral functions and transport coefficients in Yang–Mills theory, *Phys. Rev. D* 90, 091501, 2014.

[57] N. Christiansen, M. Haas, J. M. Pawlowski, and N. Strodthoff, Transport Coefficients in Yang–Mills Theory and QCD, *Phys. Rev. Lett.* 115, 11, 112002, 2015.

[58] R. Kubo, Statistical-mechanical theory of irreversible processes. I. general theory and simple applications to magnetic and conduction problems, *J. Phys. Soc. Jap.* , 12, 570–586, jun 1957.

[59] G. Jackson and A. Peshier, Re-running the QCD shear viscosity, *J. Phys. G* 45, 9, 095001, 2018.

[60] P. Zhuang, J. Hufner, S. P. Klevansky, and L. Neise, Transport properties of a quark plasma and critical scattering at the chiral phase transition, *Phys. Rev. D* 51, 3728–3738, 1995.

[61] C. Sasaki and K. Redlich, Transport coefficients near chiral phase transition, *Nucl. Phys. A* 832, 62–75, 2010.

[62] R. Marty, E. Bratkovskaya, W. Cassing, J. Aichelin, and H. Berrehrah, Transport coefficients from the Nambu-Jona-Lasinio model for $SU(3)_f$, *Phys. Rev. C* 88, p. 045204, 2013.

[63] S. Ghosh, A. Lahiri, S. Majumder, R. Ray, and S. K. Ghosh, Shear viscosity due to Landau damping from the quark-pion interaction, *Phys. Rev. C* 88, 6, 068201, 2013.

[64] S. K. Ghosh, S. Raha, R. Ray, K. Saha, and S. Upadhaya, Shear viscosity and phase diagram from Polyakov–Nambu–Jona-Lasinio model, *Phys. Rev. D* 91, 5, 054005, 2015.

[65] S. Ghosh, T. C. Peixoto, V. Roy, F. E. Serna, and G. a. Krein, Shear and bulk viscosities of quark matter from quark-meson fluctuations in the Nambu–Jona-Lasinio model, *Phys. Rev. C* 93, 4, 045205, 2016.

[66] P. Deb, G. P. Kadam, and H. Mishra, Estimating transport coefficients in hot and dense quark matter, *Phys. Rev. D* 94, 9, 094002, 2016.

[67] A. Harutyunyan, D. H. Rischke, and A. Sedrakian, Transport coefficients of two-flavor quark matter from the Kubo formalism, *Phys. Rev. D* 95, 11, 114021, 2017.

[68] A. N. Tawfik, A. M. Diab, and M. T. Hussein, SU(3) polyakov linear-sigma model: Conductivity and viscous properties of QCD matter in thermal medium, *Int. J. Mod. Phys. A* 31, 1650175, 2016.

[69] A. Abhishek, H. Mishra, and S. Ghosh, Transport coefficients in the Polyakov quark meson coupling model: A relaxation time approximation, *Phys. Rev. D* 97, 1, 014005, 2018.

[70] W. Florkowski, R. Ryblewski, N. Su, and K. Tywoniuk, Transport coefficients of the Gribov-Zwanziger plasma, *Phys. Rev. C* 94, 4, 044904, 2016.

[71] S. Plumari, A. Puglisi, F. Scardina, and V. Greco, Shear Viscosity of a strongly interacting system: Green-Kubo vs. Chapman-Enskog and Relaxation Time Approximation, *Phys. Rev. C* 86, 054902, 2012.

[72] S. Plumari, Anisotropic flows and the shear viscosity of the QGP within an event-by-event massive parton transport approach, *Eur. Phys. J. C* 79, 1, 2019.

[73] Z. Xu and C. Greiner, Shear viscosity in a gluon gas, *Phys. Rev. Lett.* 100, 172301, 2008.

[74] Z. Xu, C. Greiner, and H. Stocker, PQCD calculations of elliptic flow and shear viscosity at RHIC, *Phys. Rev. Lett.* 101, 082302, 2008.

[75] M. Alqahtani, M. Nopoush, R. Ryblewski, and M. Strickland, (3+1)D Quasiparticle Anisotropic Hydrodynamics for Ultrarelativistic Heavy-Ion Collisions, *Phys. Rev. Lett.* 119, 4, 042301, 2017.

[76] M. Alqahtani, M. Nopoush, and M. Strickland, Relativistic anisotropic hydrodynamics, *Prog. Part. Nucl. Phys.* 101, 204–248, 2018.

[77] A. Peshier and W. Cassing, The Hot non-perturbative gluon plasma is an almost ideal colored liquid, *Phys. Rev. Lett.* 94, 172301, 2005.

[78] A. Hosoya and K. Kajantie, Transport Coefficients of QCD Matter, *Nucl. Phys. B* 250, 666–688, 1985.

[79] S. Gavin, Transport Coefficients in Ultrarelativistic Heavy Ion Collisions, *Nucl. Phys. A* 435, 826–843, 1985.

[80] C. Sasaki and K. Redlich, Bulk viscosity in quasi particle models, *Phys. Rev. C* 79, 055207, 2009.

[81] M. Bluhm, B. Kampfer, and K. Redlich, Viscosities in the Gluon-Plasma within a Quasiparticle Model, *Nucl. Phys. A* 830, 737–740, 2009.

[82] A. S. Khvorostukhin, V. D. Toneev, and D. N. Voskresensky, Shear and bulk viscosities for pure glue matter, *Phys. Rev. C* 83, 035204, 2011.

[83] M. Bluhm, B. Kampfer, and K. Redlich, Bulk and shear viscosities of the gluon plasma in a quasiparticle description, *Phys. Rev. C* 84, 025201, 2011.

[84] A. S. Khvorostukhin, V. D. Toneev, and D. N. Voskresensky, Relaxation time ansatz and shear and bulk viscosities of gluon matter, *Phys. Rev. C* 84, 035202, 2011.

[85] P. Chakraborty and J. I. Kapusta, Quasi-Particle Theory of Shear and Bulk Viscosities of Hadronic Matter, *Phys. Rev. C* 83, 014906, 2011.

[86] M. Albright and J. I. Kapusta, Quasiparticle Theory of Transport Coefficients for Hadronic Matter at Finite Temperature and Baryon Density, *Phys. Rev. C* 93, 1, 014903, 2016.

[87] S. Plumari, W. M. Alberico, V. Greco, and C. Ratti, Recent thermodynamic results from lattice QCD analyzed within a quasi-particle model, *Phys. Rev. D* 84, 094004, 2011.

[88] V. Chandra, Transport properties of anisotropically expanding quark-gluon plasma within a quasi-particle model, *Phys. Rev. D* 86, 114008, 2012.

[89] S. Mitra and V. Chandra, Transport coefficients of a hot QCD medium and their relative significance in heavy-ion collisions, *Phys. Rev. D* 96, 9, 094003, 2017.

[90] V. Ozvenchuk, O. Linnyk, M. I. Gorenstein, E. L. Bratkovskaya, and W. Cassing, Shear and bulk viscosities of strongly interacting "infinite" parton-hadron matter within the parton-hadron-string dynamics transport approach, *Phys. Rev. C* 87, 6, 064903, 2013.

[91] H. Berrehrah, E. Bratkovskaya, T. Steinert, and W. Cassing, A dynamical quasiparticle approach for the QGP bulk and transport properties, *Int. J. Mod. Phys. E* 25, 07, 1642003, 2016.

[92] P. Moreau, O. Soloveva, L. Oliva, T. Song, W. Cassing, and E. Bratkovskaya, Exploring the partonic phase at finite chemical potential within an extended off-shell transport approach, *Phys. Rev. C* 100, 1, 014911, 2019.

[93] A. Muronga, Relativistic Dynamics of Non-ideal Fluids: Viscous and heat-conducting fluids. I. General Aspects and 3+1 Formulation for Nuclear Collisions, *Phys. Rev. C* 76, 014909, 2007.

[94] A. Muronga, Relativistic Dynamics of Non-ideal Fluids: Viscous and heat-conducting fluids. II. Transport properties and microscopic description of relativistic nuclear matter, *Phys. Rev. C* 76, 014910, 2007.

[95] W. Florkowski, A. Jaiswal, E. Maksymiuk, R. Ryblewski, and M. Strickland, Relativistic quantum transport coefficients for second-order viscous hydrodynamics, *Phys. Rev. C* 91, 054907, 2015.

[96] K. Paech and S. Pratt, Origins of bulk viscosity in relativistic heavy ion collisions, *Phys. Rev. C* 74, 014901, 2006. [Erratum: Phys.Rev.C 93, 059902 (2016)].

[97] G. Torrieri, B. Tomasik, and I. Mishustin, Bulk Viscosity driven clusterization of quark-gluon plasma and early freeze-out in relativistic heavy-ion collisions, *Phys. Rev. C* 77, 034903, 2008.

[98] D. Kharzeev and K. Tuchin, Bulk viscosity of QCD matter near the critical temperature, *JHEP* 09, 093, 2008.

[99] F. Karsch, D. Kharzeev, and K. Tuchin, Universal properties of bulk viscosity near the QCD phase transition, *Phys. Lett. B* 663, 217–221, 2008.

[100] D. T. Son and M. A. Stephanov, Dynamic universality class of the QCD critical point, *Phys. Rev. D* 70, 056001, 2004.

[101] O. Soloveva, P. Moreau, and E. Bratkovskaya, Transport coefficients for the hot quark-gluon plasma at finite chemical potential μ_B, *Phys. Rev. C* 101, 4, 045203, 2020.

[102] P. Singha, A. Abhishek, G. Kadam, S. Ghosh, and H. Mishra, Calculations of shear, bulk viscosities and electrical conductivity in the Polyakov-quark–meson model, *J. Phys. G* 46, 1, 015201, 2019.

[103] A. Harutyunyan and A. Sedrakian, Bulk viscosity of two-flavor quark matter from the Kubo formalism, *Phys. Rev. D* 96, 3, 034006, 2017.

[104] A. Czajka and S. Jeon, Kubo formulas for the shear and bulk viscosity relaxation times and the scalar field theory shear τ_π calculation, *Phys. Rev. C* 95, 6, 064906, 2017.

[105] S. S. Gubser, A. Nellore, S. S. Pufu, and F. D. Rocha, Thermodynamics and bulk viscosity of approximate black hole duals to finite temperature quantum chromodynamics, *Phys. Rev. Lett.* 101, 131601, 2008.

[106] D. Li, S. He, and M. Huang, Temperature dependent transport coefficients in a dynamical holographic QCD model, *JHEP* 06, 046, 2015.

[107] S. Heshmatian, R. Morad, and M. Akbari, Jet suppression in non-conformal plasma using AdS/CFT, *JHEP* 03, 045, 2019.

[108] W. Florkowski, R. Ryblewski, N. Su, and K. Tywoniuk, Bulk viscosity in a plasma of Gribov-Zwanziger gluons, *Acta Phys. Polon. B* 47, 1833, 2016.

[109] V. Begun, W. Florkowski, and R. Ryblewski, Thermodynamics and kinetics of Gribov-Zwanziger plasma with temperature dependent Gribov parameter, *Acta Phys. Polon. B* 48, 125, 2017.

[110] A. Jaiswal and N. Haque, Covariant kinetic theory and transport coefficients for Gribov plasma, *Phys. Lett. B* 811, 135936, 2020.

[111] M. Martinez, T. Schäfer, and V. Skokov, Critical behavior of the bulk viscosity in QCD, *Phys. Rev. D* 100, 7, 074017, 2019.

[112] S. Sakai and A. Nakamura, Lattice calculation of the QGP viscosities: Present results and next project, *PoS* LATTICE2007, 221, 2007.

[113] N. Y. Astrakhantsev, V. V. Braguta, and A. Y. Kotov, Temperature dependence of the bulk viscosity within lattice simulation of $SU(3)$ gluodynamics, *Phys. Rev. D* 98, 5, 054515, 2018.

[114] S. Gupta, The Electrical conductivity and soft photon emissivity of the QCD plasma, *Phys. Lett. B* 597, 57–62, 2004.

[115] G. Aarts, C. Allton, J. Foley, S. Hands, and S. Kim, Spectral functions at small energies and the electrical conductivity in hot, quenched lattice QCD, *Phys. Rev. Lett.* 99, 022002, 2007.

[116] H. T. Ding, A. Francis, O. Kaczmarek, F. Karsch, E. Laermann, and W. Soeldner, Thermal dilepton rate and electrical conductivity: An analysis of vector current correlation functions in quenched lattice QCD, *Phys. Rev. D* 83, 034504, 2011.

[117] B. B. Brandt, A. Francis, H. B. Meyer, and H. Wittig, Thermal Correlators in the \rho\ channel of two-flavor QCD, *JHEP* 03, 100, 2013.

[118] A. Amato, G. Aarts, C. Allton, P. Giudice, S. Hands, and J.-I. Skullerud, Electrical conductivity of the quark-gluon plasma across the deconfinement transition, *Phys. Rev. Lett.* 111, 17, 172001, 2013.

[119] G. Aarts, C. Allton, A. Amato, P. Giudice, S. Hands, and J.-I. Skullerud, Electrical conductivity and charge diffusion in thermal QCD from the lattice, *JHEP* 02, 186, 2015.

[120] G. Baym and H. Heiselberg, The Electrical conductivity in the early universe, *Phys. Rev. D* 56, 5254–5259, 1997.

[121] G. D. Moore and J.-M. Robert, Dileptons, spectral weights, and conductivity in the quark-gluon plasma, 7 2006.

[122] D. Fernandez-Fraile and A. Gomez Nicola, The Electrical conductivity of a pion gas, *Phys. Rev. D* 73, 045025, 2006.

[123] O. Linnyk, W. Cassing, and E. L. Bratkovskaya, Centrality dependence of the direct photon yield and elliptic flow in heavy-ion collisions at $\sqrt{s_{NN}} = 200$ GeV, *Phys. Rev. C* 89, 3, 034908, 2014.

[124] Y. Hirono, M. Hongo, and T. Hirano, Estimation of electric conductivity of the quark gluon plasma via asymmetric heavy-ion collisions, *Phys. Rev. C* 90, 2, 021903, 2014.

[125] K. Tuchin, Particle production in strong electromagnetic fields in relativistic heavy-ion collisions, *Adv. High Energy Phys.* 2013, 490495, 2013.

[126] L. McLerran and V. Skokov, Comments About the Electromagnetic Field in Heavy-Ion Collisions, *Nucl. Phys. A* 929, 184–190, 2014.

[127] U. Gursoy, D. Kharzeev, and K. Rajagopal, Magnetohydrodynamics, charged currents and directed flow in heavy ion collisions, *Phys. Rev. C* 89, 5, p. 054905, 2014.

[128] K. Fukushima, D. E. Kharzeev, and H. J. Warringa, The Chiral Magnetic Effect, *Phys. Rev. D* 78, p. 074033, 2008.

[129] A. Puglisi, S. Plumari, and V. Greco, Electric Conductivity from the solution of the Relativistic Boltzmann Equation, *Phys. Rev. D* 90, p. 114009, 2014.

[130] A. Puglisi, S. Plumari, and V. Greco, Shear viscosity η to electric conductivity σ_{el} ratio for the quark–gluon plasma, *Phys. Lett. B* 751, 326–330, 2015.

[131] L. Thakur, P. K. Srivastava, G. P. Kadam, M. George, and H. Mishra, Shear viscosity η to electrical conductivity σ_{el} ratio for an anisotropic QGP, *Phys. Rev. D* 95, 9, 096009, 2017.

[132] M. Greif, I. Bouras, C. Greiner, and Z. Xu, Electric conductivity of the quark-gluon plasma investigated using a perturbative QCD based parton cascade, *Phys. Rev. D* 90, 9, 094014, 2014.

[133] W. Cassing, O. Linnyk, T. Steinert, and V. Ozvenchuk, Electrical Conductivity of Hot QCD Matter, *Phys. Rev. Lett.* 110, 18, 182301, 2013.

[134] S. Caron-Huot, P. Kovtun, G. D. Moore, A. Starinets, and L. G. Yaffe, Photon and dilepton production in supersymmetric Yang-Mills plasma, *JHEP* 12, 015, 2006.

[135] P. Sahoo, S. K. Tiwari, and R. Sahoo, Electrical conductivity of hot and dense QCD matter created in heavy-ion collisions: A color string percolation approach, *Phys. Rev. D* 98, 5, 054005, 2018.

[136] T. Matsui, B. Svetitsky, and L. D. McLerran, Strangeness Production in Ultrarelativistic Heavy Ion Collisions. 1. Chemical Kinetics in the Quark - Gluon Plasma, *Phys. Rev. D* 34, 783, 1986. [Erratum: Phys.Rev.D 37, 844 (1988)].

[137] W. Florkowski, E. Maksymiuk, and R. Ryblewski, Coupled kinetic equations for fermions and bosons in the relaxation-time approximation, *Phys. Rev. C* 97, 2, 024915, 2018.

[138] V. Mykhaylova, M. Bluhm, K. Redlich, and C. Sasaki, Quark-flavor dependence of the shear viscosity in a quasiparticle model, *Phys. Rev. D* 100, 3, 034002, 2019.

[139] M. Bluhm, B. Kampfer, and K. Redlich, Ratio of bulk to shear viscosity in a quasigluon plasma: from weak to strong coupling, *Phys. Lett. B* 709, 77–81, 2012.

[140] M. Bluhm, B. Kampfer, and G. Soff, The QCD equation of state near T(c) within a quasi-particle model, *Phys. Lett. B* 620, 131–136, 2005.

[141] V. Chandra, Transport properties of anisotropically expanding quark-gluon plasma within a quasiparticle model, *Physical Review D* 86, 2012.

[142] H. Eschrig, The Particle World of Condensed Matter: An Introduction to the Notion of Quasi Particle. *Ed. am Gutenbergplatz*, 2005.

[143] C. Kittel, Introduction to Solid State Physics. *Wiley*, 2004.

[144] S. Mrówczyński, A. Rebhan, and M. Strickland, Hard-loop effective action for anisotropic plasmas, *Phys. Rev. D* 70, 025004, Jul 2004.

[145] P. F. Kelly, Q. Liu, C. Lucchesi, and C. Manuel, Deriving the hard thermal loops of QCD from classical transport theory, *Phys. Rev. Lett.* 72, 3461–3463, 1994.

[146] E. Braaten and R. D. Pisarski, Simple effective Lagrangian for hard thermal loops, *Phys. Rev. D* 45, 6, R1827, 1992.

[147] J. Alam, S. Sarkar, P. Roy, T. Hatsuda, and B. Sinha, Thermal photons and lepton pairs from quark gluon plasma and hot hadronic matter, *Annals Phys.* 286, 159–248, 2001.

[148] Y. B. Ivanov, V. V. Skokov, and V. D. Toneev, Equation of state of deconfined matter within dynamical quasiparticle description, *Phys. Rev. D* 71, 014005, 2005.

[149] T. S. Biró, P. Lévai, and B. Müller, Strangeness production with "massive"gluons, *Phys. Rev. D* 42, 3078–3087, 1990.

[150] M. Bluhm, B. Kampfer, R. Schulze, and D. Seipt, Quasi-Particle Description of Strongly Interacting Matter: Towards a Foundation, *Eur. Phys. J. C* 49, 205–211, 2007.

[151] R. D. Pisarski, Renormalized Fermion Propagator in Hot Gauge Theories, *Nucl. Phys. A* 498, 423–428, 1989.

[152] A. Peshier, B. Kampfer, and G. Soff, From QCD lattice calculations to the equation of state of quark matter, *Phys. Rev. D* 66, 094003, 2002.

[153] M. L. Bellac, *Thermal Field Theory*. Cambridge Monographs on Mathematical Physics, Cambridge University Press, 3 2011.

[154] S. Borsanyi, G. Endrodi, Z. Fodor, S. D. Katz, and K. K. Szabo, Precision SU(3) lattice thermodynamics for a large temperature range, *JHEP* 07, 056, 2012.

[155] S. Borsanyi, Z. Fodor, C. Hoelbling, S. D. Katz, S. Krieg, and K. K. Szabo, Full result for the QCD equation of state with 2+1 flavors, *Phys. Lett. B* 730, 99–104, 2014.

[156] V. Goloviznin and H. Satz, The Refractive properties of the gluon plasma in SU(2) theory, *Z. Phys. C* 57, 671–676, 1993.

[157] A. Peshier, B. Kampfer, O. P. Pavlenko, and G. Soff, An Effective model of the quark - gluon plasma with thermal parton masses, *Phys. Lett. B* 337, 235–239, 1994.

[158] M. I. Gorenstein and S. N. Yang, Gluon plasma with a medium-dependent dispersion relation, *Phys. Rev. D* 52, 5206–5212, 1995.

[159] M. Bluhm, B. Kampfer, R. Schulze, D. Seipt, and U. Heinz, A family of equations of state based on lattice QCD: Impact on flow in ultrarelativistic heavy-ion collisions, *Phys. Rev. C* 76, 034901, 2007.

[160] H. B. Meyer, High-Precision Thermodynamics and Hagedorn Density of States, *Phys. Rev. D* 80, 051502, 2009.

[161] P. Castorina, J. Cleymans, D. E. Miller, and H. Satz, The Speed of Sound in Hadronic Matter, *Eur. Phys. J. C* 66, 207–213, 2010.

[162] A. Khuntia, P. Sahoo, P. Garg, R. Sahoo, and J. Cleymans, Speed of sound in hadronic matter using non-extensive Tsallis statistics, *Eur. Phys. J. A* 52, 9, 292, 2016.

[163] A. Bazavov *et al.*, Equation of state in (2+1)-flavor QCD, *Phys. Rev. D* 90, 094503, 2014.

[164] C. Eckart, The thermodynamics of irreversible processes. iii. relativistic theory of the simple fluid, *Phys. Rev.* 58, 919–924, 1940.

[165] L. Landau and E. Lifshitz, Fluid Mechanics (Second Edition), 1–43, *Pergamon*, 1987.

[166] A. Muronga, Second-order dissipative fluid dynamics for ultrarelativistic nuclear collisions, *Phys. Rev. Lett.* 88, 062302, 2002.

[167] D. T. Son, Vanishing bulk viscosities and conformal invariance of unitary Fermi gas, *Phys. Rev. Lett.* 98, 020604, 2007.

[168] W. Israel, Nonstationary irreversible thermodynamics: A Causal relativistic theory, *Annals Phys.* 100, 310–331, 1976.

[169] M. S. Green, Markoff random processes and the statistical mechanics of time-dependent phenomena. ii. irreversible processes in fluids, *The Journal of Chemical Physics* 22, 3, 398–413, 1954.

[170] W. A. Hiscock and L. Lindblom, Stability and causality in dissipative relativistic fluids, *Annals of Physics* 151, 2, 466–496, 1983.

[171] W. A. Hiscock and L. Lindblom, Generic instabilities in first-order dissipative relativistic fluid theories, *Phys. Rev. D*, 31, 725–733, Feb 1985.

[172] P. Van and T. S. Biro, Relativistic hydrodynamics - causality and stability, *Eur. Phys. J. ST* 155, 201–212, 2008.

[173] W. Israel and J. Stewart, Transient relativistic thermodynamics and kinetic theory, *Annals of Physics* 118, 2, 341–372, 1979.

[174] R. Baier, P. Romatschke, D. T. Son, A. O. Starinets, and M. A. Stephanov, Relativistic viscous hydrodynamics, conformal invariance, and holography, *JHEP* 04, 100, 2008.

[175] W. Florkowski, M. P. Heller, and M. Spalinski, New theories of relativistic hydrodynamics in the LHC era, *Rept. Prog. Phys.* 81, 4, 046001, 2018.

[176] P. Romatschke, New Developments in Relativistic Viscous Hydrodynamics, *Int. J. Mod. Phys. E* 19, 1–53, 2010.

[177] I. Karpenko, P. Huovinen, and M. Bleicher, A 3+1 dimensional viscous hydrodynamic code for relativistic heavy ion collisions, *Comput. Phys. Commun.* 185, 3016–3027, 2014.

[178] P. Huovinen and P. V. Ruuskanen, Hydrodynamic Models for Heavy Ion Collisions, *Ann. Rev. Nucl. Part. Sci.* 56, 163–206, 2006.

[179] K. Dusling and T. Schäfer, Bulk viscosity, particle spectra and flow in heavy-ion collisions, *Phys. Rev. C* 85, 044909, 2012.

[180] F. Reif, Fundamentals of statistical and thermal physics, *American Journal of Physics* 66, 2, 164–167, 1998.

[181] P. Danielewicz and M. Gyulassy, Dissipative phenomena in quark-gluon plasmas, *Phys. Rev. D* 31, 53–62, 1985.

[182] P. Koch, B. Muller, and J. Rafelski, Strangeness in Relativistic Heavy Ion Collisions, *Phys. Rept.* 142, 167–262, 1986.

[183] J. Anderson and H. Witting, A relativistic relaxation-time model for the Boltzmann equation, *Physica*, 74, 3, 466–488, 1974.

[184] V. Mykhaylova and C. Sasaki, Impact of quark quasiparticles on transport coefficients in hot QCD, *Phys. Rev. D* 103, 1, p. 014007, 2021.

[185] H. Berrehrah, E. Bratkovskaya, W. Cassing, P. B. Gossiaux, J. Aichelin, and M. Bleicher, Collisional processes of on-shell and off-shell heavy quarks in vacuum and in the Quark-Gluon-Plasma, *Phys. Rev. C* 89, 5, p. 054901, 2014.

[186] O. Soloveva, D. Fuseau, J. Aichelin, and E. Bratkovskaya, Shear viscosity and electric conductivity of a hot and dense qgp with a chiral phase transition, *Phys. Rev. C* 103, 054901, May 2021.

[187] E. Lifshitz and L. Pitaevski, Physical Kinetics, 10 Course of Theoretical Physics, *Pergamon*, 1981.

[188] B. L. Combridge, Associated Production of Heavy Flavor States in p p and anti-p p Interactions: Some QCD Estimates, *Nucl. Phys. B* 151, 429–456, 1979.

[189] S. Jeon and L. G. Yaffe, From quantum field theory to hydrodynamics: Transport coefficients and effective kinetic theory, *Phys. Rev. D* 53, 5799–5809, 1996.

[190] J. Auvinen, K. J. Eskola, P. Huovinen, H. Niemi, R. Paatelainen, and P. Petreczky, Temperature dependence of η/s of strongly interacting matter: Effects of the equation of state and the parametric form of $(\eta/s)(T)$, *Phys. Rev. C* 102, 4, 044911, 2020.

[191] C. Cao, E. Elliott, J. Joseph, H. Wu, J. Petricka, T. Schäfer, and J. E. Thomas, Universal Quantum Viscosity in a Unitary Fermi Gas, *Science* 331, 58, 2011.

[192] E. Elliott, J. Joseph, and J. Thomas, Anomalous minimum in the shear viscosity of a fermi gas, *Phys. Rev. Lett.* 113, 2014.

[193] J. Joseph, E. Elliott, and J. Thomas, Shear viscosity of a unitary fermi gas near the superfluid phase transition, *Phys. Rev. Lett.* 115, 2015.

[194] M. Bluhm and T. Schäfer, Dissipative fluid dynamics for the dilute Fermi gas at unitarity: Anisotropic fluid dynamics, *Phys. Rev. A* 92, 4, 043602, 2015.

[195] M. Bluhm, J. Hou, and T. Schäfer, Determination of the density and temperature dependence of the shear viscosity of a unitary Fermi gas based on hydrodynamic flow, *Phys. Rev. Lett.* 119, 6, 065302, 2017.

[196] M. Bluhm and T. Schaefer, Model-independent determination of the shear viscosity of a trapped unitary Fermi gas: Application to high temperature data, *Phys. Rev. Lett.* 116, 11, 115301, 2016.

[197] V. Mykhaylova, Shear viscosity to electrical conductivity ratio in the quasiparticle models, *Eur. Phys. J. ST* 229, 22-23, 3487–3496, 2020.

[198] V. Mykhaylova, K. Redlich, and C. Sasaki, To appear on ArXiv, 2023.

[199] H. B. Meyer, A Calculation of the bulk viscosity in SU(3) gluodynamics, *Phys. Rev. Lett.* 100, 162001, 2008.

[200] P. B. Arnold, C. Dogan, and G. D. Moore, The Bulk Viscosity of High-Temperature QCD, *Phys. Rev. D* 74, 085021, 2006.

[201] S. Weinberg, Entropy generation and the survival of protogalaxies in an expanding universe, *Astrophys. J.* 168, 175, 1971.

[202] Y. Kim, I. J. Shin, and T. Tsukioka, Holographic QCD: Past, Present, and Future, *Prog. Part. Nucl. Phys.* 68, 55–112, 2013.

[203] A. Buchel, Transport properties of cascading gauge theories, *Phys. Rev. D* 72, 106002, 2005.

[204] V. Gribov, Quantization of non-abelian gauge theories, *Nuclear Physics B* 139, 1, 1–19, 1978.

[205] D. Zwanziger, Local and renormalizable action from the gribov horizon, *Nuclear Physics B* 323, 3, 513–544, 1989.

[206] A. Jaiswal, B. Friman, and K. Redlich, Weak and strong coupling limits of the Boltzmann equation in the relaxation-time approximation, [arXiv:1602.05424 [nucl-th]], 2016.

[207] A. Czajka, K. Dasgupta, C. Gale, S. Jeon, A. Misra, M. Richard, and K. Sil, Bulk Viscosity at Extreme Limits: From Kinetic Theory to Strings, *JHEP* 07, 145, 2019.

[208] X. Zhu and S.-Q. Feng, Shear viscosity coefficient of magnetized QCD medium near chiral phase transition, *Phys. Rev. D* 107, 1, 016018, 2023.

[209] M. Kurian and V. Chandra, Bulk viscosity of a hot qcd medium in a strong magnetic field within the relaxation-time approximation, *Phys. Rev. D* 97, 116008, Jun 2018.

[210] G. Almirante, N. Astrakhantsev, V. Braguta, M. D'Elia, L. Maio, M. Naviglio, F. Sanfilippo, and A. Trunin, Electromagnetic conductivity of quark-gluon plasma at finite baryon chemical potential and electromagnetic field, *PoS* LATTICE2022, 155, 2023.

[211] G. Boyd, J. Engels, F. Karsch, E. Laermann, C. Legeland, M. Lutgemeier, and B. Petersson, Thermodynamics of SU(3) lattice gauge theory, *Nucl. Phys. B* 469, 419–444, 1996.

[212] J. Dey, S. Satapathy, P. Murmu, and S. Ghosh, Shear viscosity and electrical conductivity of the relativistic fluid in the presence of a magnetic field: A massless case, *Pramana* 95, 3, 125, 2021.

[213] T. Matsui and H. Satz, J/ψ Suppression by Quark-Gluon Plasma Formation, *Phys. Lett. B* 178, 416–422, 1986.

[214] R. Rapp, D. Blaschke, and P. Crochet, Charmonium and bottomonium production in heavy-ion collisions, *Prog. Part. Nucl. Phys.* 65, 209–266, 2010.

[215] A. Mocsy, P. Petreczky, and M. Strickland, Quarkonia in the Quark Gluon Plasma, *Int. J. Mod. Phys. A* 28, 1340012, 2013.

[216] L. Apolinário, Y.-J. Lee, and M. Winn, Heavy quarks and jets as probes of the QGP, *Prog. Part. Nucl. Phys.* 127, 103990, 2022.

[217] M. He, H. van Hees, and R. Rapp, Heavy-Quark Diffusion in the Quark-Gluon Plasma, [arXiv:2204.09299 [hep-ph]], 2022.

[218] N. Brambilla *et al.*, Heavy Quarkonium: Progress, Puzzles, and Opportunities, *Eur. Phys. J. C* 71, 1534, 2011.

[219] P. Levai and R. Vogt, Thermal charm production by massive gluons and quarks, *Phys. Rev. C* 56, 2707–2717, 1997.

[220] T. S. Biro, E. van Doorn, B. Muller, M. H. Thoma, and X. N. Wang, Parton equilibration in relativistic heavy ion collisions, *Phys. Rev. C* 48, 1275–1284, 1993.

[221] B.-W. Zhang, C.-M. Ko, and W. Liu, Thermal charm production in a quark-gluon plasma in Pb-Pb collisions at $\sqrt{s_{NN}} = 5.5$-TeV, *Phys. Rev. C* 77, 024901, 2008.

[222] V. Mykhaylova, Charm quark fugacity in hot QCD, *EPJ Web Conf.* 274, 05006, 2022.

[223] F. Jüttner, Das maxwellsche gesetz der geschwindigkeitsverteilung in der relativtheorie, *Ann. der Phys.* 339, 856 – 882, 03 2006.

[224] J. D. Bjorken, Highly relativistic nucleus-nucleus collisions: The central rapidity region, *Phys. Rev. D* 27, 140–151, Jan 1983.

[225] L. Alvarez-Ruso and V. Koch, Phi meson propagation in a hot hadronic gas, *Phys. Rev. C* 65, 054901, 2002.

[226] P. Braun-Munzinger and K. Redlich, Charmonium production from the secondary collisions at LHC energy, *Eur. Phys. J. C* 16, 519–525, 2000.

[227] E. Schnedermann, J. Sollfrank, and U. W. Heinz, Thermal phenomenology of hadrons from 200-A/GeV S+S collisions, *Phys. Rev. C* 48, 2462–2475, 1993.

[228] M. P. Heller and M. Spalinski, Hydrodynamics Beyond the Gradient Expansion: Resurgence and Resummation, *Phys. Rev. Lett.* 115, 7, 072501, 2015.

[229] A. Andronic, P. Braun-Munzinger, K. Redlich, and J. Stachel, Statistical hadronization of heavy quarks in ultra-relativistic nucleus-nucleus collisions, *Nucl. Phys. A* 789, 334–356, 2007.

[230] S. Borsanyi *et al.*, Calculation of the axion mass based on high-temperature lattice quantum chromodynamics, *Nature* 539, 7627, 69–71, 2016.